Coordination Chemistry Reviews 289–290 (2015) 149–176

Contents lists available at ScienceDirect

Coordination Chemistry Reviews

journal homepage: www.elsevier.com/locate/ccr

Review

Radical ligand-containing single-molecule magnets

Selvan Demir[a], Ie-Rang Jeon[b], Jeffrey R. Long[a,*], T. David Harris[b,**]

[a] Department of Chemistry, University of California, Berkeley, CA 94720, USA
[b] Department of Chemistry, Northwestern University, Evanston, IL 60208, USA

Contents

Abbreviations: 2,6-NITpy, 2,6-bis-(3′-oxide-1′-oxyl-4′,4′,5′,5′-tetramethylimidazolin-2′-yl)pyridine; 2pyNO, *tert*-butyl 2-pyridyl nitroxide; 3,5-DBSQ, 3,5-di-*tert*-butyl-o-semiquinone; 3,6-DBSQ, 3,6-di-*tert*-butyl-o-semiquinone; 6,6′-NITbpy, 6,6′-bis-(3″-oxide-1″-oxyl-4″,4″,5″,5″-tetramethylimidazolin-2″-yl)-2,2′-bipyridine; 6bpyNO, 2,2′-bipyridin-6-yl *tert*-butyl nitroxide; $(^{Ad}ArO)_3$tacn, 1,4,7-tris(3-adamantyl-5-*tert*-butyl-2-hydroxybenzyl)-1,4,7-triazacyclonane; $(^{t\text{-}Bu}ArO)_3$tacn, 1,4,7-tris(3,5-di-*tert*-butyl-2-hydroxybenzyl)-1,4,7-triazacyclononane; ADBP, 2-anilino-4,6-di-*tert*-butylphenol; ap, amidophenolate; AZP, azophenine; bipy, 2,2′-bipyridine; bipyvd, 1,5-dimethyl-3-(2,2′-bipyridin-6-yl)-6-oxoverdazyl; boaDTDA, 4-(benzoxazol-2′-yl)-1,2,3,5-dithiadiazolyl; bpym, 2,2-bipyrimidine; Bu, butyl; Bz, benzyl; cbvd, 1,5-dimethyl-3-(carboxylate)-6-oxoverdazyl; Cp*, pentamethylcyclopentadienyl; Cp′, 1,2,4-tri-*tert*-butyl cyclopentadienyl; Cp^P, 1-(7,7-dimethylbenzyl)cyclopentadienyl; CTH, *dl*-5,7,7,12,14,14-hexamethyl-1,4,8,11-tetraazacyclotetradecane; dad, 1,4-diazabutadiene; ^{dipp}iq, 4,6-di-*tert*-butyl-2-[(2,6-diisopropylphenyl)-imino]quinone; dmmpoNO, 4,4-dimethyl-2,2-bis[2-(3-methylpyridyl)]oxazolidine-N-oxide; dmp_2Nin, bis(2,6-dimethylphenyl)nindigo; dmpoNO, 4,4-dimethyl-2,2-di(2-pyridyl)oxazolidine-N-oxyl; dmtacn, 1,4-dimethyl-1,4,7-triazacyclononane; dpvd, 1,3-di-(2-pyridyl)-6-oxoverdazyl; DTBNO, di-*tert*-butyl nitroxide; dtbsq, 3,5-di-*tert*-butylsemiquinonato; EBAMP, 4-ethoxy-2,6-bis(N,N-dimethylaminomethylene)pyridine; Et, ethyl; ^{F}ADBP, 2-(3,5-difluoroanilino)-4,6-di-*tert*-butylphenol; ^{F}PDA, N,N′-Bis(pentafluorophenyl)-o-phenylenediamine; H_2Pc, phthalocyanine; $Hbpz_3$, hydrotris(pyrazolyl)borate; H_c, coercive field; HDVV, Heisenberg, Dirac, van Vleck Hamiltonian; hfac, (1,1,1,5,5,5)-hexafluoroacetylacetonate; HMM, Hubbard molecule model; im, imidazole; imvd, 1,5-dimethyl-(3-(2′-imidazolyl)-6-oxoverdazyl); ind, indazole; ^{i}pr, *iso*-propyl; isq, iminobenzosemiquinone; *m*bis, 1,3-bis-(1′-oxyl-3′-oxido-4′,4′,5′,5′-tetramethyl-4,5-hydro-1H-imidazol-2-yl)benzene; Me, methyl; Me_4cyclam, 1,4,8,11-tetraaza-1,4,8,11-tetramethylcyclotetradecane; ^{MeS}ADBP, 2-(2-methylthioanilino)-4,6-di-*tert*-butylphenol; Nap, naphthalene; $NH(py)_2$, di-2-pyridylamine; Nindigo, inidigo *N,N′*-diarylimine; NIT2Py, 2-(2-pyridyl)-4,4,5,5-tetramethyl-4,5-dihydro1-H-imidazolyl-1-oxy 3-oxide; NITbpy, 6,6′-bis(3″-oxide-1″-oxyl-4″,4″,5″,5″-tetramethylimidazoline-2″-yl)-2,2′-bipyridine; NITBzImH, 2-(2-benzimidazolyl)-4,4,5,5-tetramethyl-4,5-dihydro-1H-imidazolyl-3-oxide-1-oxide; NITImH, 2-(2-imidazolyl)-4,4,5,5-tetramethyl-4,5-dihydro-1H-imidazolyl-3-oxide-1-oxide; NITPh, 2-(2-pyridyl)-4,4,5,5-tetramethyl-4,5-dihydro-1H-imidazolyl-3-oxide-1-oxide; NITPhOMe, 4′-methoxy-phenyl-4,4,5,5-tetramethylimidazoline-1-oxyl-3-oxide; NITtrz, 2-(4,5-dimethyl-4H-1,2,4-triazol-3-yl)-4,4,5,5-tetramethyl-3-oxo-4,5-dihydro-1H-imidazol-1-oxyl; *o*-Cl_4SQ, tetrachloro-*o*-benzosemiquinone; Pc, phthalocyaninate; Pc′, octa(isopropylidenedioxy)phthalocyaninate; $Pc(\alpha\text{-}OC_5H_{11})_4$, 1,8,15,22-tetrakis(3-pentyloxy)phthalocyaninate; PDI, pyridine(diimine); pfpr, pentafluoropropionate; ph, phenyl; phenSQ, 9,10-phenanthrenesemiquinone; phpyNO, *tert*-butyl 5-phenyl-2-pyridyl nitroxide; Phtfac, phenyltrifluoroacetylacetonate; pic, picolinate; pmvd, 1,5-dimethyl-3-(4,6-dimethylpyrimidin-2-yl)-6-oxoverdazyl; proxyl, 2,2,5,5-tetramethylpyrrolidinyl-1-oxy; *p*-tolsal, *N*-*p*-tolylsalicylidenimine; py, pyridine; pyDTDA, 4-(2′-pyridyl)-1,2,3,5-dithiadiazolyl; pyvd, 1,5-dimethyl-3-(2-pyridyl)-6-oxoverdazyl; salen, *N,N′*-ethylenebis(salicylidenimine); *S*-DOP, *S*-dodexyloxypropane; T_B, magnetic blocking temperature; TBA, tetrabutylammonium; TBPNOpy, 4-{*N*-(2,4,6-Tri-*tert*-butylphenyl)-*N*-hydroxylamino}pyridine; *t*Bu, *tert*-butyl; ^{tBu}ADBP, 2-(3,5-di-*tert*-butylanilino)-4,6-di-*tert*-butylphenol; ^{tBu}PDA, *N,N*-bis(3,5-di-*tert*-butylphenyl)-1,2-phenylenediamine; TClPP, meso-tetrakis-(4-chlorophenyl)porphyrinate; TCNE, tetracyanoethylene; TCNQ, tetracyanoquinodimethane; tempo, 2,2,6,6-tetramethylpiperidinyl-1-oxyl; terpy, 2,2′:6′,2″-terpyridine; tfa, trifluoroacetylacetonate; Tp*, hydrotris(3,5-dimethylpyrazolyl)borate; tppz, tetra-2-pyridinylpyrazine; TPyA, tris(2-pyridylmethyl)amine; tren, tris(2-aminoethyl)amine; ttf, tetrathiafulvalene; U_{eff}, *effective* spin-reversal barrier; X-hfpip, 1,1,1,5,5,5-hexafluoro-4-(4-X-phenylimino)$_2$-pentanonate; τ_0, preexponential factor.

* Corresponding author.
** Corresponding author. Tel.: +1 847 467 4176.
E-mail addresses: jrlong@berkeley.edu (J.R. Long), dharris@northwestern.edu (T.D. Harris).

http://dx.doi.org/10.1016/j.ccr.2014.10.012

ARTICLE INFO

Article history:
Received 21 July 2014
Received in revised form 26 October 2014
Accepted 30 October 2014
Available online 13 November 2014

Keywords:
Single-molecule magnets
Exchange coupling
Radical ligands
Redox-active ligands
Zero-field splitting

ABSTRACT

Single-molecule magnets represent the ultimate size limit for spin-based information storage and processing; however, such applications require large spin relaxation barriers and blocking temperatures. Ongoing efforts to synthesize single-molecule magnets with higher barriers must take into consideration key physical parameters, such as spin ground state, *S*, and axial zero-field splitting parameter, *D*, which are both correlated to the barrier height. A third critical parameter that has received less attention is the exchange coupling constant, *J*. This constant determines the degree of separation between spin ground state and excited states, which must be sufficiently large in a single-molecule magnet to maintain slow magnetization dynamics at elevated temperatures, and also serves to shut down fast quantum relaxation pathways. Toward this end, one synthetic strategy to engender strong magnetic exchange is the incorporation of radical ligands into metal complexes. Within these complexes, the presence of direct exchange between paramagnetic ligand and metal units can result in exceptionally strong magnetic coupling, much stronger in fact than more common superexchange interactions. This review article provides a survey of radical ligand-containing single-molecule magnets, with a brief overview of other classes of metal–ligand radical complexes that could be exploited in the design of new single-molecule magnets. Furthermore, ligand-field and electronic structure considerations in dictating exchange strength and slow magnetic relaxation are highlighted, with the aim of helping to guide the synthesis of future radical ligand-containing single-molecule magnets with even stronger exchange coupling.

1. General introduction

Single-molecule magnets are molecules exhibiting an energy barrier to magnetic relaxation that enables them to retain their magnetization orientation after removal of an applied field. Remarkably, these molecules exhibit bulk magnet-like properties such as magnetic hysteresis, while their molecular nature also leads to quantum phenomena such as quantum tunneling of the magnetization. Indeed, the discovery of slow magnetic relaxation in molecules has sparked a tremendous interest in single-molecule magnets, owing largely to the potential for their use in applications such as molecular spintronics [1–6] and quantum information storage and processing [7,8]. However, in order for these applications to be realized, much higher spin relaxation barriers must be attained.

The magnitude of relaxation barrier in a single-molecule magnet, theoretically predicted as $U = S^2|D|$ for integer-spin molecules and $U = (S^2 - ¼)|D|$ for half-integer-spin molecules, arises from the impact of a uniaxial magnetic anisotropy, quantified by the axial zero-field splitting parameter, *D*, on a high-spin ground state, *S*. By convention, a negative value of *D* positions the largest $M_S = \pm S$ levels lowest in energy, thereby effecting an energy barrier to spin relaxation from $M_S = +S$ to $-S$ that is ultimately responsible for single-molecule magnet behavior. As such, increasing the spin relaxation barrier of a single-molecule magnet necessitates the maximization of both *S* and *D*. Toward this end, an extraordinary effort has been undertaken by numerous researchers to synthesize molecules that possess high spin ground states with a large magnetic anisotropy.

In addition to the importance placed on designing molecules with large values of *S* and *D*, the exchange coupling constant, *J*, must also be considered. In a multinuclear complex, the energetic separation between spin ground state and excited states is directly correlated to the strength of exchange coupling between paramagnetic centers and therefore the magnitude of *J*. If this separation is not sufficiently large, the magnetization of the molecule can undergo fast relaxation through pathways involving spin excited states. As such, even an exceptionally large anisotropy barrier will not necessarily lead to a high blocking temperature if the exchange coupling is not strong. In addition, strong exchange coupling can serve to shut down quantum tunneling processes within a single spin state manifold. Indeed, tunneling remains an important problem in the design of single-molecule magnets with higher blocking temperatures, especially in f-element-containing species, as it provides a mechanism through which relaxation

can short cut the overall anisotropy barrier. Despite the importance of exchange coupling strength in single-molecule magnets, an overwhelming majority of these molecules feature structures comprised of paramagnetic metal centers bridged by diamagnetic ligands. Here, magnetic coupling between metal centers occurs via an indirect superexchange mechanism, which is often relatively weak, especially in the case of multi-atom bridging ligands. As an alternative, connecting paramagnetic metal centers by paramagnetic bridging ligands can give rise to much stronger direct exchange coupling between the metals and the spin of the ligand radical. This strategy can be particularly effective in lanthanide-containing single-molecule magnets, since radical ligands possess diffuse spin orbitals that can potentially penetrate the core electron density of the lanthanide ions to reach the deeply buried 4f orbitals. Encouragingly, despite the paucity of ligand radical-containing single-molecule magnets, the literature is replete with examples of exceptionally strong metal-radical ligand coupling in molecules that do not exhibit slow magnetic relaxation, and knowledge learned from these work can undoubtedly be extended to the area of single-molecule magnets.

Herein, we review the current literature of radical ligand-containing single-molecule magnets. While not intended to provide a comprehensive review on other metal–ligand radical complexes that do not exhibit slow magnetic relaxation, this article will nevertheless briefly survey classes of molecules that could potentially be exploited to realize new, metal-radical ligand single-molecule magnets. For a more comprehensive account of other metal-radical ligand complexes, the reader is referred to broader and more inclusive review articles [9–21]. For the latest advances on single-molecule magnets, the reader is referred to some recent review articles [22–30]. The scope of this review includes mono- and multinuclear molecular complexes, spanning transition metal-, lanthanide-, and actinide-containing species. Note that organic radicals that do not possess the ability to coordinate to metal ions, and thus cannot act as ligands, are not addressed here. Finally, in the following discussion, an emphasis is placed on highlighting the importance of ligand-field and electronic structure considerations in dictating exchange strength and slow magnetic relaxation. The values of magnetic exchange coupling constant (J) reported in this review are converted based on the general Hamiltonian $H = -2JS_AS_B$, with A and B indicating two interacting paramagnetic centers, metal ions and/or radical ligands. Fig. 1 provides a summary of the radical ligands that will be discussed in this article.

2. Transition metal-radical ligand single-molecule magnets

2.1. Introduction

After the discovery of the first single-molecule magnet, cluster compound $Mn_{12}O_{12}(O_2CMe)_{16}(H_2O)_4$ [31], efforts to increase the spin relaxation barrier primarily involved research aimed at synthesizing larger metal clusters with higher values of S, typically featuring oxo bridging ligands between metal centers [31–49]. Here, the magnetic interactions between the metal centers occur via superexchange coupling through the diamagnetic oxido unit, and these interactions can indeed reach appreciable magnitudes for such one-atom bridging ligands. However, introducing a paramagnetic center as the bridging moiety can provide even stronger exchange coupling.

The presence of strong coupling arising from the direct orbital overlap between radical and transition metal ion has provided researchers with great impetus for studying the magnetic interactions between two different paramagnetic centers [50]. The ligands being utilized for this purpose span a wide range, from the more established nitronyl nitroxide and benzosemiquinonoid ligands [51–54], to the more recently developed verdazyl, thiazyl, and carbene ligands that already show great promise in generating materials with interesting magnetic properties [55–57]. Although tetracyanoethylene, 7,7,8,8-tetracyanoquinodimethane, *N,N′*-dicyanoquinonediimine, and perchlorotriphenylmethyl radicals have found enormous success in the rational design of molecule-based magnetic materials, they will not be covered in this section, owing to the lack of the corresponding molecular analogs [58–75].

The use of organic radicals to bridge two or more paramagnetic transition metal ions in order to build magnetic materials has provided two remarkable benchmarks, the first room temperature molecule-based magnet, $V(TCNE)_x{\cdot}nCH_2Cl_2$ ($x \approx 2$, $n \approx 1/2$) [60] and the first experimental observation of slow dynamics in a one-dimensional compound, as observed in $(NITPhOMe)Co(hfac)_2$ [76]. Nevertheless, transition metal-based single-molecule magnets incorporating a radical ligand in either mono- or multinuclear compounds are scarce [77–87]. The following sections will survey radical ligand-containing mononuclear and radical ligand-bridged multinuclear transition metal complexes that have been shown to exhibit single-molecule magnet behavior or that represent classes of molecules that could lead to new single-molecule magnets.

2.2. Mononuclear transition metal-radical complexes

2.2.1. Nitroxide radical-containing complexes

Nitronyl nitroxides, which are among the most widely studied stable free radicals, feature an unpaired electron that is delocalized over the coordinating oxygen atoms (Fig. 1). Consequently, this family of ligands has been and continues to be an attractive choice for spin carriers in magnetic materials. A limitation of these ligands, however, is the poor ability of the weakly Lewis basic N—O group to coordinate to a metal center. Nevertheless, enhanced binding of monodentate nitroxides can often be achieved through employment of electron withdrawing groups, such as (1,1,1,5,5,5)-hexafluoroacetylacetonate (hfac) [88–92], halides [93], and halocarboxylate [94,95], as ancillary ligands in order to increase the Lewis acidity of metal ions and generate compounds of the form $L_nM(L')_2$ (L = nitroxide radical; L′ = ancillary ligand; n = 1 or 2). The first structurally [88] and magnetically [96] characterized complex of this form, $(tempo)Cu(hfac)_2$ (tempo = 2,2,6,6-tetramethylpiperidinyl-1-oxyl), comprises a distorted square pyramidal Cu^{II} center with the nitroxyl oxygen atom occupying a basal coordination site. The bent metal–ligand bonding configuration with Cu—O—N angle of 123.9(4)° offers appropriate symmetry for overlap of nitroxyl π* and copper $d_{x^2-y^2}$ orbitals, enabling strong antiferromagnetic coupling ($J \leq -225\,cm^{-1}$ [97]; Table 1). While long axial bonds of the NO groups coordinated to Cu^{II} results in moderate ferromagnetic coupling between nitroxide radical and the metal ion [91,98], short equatorial coordination induces strong antiferromagnetic exchange interactions [95,96], as rationalized by extended Hückel calculations [98]. Axial coordination of the nitroxide leads to an orthogonality between the ligand π* orbital and the metal $d_{x^2-y^2}$ orbital resulting in ferromagnetic coupling. In contrast, orbital overlap increases rapidly for equatorial coordination, giving rise to antiferromagnetic coupling.

A number of heterocycle-based derivatives of nitronyl nitroxide have also been employed [99–106], as the chelate effect arising from the heterocycle nitrogen donors enhances the ability of the nitroxyl group to coordinate a poor electrophilic metal center. However, the formation of the chelate ring substantially weakens the magnitude of the coupling [102], most likely due to the σ–π mixing of the lone pair of nitrogen and the nitroxide [54]. Recently, the ligand 4,4-dimethyl-2,2-di(2-pyridyl)oxazolidine-*N*-oxyl (dmpoNO) [107], which bears two pyridyl donors, was treated

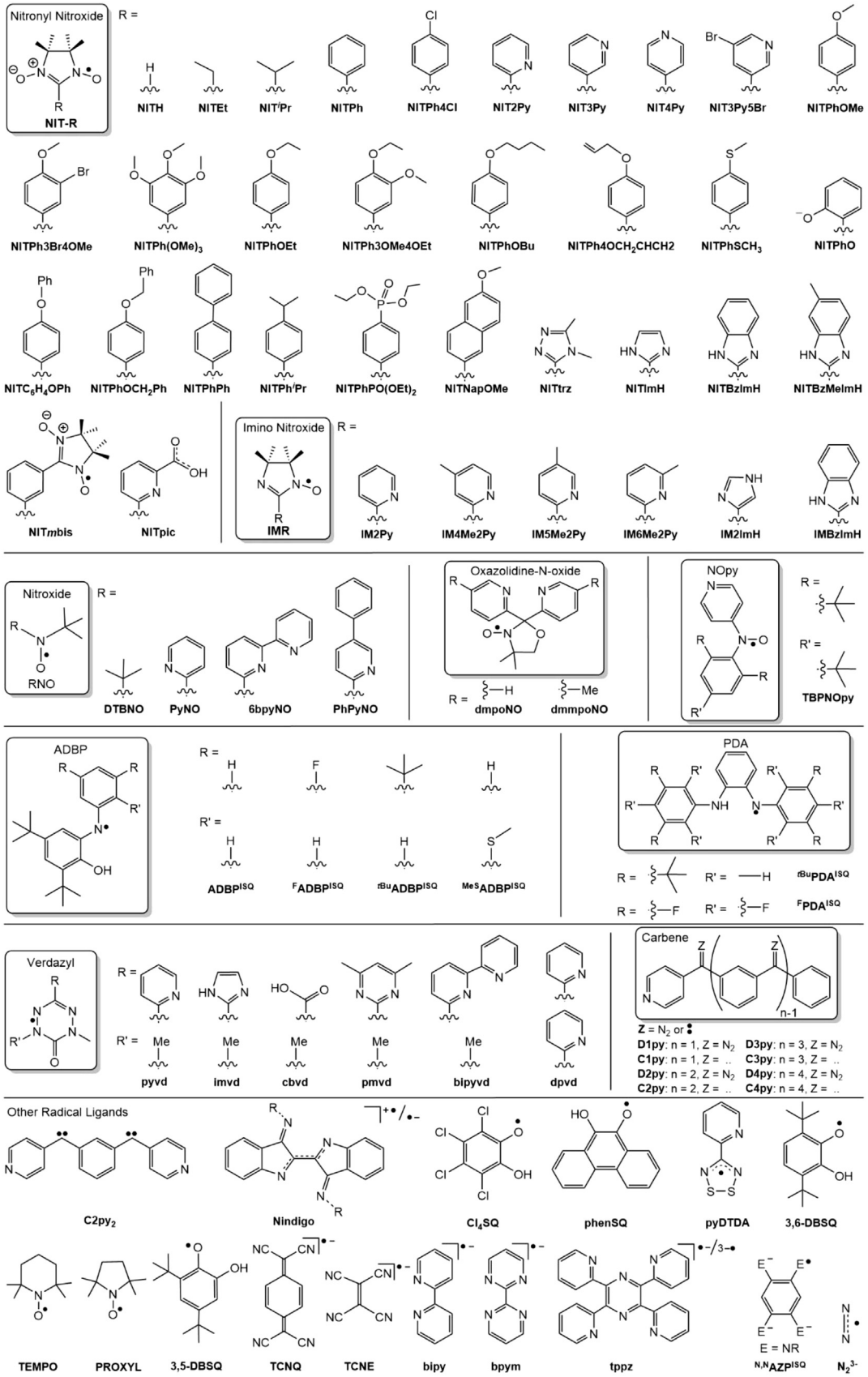

Fig. 1. Radical accessible ligands covered in this review from top-to-bottom, left-to-right: nitronyl nitroxide, imino nitroxide, nitroxide, oxazolidine-*N*-oxide, NOpy, ADBP, DPA, verdazyl, carbene and various other radical ligands.

Table 1
Summary of magnetic exchange interactions in selected structurally characterized mononuclear transition metal complexes that contain radical ligands.

Compounds	J_1 [a]	J_{L-L} [a]	Reference	Compounds	J_1 [a]	J_{L-L} [a]	Reference
Nitroxide (monodentate)				$M(Cl_4SQ)_3$ (M = Fe, Cr)	−60 (Fe), −400 (Cr)		[116,118]
(tempo)Cu(hfac)$_2$	≤−225		[88,96]	$M(phenSQ)_3$ (M = Fe, Cr)	−100 (Fe), −350 (Cr)		[116,118]
(tempo)$_2$Mn(hfac)$_2$ [b]	−79[c]		[89]	$Fe(^{F}ADBP^{ISQ})_3$	−184(5)	0[k]	[158]
(proxyl)$_2$Mn(hfac)$_2$	−105[c]		[89]	$M(phenSQ)_2(py)_2$ (M = Ni, Co)	~0 (Ni), −3.6 (Co)		[118,159]
$(NITPh)_2CuCl_2$	−7[d]		[93]	Ni(phenSQ)$_2$(bpy)	−0.7		[118]
$(NITPh)_2Cu(hfac)_2$	<+5		[91]	$Fe(3,6\text{-}DBSQ)_3$	−139	−235	[119]
(NITPh)Cu(hfac)$_2$	nr[e]		[91]	$Cu(3,6\text{-}DBSQ)_2$	+100		[160]
$(NITPh)_2Ni(hfac)_2$	−200		[92]	$Ni(3,6\text{-}DBBQ)(3,6\text{-}DBSQ)_2$	+89.1	−89.9	[161]
$(NITPh)_2Cu(tfac)_2$	<−500[c]		[95]	$Mn(3,6\text{-}DBSQ)_2(3,6\text{-}DBCat)$	nr[f]		[162]
Nitroxide (bidentate)				$[Cr(Cl_4SQ)_2(Cl_4cat)]^-$	nr[i]		[163]
$(NIT2Py)_2MCl_2$ (M = Ni, Mn)	−110 (Ni), −79 (Mn)		[99]	$Cu(ADBP^{ISQ})_2$	+195[j]	−400	[127]
(NIT2Py)M(hfac)$_2$ (M = Ni, Mn)	−167 (Ni), −65 (Mn)		[99]	$Fe(ADBP^{ISQ})_2X$ (X = Cl, Br, I)	nr[k] (Cl), −145 (Br), −100 (I)		[164]
$[(NITImH)_3Mn]^{2+}$	−53(2)		[102]	$Mn^{III}(ADBP^{ISQ})_2(ADBP^{PDI})$	−300	0[i]	[123]
$[(NITBzImH)_3Mn]^{2+}$	−79(5)		[102]	$Mn^{IV}(ADBP^{ISQ})_2(HADBP^{PDI})$	−470	0[i]	[123]
$[(NIT2Py)_3M]^{2+}$ (M = Ni, Mn)	−111 (Ni), −88 (Mn)		[102]	$Mn^{IV}(^{tBu}ADBP^{ISQ})_2(^{tBu}ADBP^{PDI})$	−292		[165]
$[(2pyNO)_2M(H_2O)_2]^{2+}$ (M = Ni, Cu)	+88 (Ni), −95 (Cu)		[105]	$Cu(^{MeS}ADBP^{ISQ})_2$	−207	−57	[127]
$[(phpyNO)_2Ni(H_2O)_2]^{2+}$ (M = Ni, Cu)	+142 (Ni), +151 (Cu)		[106]	$Ni(^{tBu}PDA^{ISQ})_2$	nr[e], −946[l]		[129]
$[(phpyNO)_2Cu(ClO_4)_2]$	+96		[106]	$[Cu(NH(py)_2)(3,5\text{-}DBSQ)]^+$	+110		[121]
$[(phpyNO)_2Cu(CF_3SO_3)_2]$	−327		[106]	$[Ni(CTH)(3,5\text{-}DBSQ)]^+$	nr[k], +178[l]		[120,159]
Nitroxide (tridentate)				$[Ni(CTH)(phenSQ)]^+$	nr[k], +142[l]		[120]
$[(2,6\text{-}NITpy)_2Ni]^{2+}$ (M = Ni, Co, Mn)	−167 (Ni), nr[f] (Co), −83 (Mn)	−10	[103]	$[Cr(tren)(3,6\text{-}DBSQ)]^{2+}$	<−350[h]		[166]
$[(2,6\text{-}NITpy)_2Cu]^{2+}$	−320 (eq), +7 (ax)	−14	[103]	$[Cu(dmtacn)(ADBP^{ISQ})]^+$	+195		[167]
$[(6bpyNO)_2Ni]^{2+}$ (M = Ni, Cu)	+133 (Ni), +140 (Cu)		[104]	$[Co(Me_4cyclam)(phenSQ)]^+$	−13		[168]
$[(dmpoNO)_2Cu]^{2+}$	−82		[107]	$[Ni(tren)(ADBP^{ISQ})]^+$ (M = Ni, Fe)	+200 (Ni), nr[e] (Fe)		[169]
$[(dmmpoNO)_2Cu]^{2+}$	−78		[107]	$[Fe(^{F}PDA^{ISQ})(^{F}PDA^{PDI})]$	nr[h], −640[l]		[130]
$[(dmpoNO)_2Co]^{2+}$ [g]	+64		[109]	**Verdazyl and Thiazyl**			
Nitroxide (tetradentate)				(pyvd)M(hfac)$_2$ (M = Mn, Ni)	−23 (Mn), +120 (Ni)		[170]
$(NITbpy)Cu(ClO_4)_2$	−168		[100]	(imvd)M(hfac)$_2$ (M = Mn, Ni)	−31 (Mn), +97 (Ni)		[139]
$[(NITbpy)Ni(H_2O)_2]^{2+}$	+39.6 ($J_{Ni\text{-}rad}$)		[101]	(pyDTDA)Mn(hfac)$_2$ (M = Mn, Fe, Co, Ni, Cu)	nr[m] (Mn), −41.9 (Fe), nr[m] (Cu), +91.7 (Ni), +41.1 (Co)		[142–144]
$[(NITbpy)Ni(H_2O)(ClO_4)]^+$	+27.8 ($J_{Ni\text{-}rad}$)		[101]	$[(bipyvd)_2Mn]^{2+}$ (M = Mn, Ni, Cu)	−46.5 (Mn), +120 (Ni), −2.3 (Cu)		[147]
$[(NITbpy)Mn(H_2O)(ClO_4)]^+$	−65.3		[101]	$[(dpvd)_2Ni]^{2+}$	>+110	>+50	[148]
$[(NITbpy)Co(H_2O)(ClO_4)]^+$	+0.4 ($J_{Ni\text{-}rad}$)		[101]	$(cbvd)_2Ni(H_2O)_2$ (M = Ni, Co)	+188 (Ni), +68 (Co)	−42	[171]
Benzosemiquinonoid				**Carbene**			
$Fe(3,5\text{-}DBSQ)_3$	−190[h]		[116,118]	[Co(EBAMP)(NCO)$_2$(C1py)]	−35.6		[156]

[a] J values were estimated based on the general Hamiltonian $H = -2J_1S_MS_{L1} - 2J_2S_MS_{L2} - 2J_{L\text{-}L}S_{L1}S_{L2}$ and are shown in units of cm^{-1}.
[b] For (tempo)$_2$M(hfac)$_2$ (M = Ni, Co), the magnetic interaction was shown to be antiferromagnetic, but no values of J were reported.
[c] No Hamiltonian was reported.
[d] A chain model based on Bonner–Fisher theory was used due to the presence of intermolecular interactions.
[e] Diamagnetic at room temperature.
[f] Antiferromagnetic.
[g] Single-molecule magnet.
[h] $S = 1$ at room temperature.
[i] $S = 1/2$ at room temperature.
[j] This value was fixed to fit the susceptibility data.
[k] $S = 3/2$ at room temperature.
[l] Theoretical value obtained from DFT calculation.
[m] Magnetic behavior of isolated metal ion due to intermolecular ligand dimerization; nr = not reported.

with divalent metal salts in a 2:1 ratio to afford the compounds $[(dmpoNO)_2M^{II}]^{2+}$ (M = Co (**1**; Fig. 2), Fe, Cu) [107–109]. Among these complexes, the cobalt analog **1** is intriguing not only due to the observation of spin crossover but also to its single-molecule magnet behavior. Variable-temperature dc magnetic susceptibility data for **1** showed a gradual decrease in $\chi_M T$ from 400 K to 218 K, reflecting the presence of an incomplete spin crossover. Below 200 K, the magnetic behavior is governed by the interactions between spin centers, and a fit to the data provided the coupling constants $J_{Co\text{-}L} = +63.8$ and $J_{L\text{-}L} = +63.9\ cm^{-1}$, respectively, for the cobalt-radical and the intramolecular radical–radical interactions. Overall, this affords a ground state of $S = 3/2$. The observation of

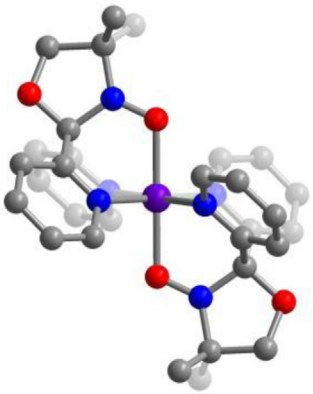

Fig. 2. Crystal structure of $(TBPNOpy)_4Co(NCS)_2$ (**1**), as observed at 123 K. Purple, blue, red, and gray spheres represent Co, N, O, and C atoms, respectively; H atoms are omitted and selected C and N atoms are faded for clarity.

a ferromagnetic Co-radical interaction presumably arises from the orthogonality of the Co^{II} $3d_{z^2}$ orbital and nitroxide π^* orbital, while the small overlap between two radical orbitals due to a lack of prominent spin polarization through the low spin Co^{II} center is responsible for the radical–radical ferromagnetic interactions. Ac magnetic susceptibility data reveal frequency-dependent peaks in external dc magnetic fields of 2000 and 5000 Oe, leading to spin relaxation barriers of U_{eff} = 7.4 and 5.3 cm^{-1}, respectively. Similarly, some mononuclear Co^{II} complexes with *N*-aryl-*N*-pyridylaminoxyl ligands of general formula L_4CoX_2 $(NOPy)_4CoX_2$ (X^- = NCS^- or NCO^-), where a pyridyl nitrogen atom instead of the nitronyl nitroxide unit is coordinated to the metal ion, have shown slow magnetic relaxation [110,111]. Finally, note that the strategy of combining transition metal ions and radicals has also led to systems with higher nuclearity and dimensionality greater than zero, resulting in high spin clusters [112], single-chain magnets [76], and compounds exhibiting long-range magnetic order [113]; however, these compounds are beyond the scope of this review.

2.2.2. Benzosemiquinonoid radical-containing complexes

Compared to nitronyl nitroxides, benzosemiquinonoid radicals contain much stronger oxygen donors, resulting in stronger magnetic exchange coupling with metal ions [114,115]. Additionally, the metal and benzosemiquinonoid radical orbitals are closer in energy, thus providing a more efficient exchange bias.

Homoleptic compounds of formula MSQ_3 (M = Cr^{III}, Fe^{III}; SQ^- = benzosemiquinone radical anion) exhibit strong intramolecular antiferromagnetic exchange interactions between the metal center and the radical ligands, resulting in spin ground states of *S* = 0 and *S* = 1 for Cr^{III} and Fe^{III}, respectively [51,116–119]. The strength of the exchange can be readily modulated by varying the substituents on the benzosemiquinone ligands. For instance, incorporation of aryl rings or electron-withdrawing groups such as chloride onto *o*-benzosemiquinone decreases the amount of electron density on the oxygen atoms, resulting in weaker magnetic coupling (Table 1). In contrast, the introduction of electron-donating substituents such as *t*-butyl groups provides stronger exchange, stabilizing the spin ground states of both Cr^{III} and Fe^{III} complexes well below their excited states even at 300 K. In addition, as expected, the orthogonality of the magnetic orbitals of the benzosemiquinone radical anions and the Ni^{II} or Cu^{II} ions in C_{2v} symmetry was shown to provide an efficient pathway for strong ferromagnetic coupling [120,121].

The more diffuse orbitals and lower electronegativity of the nitrogen donor atoms in *o*-iminobenzosemiquinone and *o*-diiminobenzosemiquinone radical ligands have been found to provide better orbital overlap within the metal–nitrogen bond, leading to an increase in the strength of the exchange coupling [122–131]. Moreover, functionalization at the nitrogen atoms allows control of the steric hindrance at the metal center and ultimately the electronic environment of the ligand. The presence of strong magnetic coupling between the metal centers and the *o*-diiminobenzosemiquinone ligands is reflected in all reported mononuclear compounds, which exhibit temperature-independent $\chi_M T$ values up to 300 K. Theoretical calculations performed on $Ni(^{tBu}PDA^{ISQ})_2$ (^{tBu}PDA = *N*,*N*-bis(3,5-di-*tert*-butylphenyl)-1,2-phenylenediamine) afforded an exceptionally large coupling constant of $J = -946\ cm^{-1}$ [129].

In addition to strong magnetic exchange, the aromatic π orbitals in benzosemiquinone radicals can facilitate electron delocalization between two ligands coupled through a central metal ion. For instance, DFT calculations of the coupling constant in $Fe(^{tBu}PDA^{ISQ})(^{tBu}PDA^{PDI})$ resulted in values near $J = -640\ cm^{-1}$, corresponding to an intermediate spin of *S* = 3/2 for the Fe^{III} center that is strongly antiferromagnetically coupled to the *S* = 1/2 radical ligand [130]. The ligand-to-ligand intervalence charge-transfer band located at 1190 nm suggests that the complex can be assigned to a fully delocalized class III mixed-valence system, as a result of electron delocalization between one benzosemiquinone radical and one closed-shell dianion ligand, similar to related compounds of Ni^{II}, Pd^{II}, and Pt^{II} [129,132]. The significant enhancement of coupling between ligands via electron delocalization was explained by efficient back-bonding interactions to the central metal center [133]. Here, the close proximity of energies between frontier orbitals for the metal centers and radical ligands not only leads to strong coupling, but can also induce electron transfer between the metal and the ligand in these complexes. This electron-transfer process is known as valence tautomerism, and is currently an active area of research in the field of molecular magnetism [52,134–138].

2.2.3. Verdazyl and thiazyl radical-containing complexes

Verdazyl radicals represent another class of free radicals that show remarkable air and moisture stability, even without the use of bulky substituents [10]. This stability, in conjunction with the ease through which they can be functionalized, make verdazyl ligands attractive alternatives to nitronyl nitroxides for the construction of molecular magnets.

Variable-temperature dc magnetic susceptibility measurements performed on $LM(hfac)_2$ (L = pyvd, imvd; M = Ni, Mn) complexes revealed that the metal–verdazyl radical coupling is antiferro- and ferromagnetic for the Mn^{II} and Ni^{II} congeners, respectively (Table 1) [139]. This difference in the type of magnetic interaction can be explained by orbital symmetry considerations. The unpaired electrons of the Ni^{II} center and the verdazyl radical reside in orbitals of σ and π symmetry, respectively, which are orthogonal to each other. By contrast, π overlap between the half-filled t_{2g} orbitals of Mn^{II} and the verdazyl SOMO induces antiferromagnetic coupling. Wave function calculations of the system confirmed the experimentally obtained values and suggested that the π^* donor character and a spin polarization effect on the verdazyl serves as the main contribution to the strong ferromagnetic exchange interaction in the Ni analog [140]. In addition, verdazyl radical-bridged dinuclear complexes $[(hfac)_2M(pmvd)M(hfac)_2]$ (M = Mn, Ni; pmvd = 1,5-dimethyl-3-(4,6-dimethylpyrimidin-2-yl)-6-oxoverdazyl radical) were found to have metal-radical coupling constants similar to those found in the mononuclear complexes [141].

The ligand 4-(2′-pyridyl)-1,2,3,5-dithiadiazolyl (pyDTDA) [142], is similar to the aforementioned verdazyl-derived ligands in terms of coordination environment and distribution of electron density on the ligand. Although the ligand composition within the molecule is identical in complexes of the type $(pyDTDA)M(hfac)_2$ (M = Mn^{II}, Fe^{II}, Co^{II}, Ni^{II}, Cu^{II}) [142–144], subtle differences in coordination

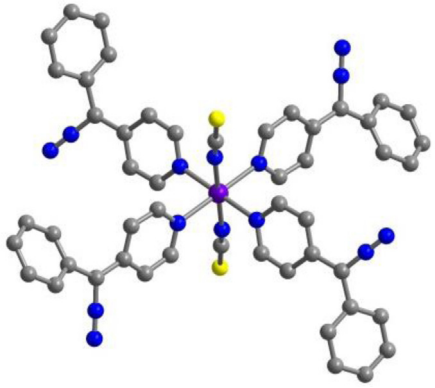

Fig. 3. Structure of $(D1py)_4Co(SCN)_2$ (**2**), with purple, blue, yellow and gray spheres representing Co, N, S, and C atoms, respectively; H atoms are omitted for clarity.

geometries around each metal ion resulted in significantly different crystal packing. Variable-temperature dc susceptibility data revealed an antiferromagnetic metal-radical interaction for the Fe^{II} species and ferromagnetic interactions for the Co^{II} and Ni^{II} complexes (Table 1). In addition, the $\chi_M T$ observed for the Mn^{II} and Cu^{II} analogs were temperature-independent above 50 K with values of 4.2 and 0.42 cm^3·K/mol, indicative of ligand dimerization and thus magnetic behavior associated with an isolated metal ion. Nevertheless, solution measurements of the magnetic moment indicated the presence of antiferromagnetic and ferromagnetic coupling between the metal center and the radical ligand in the Mn^{II} and Cu^{II} analogs, respectively. A similar trend for metal-radical coupling in dinuclear complexes was also observed with 2,2′-bipyrimidine-substituted thiazyl and selenazyl bridging ligands [145].

Strong antiferromagnetic and ferromagnetic interactions were found in the homoleptic complexes $[(bipyvd)_2M]^{2+}$ (M = Mn, Ni, Cu) and $[(dpvd)_2Ni]^{2+}$, similar to those arising within $LM(hfac)_2$ complexes [146–148]. While the intramolecular radical–radical coupling in $[(bipyvd)_2Mn]^{2+}$ was estimated as $|J| \leq 5\ cm^{-1}$, the corresponding value for $[(dpvd)_2Ni]^{2+}$ was found to be $J \geq +50\ cm^{-1}$. This observed strong ferromagnetic coupling between verdazyl radicals is in contrast to that observed in $[(bipyvd)_2M]^{2+}$, suggesting that the verdazyl-verdazyl exchange interaction is highly dependent on the relative orientation of the two verdazyl groups within the inner coordination sphere.

Although verdazyl radicals generally provide weaker exchange compared to benzosemiquinonoid radicals (Table 1), their implementation as building units within larger molecules is nonetheless advantageous due to their chemical stability and synthetic versatility. Notably, dynamic magnetic measurements have not yet been reported for verdazyl and thiazyl radical-containing transition metal complexes.

2.2.4. Carbene radical containing complexes

A recently discovered strategy for the generation of organic molecules and metal complexes with high spin multiplicities involves the photolysis of diazo compounds to yield triplet carbenes [149–154]. Indeed, reaction of D*n*py with $Co(SCN)_2$ afforded crystalline complexes of general formula $(Dnpy)_4Co(X)_2$ (X = SCN^- (**2**), Cl^-, NCO^-; Fig. 1) [77,79,155]. Here, the Co^{II} center resides in a distorted octahedral coordination environment with four pyridyl nitrogen atoms in an equatorial plane and two *trans*-disposed SCN^- ligands (Fig. 3). Variable-temperature ac susceptibility measurements carried out on a frozen solution of $(D1py)_4Co(SCN)_2$ below 10 K showed a value $\chi_M'T \approx 2\ cm^3$ K/mol prior to irradiation, in agreement with an isolated $S = 3/2$ Co^{II} ion. Upon irradiation to form $(C1py)_4Co(SCN)_2$, the magnetic moment was found to increase significantly to a value of $\chi_M'T = 11\ cm^3$ K/mol. This value is higher than the expected value for four non-interacting triplet carbenes and a Co^{II} center, suggesting the presence of ferromagnetic coupling between the Co^{II} center and the triplet C1py carbene diradical ligands [77]. Most importantly, ac susceptibility measurements of $(C1py)_4Co(SCN)_2$ performed at various frequencies revealed a set of peaks in the plot of χ_M'' vs T, with fits to the corresponding Arrhenius plot affording a relaxation barrier of $U_{eff} = 62\ cm^{-1}$. Below 2.5 K, the relaxation time was temperature-independent, indicative of quantum tunneling of the magnetization with the characteristic time estimated as $\tau_Q = 6 \times 10^2$ s. By replacing SCN^- ligands with Cl^- and NCO^-, the relaxation barrier was increased to $U_{eff} = 63$ and 90 cm^{-1}, respectively, with lengthened tunneling times of $\tau_Q = 4 \times 10^3$ and 2×10^5 s [155]. The elongation of τ_Q probably hampered the onset of quantum tunneling and consequently increased the relaxation barrier. This effect might be due to the modification of the magnetic anisotropy through changing the strength of the axial ligand field.

A 1:2 mixture of Co(*p*-tolsal)$_2$ and D*n*py yielded compounds of form $(Dnpy)_2Co(p\text{-tolsal})_2$ in solution [82]. Here, the number of carbenes in each peripheral ligand was increased by connecting diazo moieties with *m*-phenylene linkers, leading to D2py, D3py, and D4py ligands (Fig. 1). The value of $\chi_M T = 1.6\ cm^3$ K/mol observed for $(Dnpy)_2Co(p\text{-tolsal})_2$ at 10 K was increased to 6.2, 12.8, 23.8, and 32.1 cm^3 K/mol for the irradiated compounds $(Cnpy)_2Co(p\text{-tolsal})_2$ (n = 1, 2, 3, and 4, respectively), indicative of two carbenes with spin multiplicities of S = 1, 2, 3, and 4, in each case ferromagnetically coupled to a Co^{II} center. Sets of frequency-dependent peaks were observed in the χ_M'' vs T plots for these compounds, indicating the presence of slow magnetic relaxation. Interestingly, the relaxation barrier was found to gradually increase with spin ground state, affording barriers of U_{eff} = 28, 45, 51, and 51 cm^{-1}, respectively, accompanied by substantial increases in the characteristic time for quantum tunneling. Since the radical-free model complex $(py)_2Co(p\text{-tolsal})_2$, exhibits slow magnetic relaxation only under an applied dc field, these results suggest that the magnetic coupling between the carbenes and the Co^{II} center suppresses the tunneling pathway, leading to the single-molecule magnet behavior observed at zero dc field [79].

The strength of magnetic exchange between the Co^{II} center and the carbene ligands was estimated to be $J = -35.6\ cm^{-1}$ in the complex Co(EBAMP)$(NCO)_2$(C1py) [156]. This value is similar to those of $J = +33.4\ cm^{-1}$ and $-17.4\ cm^{-1}$ reported for carbene-bridged chain compounds of Cu^{II} and Mn^{II}, respectively [81,157].

2.3. Radical-bridged transition metal single-molecule magnets

2.3.1. Carbene-bridged single-molecule magnets

As discussed above, triplet carbenes are attractive targets owing to the ability to introduce multiple carbene units to increase the spin multiplicity of the ligand, thereby resulting in complexes with high spin ground states [82]. However, gains in S are offset by an overall lengthening of the ligand, which consequently increases the metal-radical distance. Indeed, the relaxation barrier was enhanced with increasing number of carbene units attached to a metal center up to certain number, after which a plateau is reached at a fixed value of U_{eff} [82]. An alternative strategy to increase the spin ground state of a carbene-based metal complex, while maintaining strong metal-carbene exchange, is to connect multiple metal centers through a carbene-based bridging ligand.

Toward this end, the didiazo-dipyridine ligand $D2py_2$ has been employed as a precursor for the corresponding carbene derivative, in which two pyridyl nitrogen atoms on each terminus of the ligand serve to link metal ions (Fig. 1). For instance, this ligand gives rise to the dinuclear complexes $(Co(X\text{-}hfpip)_2)_2(D2py_2)_2$ (X = I (**3**), H (**4**), *t*Bu (**5**)) [84,85], which exhibit a common structure consisting of a cyclic dimer comprised of two $Co(X\text{-}hfpip)_2$ units alternating

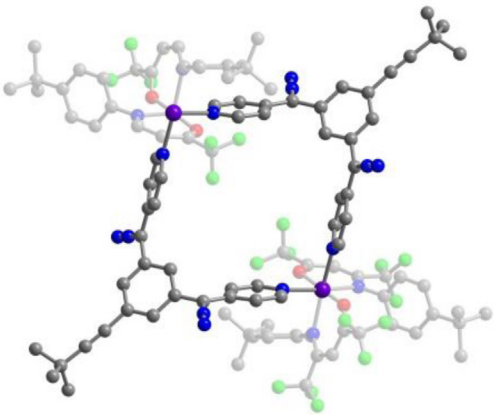

Fig. 4. Structure of $(Co(t\text{Bu-hfpip})_2)_2(D_2py_2)_2$ (**5**). Purple, blue, red, green, and gray spheres represent Co, N, O, F, and C atoms, respectively; H atoms are omitted for clarity.

with two $D2py_2$ ligands (Fig. 4). In each structure, the Co^{II} center resides in a compressed octahedral coordination environment in which two pyridine nitrogen atoms of different $D2py_2$ ligands are bound in a *cis* configuration. Notably, the structures exhibit shortest intermolecular Co···Co contacts of longer than 11 Å, suggesting the absence of significant intermolecular magnetic interactions.

Unlike the above mononuclear complexes that possess intermolecular contacts, limiting their magnetic measurements to frozen solution, the magnetically isolated dimer structure enabled irradiation and magnetic measurements of a solid-state crystalline sample. The $\chi_M T$ product of all analogs before irradiation was found to be near 4 cm^3 K/mol, and this value increased significantly upon irradiation to $\chi_M T$ = 29, 24, and 26 cm^3 K/mol for **3**, **4**, and **5**, respectively. These values are much higher than the calculated spin-only values, indicating the presence of intramolecular ferromagnetic coupling between the Co^{II} center and the carbene radicals. Indeed, variable-field dc magnetization data collected on three irradiated compounds revealed the presence of magnetic hysteresis at a field-sweep rate of 0.35 kOe/s, with the coercive fields at 1.9 K of 26, 15, and 10 kOe for **3**, **4**, and **5**, respectively (Fig. 5), demonstrating that all complexes exhibit single-molecule magnet behavior. Furthermore, relaxation barriers were determined from ac susceptibility measurements, giving U_{eff} = 97, 94, and 67 cm^{-1} for **3**, **4**, and **5**, respectively.

2.3.2. Benzosemiquinonoid radical-bridged single-molecule magnets

Efforts to generate benzosemiquinonoid-containing transition metal complexes with a nuclearity of greater than one have resulted in numerous dinuclear compounds, including those containing metal centers bridged by derivatives of 2,5-dihydroxy-1,4-benzoquinonoids [172–189], bis(pyrazolyl)benzoquinonoids [190–193], bis(phosphine)benzoquinonoids [194,195], bis(amino) benzoquinonoids [196–202], and bis(amino)diiminobenzoquinonoids [86,203–206]. Indeed, the radical form of these ligands has shown enhanced magnetic coupling compared to their non-radical redox isomers [174,180,182]. In fact, magnetic exchange coupling in benzosemiquinone radical-bridged dinuclear complexes is so strong in some cases that the spin ground state remains well-isolated from excited spin states even at 300 K [86,183].

To date, the only known example of benzosemiquinonoid radical-bridged transition metal single-molecule magnet has been generated from the radical form of azophenine ($H_2{}^{N,N}AZP^{IBQ}$; Fig. 1) [86]. The reaction of azophenine with in situ-generated $[(TPyA)Fe(MeCN)_2]^{2+}$ (TPyA = tris(2-pyridylmethyl)amine) in the

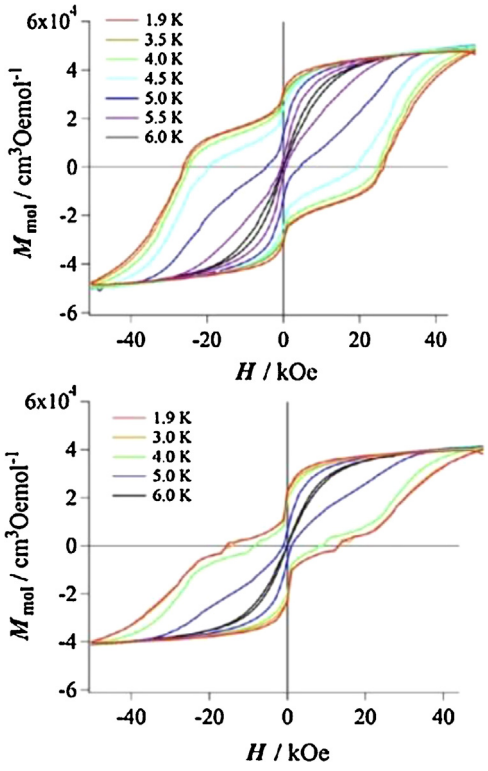

Fig. 5. Variable-field magnetization data collected for $(Co(X\text{-hfpip})_2)_2(C_2py_2)_2$ (X = I (top), H (bottom)) at a field-sweep rate of 0.35 kOe/s.

Source: Figure was reproduced from Ref. [85], with permission of the copyright holders.

presence of $Li[N(SiMe_3)_2]$ afforded the complex $[(TPyA)_2Fe^{II}{}_2(^{N,N}AZP^{IBQ})]^{2+}$. Subsequent treatment of this complex with a strong reductant resulted in the one-electron reduced radical-bridged complex $[(TPyA)_2Fe^{II}{}_2(^{N,N}AZP^{ISQ})]^{+}$ (**6**; Fig. 6). The structures of both unreduced and reduced complexes reveal two $[(TPyA)Fe]^{2+}$ units connected by a deprotonated azophenine bridging ligand, with azophenine nitrogen atoms occupying *cis*-disposed sites of each Fe^{II} center and four TPyA nitrogen atoms completing the coordination spheres. While the structures of both cationic complexes are similar, bond lengths in the bridging ligand backbone reveal several key differences. In particular, moving from the unreduced to the reduced complex, the decrease in mean benzoquinone C—C distance and in mean Fe-N_{AZP} distance, along with the increase in mean benzoquinone C—N distance, suggest the presence of a trianionic bridging ligand bearing an unpaired electron. This assignment is further supported by Mössbauer spectra of the two complexes, which reveal identical isomer shifts.

Variable-temperature dc magnetic susceptibility data collected for the $[Fe_2]^{2+}$ complex revealed the presence of weak antiferromagnetic superexchange coupling with $J = -2.90(2)$ cm^{-1}. In contrast, the plot of $\chi_M T$ vs T for the reduced complex displays a temperature-independent profile, with $\chi_M T$ = 8.84 cm^3 K/mol in the temperature range 130–300 K (Fig. 6). This value is in agreement with an $S = 7/2$ ground state, resulting from strong antiferromagnetic exchange between the radical bridging ligand and two Fe^{II} centers. While the temperature independence of $\chi_M T$ precludes an exact determination of J, simulations of the data enabled a lower-bound estimate of $J \leq -900$ cm^{-1}, the largest value yet reported for a single-molecule magnet. Finally, single-molecule magnet behavior was confirmed through variable-frequency ac susceptibility experiments, which revealed a spin relaxation barrier of U_{eff} = 50 cm^{-1} (Fig. 6).

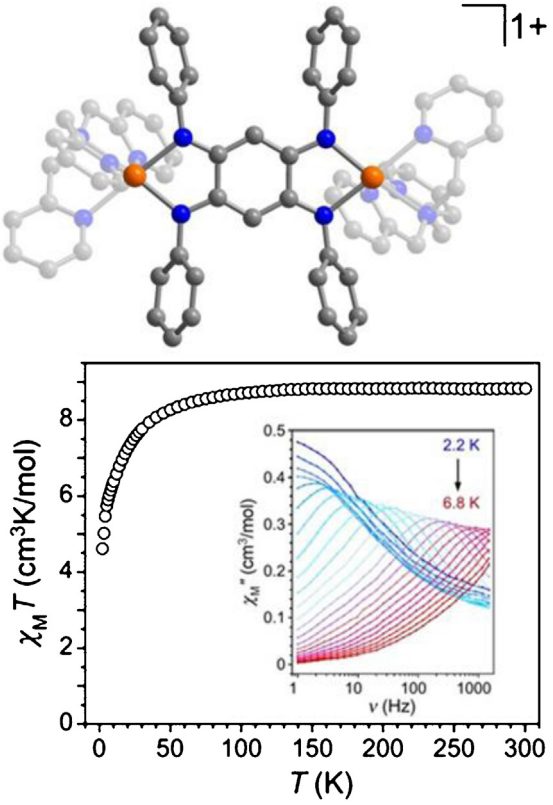

Fig. 6. Top: structure of $[(TPyA)_2Fe^{II}{}_2(^{N,N}AZP^{ISQ})]^+$ (**6**), with orange, blue, and gray spheres representing Fe, N, and C atoms, respectively; H atoms are omitted and selected N and C atoms faded for clarity. Bottom: variable-temperature dc susceptibility data for **6**, collected under an applied field of 1000 Oe. Inset: variable-frequency ac susceptibility data for **6** collected under zero applied dc field.

Source: Figure was reproduced from Ref. [86], with permission of the copyright holders.

2.3.3. Nindigo radical-bridged single-molecule magnets

A wide range of indigo *N,N′*-diarylimine (Nindigo) ligand derivatives can be synthesized by treating indigo with an excess of aniline-derivatives containing electron-rich, electron-poor, and bulky substituents in the presence of $TiCl_4$ and 1,4-diazabicyclo[2.2.2]octane. Initial investigations of their coordination chemistry with $Pd(hfac)_2$ demonstrated rich redox activity and a near-IR absorption band centered at the ligand, suggesting a promising, tunable bridging ligand [207,208].

The dinuclear Co^{II} complex $(dmp_2Nin)Co_2(N(SiMe_3)_2)_2$ (**7**) represents the only known paramagnetic metal complex of Nindigo [87]. The cyclic voltammogram of this species features four accessible oxidation states, with redox processes centered at −0.12 V, −1.45, and −2.00 V vs $[Cp_2Fe]^{0/+}$. Accordingly, chemical reduction using 1 or 2 eq. of KC_8 afforded the one- and two-electron reduced complexes, $[(dmp_2Nin)Co_2(N(SiMe_3)_2)_2]^-$ (**8**) and $[(dmp_2Nin)Co_2(N(SiMe_3)_2)_2]^{2-}$ (**9**), respectively (Fig. 7) [87]. Additionally, the one-electron oxidized complex $[(dmp_2Nin)Co_2(N(SiMe_3)_2)_2(Et_2O)_2]^+$ (**10**) was obtained upon treatment with $[Cp_2Fe]^+$ [209].

Variable-temperature dc magnetic susceptibility data collected for **7** and **9** reveal similar temperature dependence, featuring a gradual decrease in $\chi_M T$ from 5.5 cm^3 K/mol at 300 K to 0 cm^3 K/mol at 1.8 K. This temperature dependence is indicative of intramolecular antiferromagnetic interactions between high spin Co^{II} centers through the diamagnetic bridging ligand, with coupling constants of $J = -11.7$ and -14.7 cm^{-1} for **7** and **9**, respectively. Upon one-electron reduction and oxidation of **7** to **8** and **10**, respectively, the occurrence of strong magnetic coupling between ligand radical and

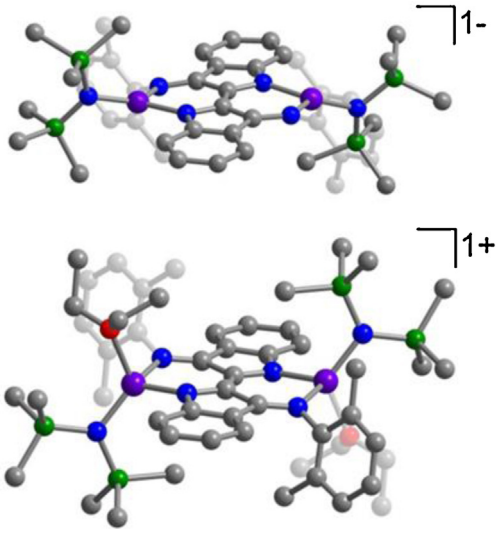

Fig. 7. Structures of $[(dmp_2Nin)Co_2(N(SiMe_3)_2)_2]^-$ (**8**) (top) and $[(dmp_2Nin)Co_2(N(SiMe_3)_2)_2(Et_2O)_2]^+$ (10) (bottom) with purple, blue, red, green, and gray spheres representing Fe, N, O, Si, and C atoms, respectively; H atoms are omitted and selected C and O atoms are faded for clarity.

Co^{II} centers significantly changed the profile of the $\chi_M T$ vs T curves. Electronic structure calculations and fits to variable-field magnetization data provided estimates of magnetic exchange constants for the complexes of $J = -133$ and -138 cm^{-1} for **8** and **10**, respectively. The values obtained indicate the presence of antiferromagnetic metal-radical interactions, leading to a spin ground state of $S = 5/2$. The stabilization of the spin ground state through strong magnetic exchange interactions between high-spin Co^{II} centers and the radical bridging ligand indeed promote slow magnetic relaxation in both **8** and **10**. Here, the relaxation dynamics of both complexes are too fast over the frequency range of 0.1–1500 Hz in the absence of an external dc field down to 1.8 K to observe in the variable-frequency plots of χ_M''. Nevertheless, the frequency dependence of χ_M'' was found to be strongly influenced upon applying an external dc field, resulting in an optimum field of 1200 Oe to provide the slowest dynamics (Fig. 8). Arrhenius fits to the relaxation times extracted from ac measurements at 1200 Oe afforded relaxation barriers of $U_{eff} = 23$ and 26 cm^{-1} for **8** and **10**, respectively. Notably, this series of redox isomers provides the unique ability to "switch" the single-molecule magnet behavior on and off over four different oxidation states.

3. Lanthanide-radical single-molecule magnets

3.1. Introduction

An alternative path to generating single-molecule magnets is to focus on molecules that comprise only one highly anisotropic metal center instead of maximizing the ground state. This strategy has yielded a number of remarkable breakthroughs in the field [210–218]. In particular, the combination of metal centers possessing large spin-orbit coupling along with appropriate coordination environments can give rise to greater relaxation barriers than those observed for exchange-coupled clusters. The discovery of slow magnetic relaxation in the series of mononuclear lanthanide complexes $[LnPc_2]^{n+}$ (Ln^{III} = Tb, Dy, Ho; H_2Pc = phthalocyanine; $n = -1$, 0, 1) was a pioneering result and milestone in the field of molecular magnetism [210–212]. The qualitative method of matching ligand field symmetry with the electron distribution of the maximal M_J state presented in this work can be used to elucidate the origin of slow magnetic relaxation in other mononuclear complexes, such

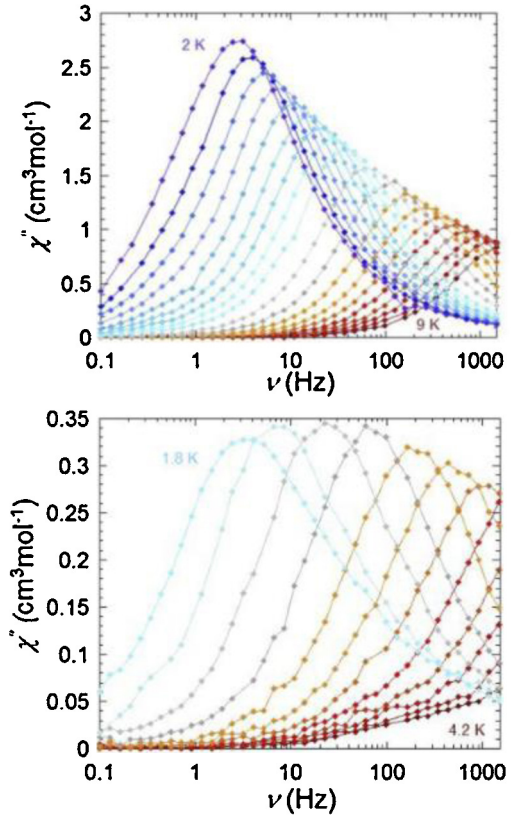

Fig. 8. Variable-frequency ac susceptibility data for $[(dmp_2Nin)Co_2(N(SiMe_3)_2)_2]^-$ (**8**) (top) and $[(dmp_2Nin)Co_2(N(SiMe_3)_2)_2(Et_2O)_2]^+$ (**10**) (bottom) collected under a 1200 Oe dc field.

Source: Figure was reproduced from Ref. [209], with permission of the copyright holders.

as $[Ln(W_5O_{18})_2]^{9-}$, $[Ln(\beta_2\text{-}SiW_{11}O_{39})_2]^{13-}$ (Ln^{III} = Dy, Ho, Er, Yb), Cp*Er(COT), $[Er(COT'')_2]^-$ and $[Er(COT)_2]^-$ [213–218]. In particular, the latter two molecules exhibit the highest blocking temperatures yet observed for mononuclear single-molecule magnets. Here, the blocking temperature is defined as the temperature at which the relaxation time (τ) is 100 s [219]. Notably, expansion to the triple-decker analogs $Er_2(COT'')_3$ and $K_2(THF)_4[Er_2(COT)_4]$ yielded enhanced magnetic properties, with both exhibiting magnetic hysteresis at up to 12 K in the solid state [220]. Despite the strikingly large relaxation barriers and blocking temperatures observed in these complexes, the corresponding hysteresis loops feature prominent steps around zero field due to facile quantum tunneling of the magnetization. Here, the tunneling is often so strong that the hysteresis loops are closed or almost closed at zero fields, as evidenced by small coercive fields H_c. The coercive field is defined as the strength of the magnetic field required to drive the magnetization of a compound back to zero following magnetization.

In the following sections, mono- and dinuclear lanthanide-radical complexes are surveyed, with emphasis on the estimated strengths of magnetic exchange and the observation of slow magnetic relaxation. An enumeration of relevant spin relaxation barriers for known radical-containing lanthanide single-molecule magnets is provided in Table 3.

3.2. Mononuclear lanthanide radical complexes

3.2.1. Mononuclear lanthanide phthalocyanine radical complexes

Consistent with the scope of this review, we will focus on the neutral phthalocyanine complexes $LnPc_2$ (Fig. 10) that are obtained

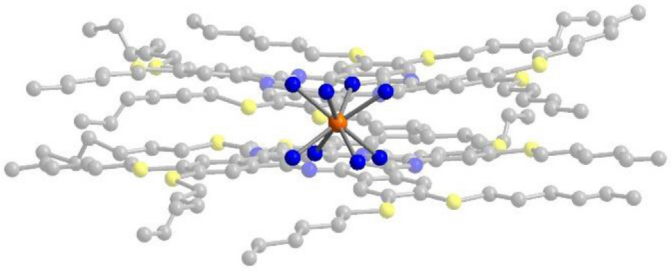

Fig. 9. Structure of $Gd[Pc(C_6S_8)]_2$ (**11**) with orange, blue, yellow and gray spheres representing Gd, N, S and C atoms, respectively; H are omitted and selected C and S atoms are faded for clarity.

through a one-electron oxidation of $[LnPc_2]^-$, where oxidation of one of the ligands occurs to give an open π electron shell. Indeed, strong exchange coupling between a lanthanide ion and the delocalized electron on the coordinated ligand was suggested long before the first lanthanide-based single-molecule magnet was discovered [221]. In particular, the variable-temperature dc susceptibility data for the Gd^{III} congener could not be fit to the Curie–Weiss law considering a $S = 7/2$ ground state. Instead, the data were best modeled using $S = 3$ to give a Weiss constant $\theta = -0.41$ K. As such, the data were interpreted as corresponding to a ground state of $^7S_3$, stemming from strong antiferromagnetic coupling between the Gd^{III} center and the phthalocyanine radical electron. In contrast, the Gd^{III}-radical coupling has been found to be ferromagnetic in the eight-fold hexylthio-substituted gadolinium phthalocyanine complex $Gd[Pc(C_6S_8)]_2$ (**11**; Fig. 9), with a coupling constant of $J = +0.2\ cm^{-1}$ [222]. This magnitude of coupling is considerably weaker than found in other radical-containing gadolinium complexes, as tabulated in Table 2.

Similarly, the complex $TbPc_2$ (**12**) is regarded as a two-spin system with an unpaired electron delocalized over both ligands ($S = 1/2$) and an $4f^8$ Tb center ($J = 6$) [223]. Ac susceptibility data collected for this molecule revealed out-of-phase (χ_M'') peaks at 50, 43 and 36 K at frequencies of 10^3, 10^2, and 10 Hz, respectively, corresponding to a relaxation barrier of $U_{eff} = 410\ cm^{-1}$ [223]. This distinctive magnetization lag to the oscillating field occurs at temperatures more than 10 K higher than in the non-radical anionic analog $[TbPc_2]^-$ (**13**), which exhibits an effective barrier of just $230\ cm^{-1}$ (Fig. 11).

However, solution ^1H NMR studies of the electronic spin dynamics of $[TbPc_2]^-$ revealed a much larger barrier of $U_{eff} = 584\ cm^{-1}$, and solid samples diluted with the diamagnetic salt $(Bu_4N)Br$, namely $(Bu_4N)[TbPc_2]\cdot 143(Bu_4N)Br$ and $(Bu_4N)[TbPc_2]\cdot 9(Bu_4N)Br$ also displayed considerably higher barriers of $641\ cm^{-1}$. In theory, the HOMOs of the anionic species $[LnPc_2]^-$ residing on the $[Pc]^{2-}$ ligands are of a π-type antibonding nature that can undergo one- or two- electron oxidations to afford $LnPc_2$ and $[LnPc_2]^+$, respectively [224]. However, the magnetic properties of charged phthalocyanine-based lanthanide compounds are better

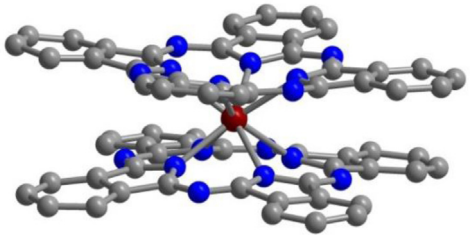

Fig. 10. General structure of a double-decker $[LnPc_2]^{n-}$ complex. Red, blue and gray spheres represent Ln, N, and C atoms; H are omitted and selected C atoms are faded for clarity.

Table 2
Summary of magnetic exchange coupling constants (cm^{-1}) for radical-containing gadolinium complexes.[a]

Complexes	Structure	J_{Gd-L1}	J_{Gd-L2}	J_{L-L}	J_{Gd-Gd}	Reference
$Gd(hfac)_3(NITH)_2$	Mononuclear	+1.81				[249]
$Gd(hfac)_3(NITH)_3$	Mononuclear	+2.68				[250]
$Gd(hfac)_3(NITPh)_2$	Mononuclear	+0.62		−2.55		[251]
$Gd(hfac)_3(NITEt)_2$	Mononuclear	+0.25		−2.15		[251]
$[Gd(hfac)_3(NITEt)]_n$	Chain	+0.21		−2.54	−0.49	[252]
$[Gd(hfac)_3(NIT^iPr)]_n$	Chain	+0.21		−2.66	−0.19	[252]
$Gd(hfac)_3(NIT^iPr)(H_2O)$	Mononuclear	+0.33/0.42[b]				[253]
$Gd(hfac)_3(NIT2Py)\cdot 0.5C_7H_{16}$	Mononuclear	+1.52				[254]
$[Gd(hfac)_3(NIT4Py)]_2$	Dinuclear	+0.89	0.09			[254]
$Gd(hfac)_3NITBzImH$	Mononuclear	+1.7				[255]
$[Gd(hfac)_3(NIT\text{-}5\text{-}Py3Br)]_2$	Dinuclear	+2.6	−0.24			[256]
$Gd(hfac)_3(NITPhOMe)_2$	Mononuclear	+1.48		−1.82		[257]
$Gd(hfac)_3(NITPhSCH_3)_2$	Mononuclear	+0.55		−0.93		[258]
$Gd(hfac)_3(NITPhOEt)_2$	Mononuclear	+0.27		−2.97		[259]
$Gd(hfac)_3(NITPhOBu)_2$	Mononuclear	+0.1		−0.96		[260]
$Gd(hfac)_3(NITPhOCH_2Ph)_2$	Mononuclear	+0.62		−7.01		[259]
$Gd(hfac)_3(NITPhPh)_2$	Mononuclear	+0.05		−0.15		[261]
$Gd(hfac)_3(NITNapOMe)_2$	Mononuclear	+3.59		−11.89		[262]
$Gd(hfac)_3(NITPh(OMe)_3)_2$	Mononuclear	+1.46		−1.89		[263]
$Gd(hfac)_3(NITPh4OCH_2CHCH_2)_2$	Mononuclear	+1.40/2.08[e]		−4.89/7.21		[264]/[265][e]
$Gd(hfac)_3(NITPh3Br4OMe)_2$	Mononuclear	+5.69		−17.1		[266]
$Gd(hfac)_3(NITPh^iPr)_2$	Mononuclear	+2.42		−8.42		[267]
$Gd(hfac)_3(NITPh4Cl)_2$	Mononuclear	+0.38		−3.00		[268]
$Gd(hfac)_3(NITPh3OMe4OEt)_2$	Mononuclear	+2.33		−5.66		[269]
$[Gd(hfac)_3(NITPhPO(OEt)_2)]_2$	Dinuclear	+1.73	Not fitted			[270]
$[Gd(Phtfac)_3(NIT4Py)]_2$	Dinuclear	+1.84	+0.12			[271]
$Gd(tfa)_3(NITBzImH)$	Mononuclear	+0.99				[272]
$Gd(NITtrz)_2(NO_3)_3$	Mononuclear	+3.05		−3.5		[273]
$[Gd(acac)_2(NITPhO)]_2$	Dinuclear	+2.75			−0.076[c]	[274]
$Gd(acac)_3(NIT2Py)\cdot 0.5NIT2Py$	Mononuclear	+2.23				[275]
$[Gd(pfpr)_3]_2(NITPhOMe)\cdot H_2O$	Mononuclear	+2.14				[276]
$Gd(hfac)_3IM2Py$	Mononuclear	−1.9/−3.00[e]				[255]/[277][e]
$Gd(TCNE)_3$	3D network	+0.05				[278]
$[Gd(hfac)_3imvd]_n$	Chain	−1.58		−0.42		[279]
$Gd[Pc(C_6S_8)]_2$	Mononuclear	+0.2[d]				[222]
$Gd(Cp^*)(IPy)_2$	Mononuclear	−1.59		−0.97		[280]
$[Gd(NITBzImH)_4]\cdot(ClO_4)_3$	Mononuclear	−1.8		−7.2		[281]
$Gd(hfac)_3(IM2ImH)$	Mononuclear	−2.59				[282]
$Gd(hfac)_3IMBzImH$	Mononuclear	−2.6				[255]
$[Gd(NITBzMeImH)_4]\cdot(ClO_4)_3$	Mononuclear	−3.8		−5.6		[281]
$Gd(hfac)_3(IM5Me2Py)$	Mononuclear	−3.8				[283]
$Gd(hfac)_3(IM4Me2Py)$	Mononuclear	−3.8				[283]
$Gd(hfac)_3(IM6Me2Py)$	Mononuclear	−4.0				[283]
$Gd(hfac)_3(DTBNO)(H_2O)$	Mononuclear	−4.03			+0.042	[284]
$Gd(NITBzImH)_2(NO_3)_3$	Mononuclear	−4.05	−0.80	−1.1		[285]
$Gd(hfac)_3(2PyNO)(H_2O)$	Mononuclear	−4.80				[249]
$Gd(hfac)_3(6bpyNO)$	Mononuclear	−5.53				[286]
$[Gd(Hbpz_3)_2(dtbsq)]\cdot 2CHCl_3$	Mononuclear	−5.7				[287]
$[(Cp^*_2Gd)_2(\mu\text{-}tppz^{\bullet})]^-$	Dinuclear	−6.29				[288]
$[(Cp^*_2Gd)_2(\mu\text{-}tppz^{\bullet})]^+$	Dinuclear	−6.91				[288]
$[(Cp^*_2Gd)_2(\mu\text{-}bpym)][BPh_4]$	Dinuclear	−10				[289]
[K(18-C-6)]{[((Me3Si)2N)2(THF)Gd]2(μ-N2)}	Dinuclear	−27			+0.07	[290]
$K\{[((Me_3Si)_2N)_2(THF)Gd]_2(\mu\text{-}N_2)\}$	Dinuclear	−27.1			−2.28[c]	[291]

[a] J values were estimated based on Hamiltonian of $H = -2J_{Gd-L1}S_{Gd}S_{L1} - 2J_{Gd-L2}S_{Gd}S_{L2} - 2J_{L-L}S_{L1}S_{L2} - 2J_{Gd-GD}S_{Gd1}S_{Gd2}$ and are presented in units of cm^{-1}.
[b] High-temperature fit (4.2–300 K)/low-temperature fit (1.2–4.2 K).
[c] Intramolecular Gd–Gd interactions.
[d] Type of Hamiltonian is not reported.
[e] Multiple values have been reported.

understood compared to their neutral counterparts of the type $LnPc_2$. In fact, relatively few reports of $LnPc_2$ have been published, possibly due to the challenging isolation of these radical-bearing congeners, which in some cases display solvent-sensitivity such as oxidation in THF [225].

Ac susceptibility measurements for the neutral complex $Tb(Pc(OEt)_8)_2$ featuring phthalocyanine ligands functionalized by octaethoxyl groups, has not been reported. However, oxidation or reduction of $Tb(Pc(OEt)_8)_2$ affords $[Tb(Pc(OEt)_8)_2]^+$ and $[Tb(Pc(OEt)_8)_2]^-$, which exhibit spin relaxation barriers of U_{eff} = 550 and 510 cm^{-1}, respectively [226]. This difference in barrier height was attributed to a contracted TbN_8 coordination sphere that is accompanied by a two-electron oxidation from $[Tb(Pc(OEt)_8)_2]^-$ to $[Tb(Pc(OEt)_8)_2]^+$. Albeit to a smaller extent, the similar temperature shift in the ac susceptibility data observed in moving from $[TbPc_2]^-$ to $TbPc_2$ likely arises from a stronger ligand field induced by removing one electron from the antibonding HOMO of $[TbPc_2]^-$. While the dynamic magnetic behavior has not been

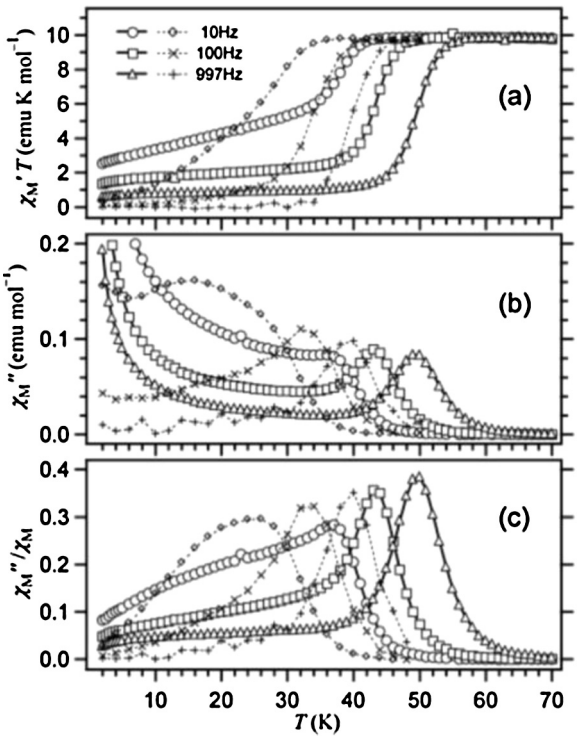

Fig. 11. Plots of (a) $\chi_M'T$, (b) χ_M'', and (c) χ_M''/χ_M vs T for solid samples of $TbPc_2$ (**12**) (solid lines) and $[TbPc_2]^-$ (**13**) (dashed lines).

Source: Figure was reproduced from Ref. [223], with permission of the copyright holders.

described for the analogous radical-containing dysprosium analog $DyPc_2$, the anionic complex $[DyPc_2]^-$ showed relatively fast relaxation, corresponding to a barrier of $U_{eff} = 28\,cm^{-1}$, owing to the small energy gap between the ground state and the first excited state [210]. While its magnetic behavior remains unclear, the complex $Dy(Pc(OEt)_8)_2$ has been used to prepare the oxidized and reduced species $[Dy(Pc(OEt)_8)_2]^+$ (**14**) and $[Dy(Pc(OEt)_8)_2]^-$ (**15**) [212]. The latter complex shows an enhancement of the barrier from $U_{eff} = 27$ to $55\,cm^{-1}$ upon two-electron oxidation, which is accompanied by a contraction of the Dy^{III} coordination environment. The magnitude of this increase stands out when compared to the Tb^{III} analogs, for which the increase is only 8%. Furthermore, $[Dy(Pc(OEt)_8)_2]^+$ displays a large nonzero remanent magnetization up to 4 K when compared to the anionic $[Dy(Pc(OEt)_8)_2]^-$ complex, in contrast to the results observed for the Tb^{III} analogs (Fig. 12). This large remanent magnetization arises from a Dy^{III} Kramers ion, which is corroborated by the lack of a remanent magnetization in the hysteresis loops for the corresponding non-Kramers Tb^{III} complex.

An intriguing investigation of the hysteretic behavior of the reduced, neutral, and oxidized species $[TbPc'_2]^{n+}$ ($n = -1$, 0, 1; Pc′ = octa(isopropylidenedioxy)phthalocyaninate) [227] was carried out by magnetic circular dichroism (MCD) spectroscopy [228]. The MCD spectra were acquired as frozen solutions in CH_2Cl_2 with 0.8 M $(Bu_4N)(BF_4)$. The intensity of the MCD bands was studied at 705, 664, and 631 nm for the complexes over a magnetic field range of $H = \pm 2$ T with a sweep rate of $1\,T\,min^{-1}$. Both the cationic and anionic species displayed waist-constricted hysteresis loops, approaching saturation at $H = \pm 2$ T with a sudden drop at $H \sim 0$ T, albeit not fully closing (Fig. 13). In addition, $[TbPc'_2]^+$ displays a higher coercive field of 0.071 T than the 0.023 T observed for $[TbPc'_2]^-$, and possesses a wider hysteresis loop that is associated with a larger separation of the ground state from the first excited state (again stemming from the contracted metal coordination

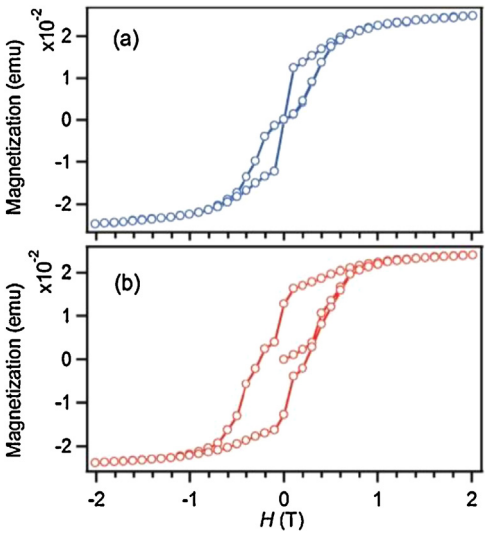

Fig. 12. Variable-field magnetization data collected on solid samples of (a) $[Dy(Pc(OEt)_8)_2]^-$ (**15**) and (**b**) $[Dy(Pc(OEt)_8)_2]^+$ (**14**) at 1.8 K.

Source: Figure was reproduced from Ref. [212], with permission of the copyright holders.

sphere). Contrary to these results, the neutral complex $TbPc'_2$ exhibits a fully open hysteresis loop over the entire magnetic field range of ±1.5 T that does not narrow around zero field. In addition, this complex exhibited a coercive field of $H_c = 0.16$ T, indicative of less apparent tunneling in this neutral species. More importantly, the hysteresis observed for the neutral complex suggests, that under the requirements of the MCD study, it is a better single-molecule magnet owing to its higher coercive field than its cationic congener. In contrast, the cationic complex was found to exhibit a slower relaxation by ac susceptibility measurements.

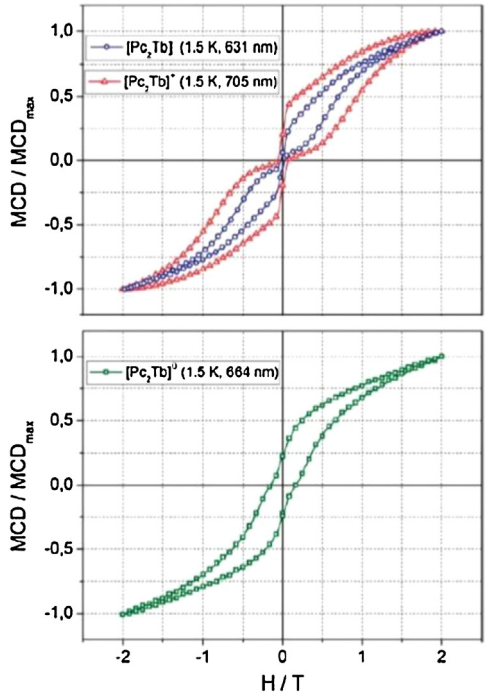

Fig. 13. Hysteresis curves of the normalized MCD intensity vs H recorded at 1.5 K and a sweep rate of $1\,T\,min^{-1}$ for the Q-band of $[TbPc'_2]^{+/-}$ (top) and $[TbPc'_2]^0$ (bottom). The symbols represent 1 of every 5 data points.

Source: Figure was reproduced from Ref. [228], with permission of the copyright holders.

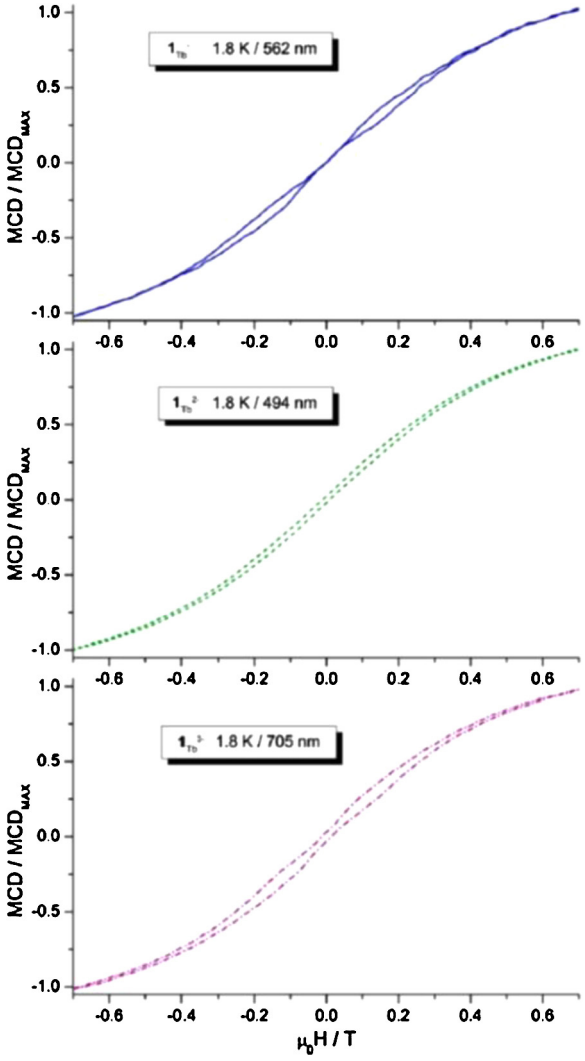

Fig. 14. Hysteresis curves of the normalized MCD intensity recorded at 1.8–1.9 K and at a sweep rate of 1 T min^{-1} for **16-1** (top), **16-2** (middle), and **16-3** (bottom).
Source: Figure was reproduced from Ref. [229], with permission of the copyright holders.

Fluorine substitution on the phthalocyanine rings in Tb(F$_{64}$Pc)$_2$ enabled generation of the reduced complexes [Tb(F$_{64}$Pc)$_2$]$^{1-}$ (**16-1**), [Tb(F$_{64}$Pc)$_2$]$^{2-\bullet}$ (**16-2**), and [Tb(F$_{64}$Pc)$_2$]$^{3-}$ (**16-3**) through bulk electrolysis [229]. The MCD intensity was measured at 562, 494, and 705 nm for **16-1**, **16-2**, and **16-3**, respectively, in frozen solutions at low temperatures, over a magnetic field range between −2 T and +2 T at a sweep rate of 1 T min^{-1} (Fig. 14). The monoanionic and trianionic species displayed waist-constricted hysteresis loops around zero field that were ascribed to quantum tunneling of the magnetization. In contrast, the dianionic radical species showed an open hysteresis loop over the entire probed magnetic field range, suggestive of a less-operative tunneling regime.

In summary, for halogenated and unsubstituted TbPc$_2$ complexes with odd charges (+1, −1, −3), butterfly-shaped hysteresis loops are observed, whereas those with even redox states (0, +2) display open hysteresis loops, presumably facilitated by the delocalized electron on the Pc ligand [230,231]. Evidently, the radical nature of the Pc ligands in the neutral and dianionic complexes suppress quantum tunneling pathways, possibly through coupling between the ligand spin and the metal center, as was previously noted for lanthanide double decker complexes [221]. Additionally, the even redox states TbPc$_2$ and [TbPc$_2$]$^{2+}$ are Kramers doublets,

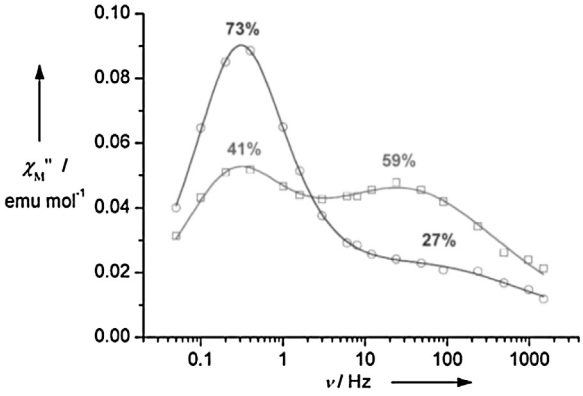

Fig. 15. Out-of-phase susceptibility (χ_M'') for **16**$_{cr}$ and **16**$_{dis}$ at 258 °C. The solid lines represent fits.
Source: Figure was reproduced from Ref. [232], with permission of the copyright holders.

rendering an electronic spin tunneling impossible and potentially playing a role in the absence of tunneling steps in the hysteresis loops.

The neutral complex Tb(Pc(*S*-DOP)$_8$)$_2$ (**17**; *S*-DOP = *S*-dodexyloxypropane) is a liquid crystal at room temperature and a single-molecule magnet at low temperatures [232]. Its mesomorphism provided a tool for probing the magnetic properties in various discrete structural situations. The synthesis of a structurally disordered species, **17**$_{dis}$, an intermediate partially ordered form, **17**$_{po}$, and an ordered crystalline sample, **17**$_{cr}$, were achieved by employing different rates of cooling. All phases display distinct ac peaks that appear simultaneously, where the ratio of slower and faster magnetic relaxation differs in each state. For instance, at 25 K, the ratio of slow to fast relaxation was found to be 73:27 for **17**$_{cr}$ and 41:59 for **17**$_{dis}$, leading to relaxation barriers of U_{eff} = 480 and 422 cm^{-1}, respectively (Fig. 15). This result underscores that the structural environment of a single-molecule magnet has a crucial impact on its magnetic properties.

The effect of peripheral substitution of Pc ligands with *tert*-butyl or *tert*-butylphenoxy groups has been demonstrated in neutral homoleptic and heteroleptic complexes of the form TbPc″$_2$ and Tb(Pc″)(Pc‴). The single delocalized electron in these compounds tends to promote higher relaxation barriers than apparent for their anionic counterparts [225]. Notably, the heteroleptic complexes bearing electron-donor groups led to significantly higher relaxation barriers and blocking temperatures relative to the corresponding homoleptic species. This observation stems from an increased ligand-field effect, owing to elongated Tb-N distances in the substituted Pc ring that positions the metal ion closer to the unsubstituted Pc ligand. In the homoleptic complex TbPc‴$_2$, where Pc‴ represents an octa-substituted (*tert*-butylphenoxy) phthalocyanine ligand, the extracted barrier is U_{eff} = 504 cm^{-1}. Notably, the heteroleptic complex Tb(Pc)(Pc‴) (**18**), where Pc‴ is functionalized with eight *tert*-butylphenoxy groups, displays the highest relaxation barrier yet reported for any molecular species, with U_{eff} = 652 cm^{-1} (Fig. 16).

In addition, the derivative Tb(Pc)(Pc*) (**19**) where Pc* is tetra-substituted Pc with four *tert*-butylphenoxy groups, possesses a similar barrier of U_{eff} = 642 cm^{-1}. The difference in relaxation barriers is attributed to the higher number and strength of electron-donating *tert*-butylphenoxy groups on the Pc ligand in complex **18**, which shifts the metal closer to the unsubstituted Pc ligand. Moreover, bulky groups on the ligand facilitate the isolation of complex **18**. Notably, both radical-containing species **18** and **19** displayed higher barriers than their reduced anionic analogs. Furthermore, at 2 K, all neutral and anionic species display hysteresis curves that are closed at H = 0, (Fig. 17).

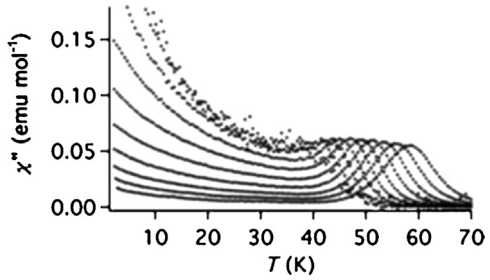

Fig. 16. Out-of-phase susceptibility (χ_M'') of **18** from 10 to 10,000 Hz.
Source: Figure was reproduced from Ref. [225], with permission of the copyright holders.

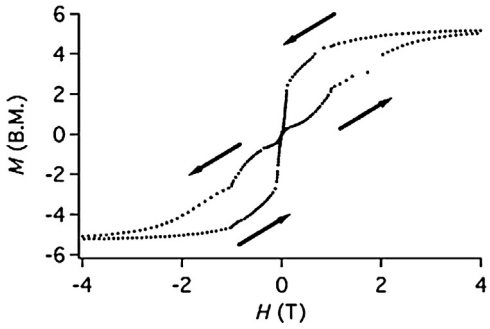

Fig. 17. Plot of magnetization vs field at 2 K for compound **19**.
Source: Figure was reproduced from Ref. [225], with permission of the copyright holders.

Structurally related to the double-decker lanthanide phthalocyanine complexes are the neutral heteroleptic complexes Dy(Pc)(TClPP) (**20**) and Dy(Pc(α-OC_5H_{11})$_4$)(TClPP) (**21**), where Pc(α-OC_5H_{11})$_4$ is a pentyloxy-substituted phthalocyaninate and TClPP is a chlorophenyl-substituted porphyrinate (Fig. 18) [233]. The interaction between Dy^{III} center and the radical was found to be ferromagnetic in **20**, consistent with the coupling observed in bis(phthalocyaninato) lanthanide complexes [221]. In the temperature range 2.4–3.5 K, **20** exhibits slow magnetic relaxation at zero dc field, with a relaxation barrier of $U_{eff} = 16\,cm^{-1}$. In contrast, as a result of a larger degree of quantum tunneling attributed to its lower symmetry, **21** displays out-of-phase signals only at applied fields of 2000 Oe, translating to a barrier of $U_{eff} = 30\,cm^{-1}$.

Overall, a tremendous effort has been directed toward an in-depth analysis of phthalocyanine containing single-molecule magnets, including exploration of their utility for surface deposition and thus possible spin-based device applications. For instance, variations of $TbPc_2$ have been deposited onto pyrolytic graphite [234–236], graphene [237,238], carbon nanotubes [239], copper (1 0 0) [240], copper (1 1 1) [241], ferro-magnetic films [242], gold films [243], gold (1 1 1) [244,245]. Interactions of $TbPc_2$ with single-walled nanotubes (SWNTs) [239,246], within the context of potential molecular spintronic devices have further been reported [247,248].

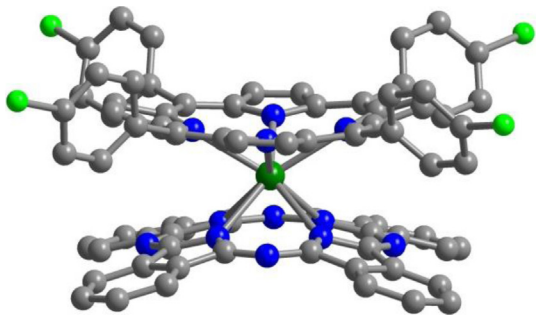

Fig. 18. Structure of Dy(Pc)(TClPP) (**20**), with green, blue and gray spheres representing Dy, N and C atoms, respectively; H and Cl atoms are omitted and selected C and O atoms are faded for clarity.

3.2.2. Mononuclear lanthanide nitroxide radical complexes

Encouraged by the success of transition metal complexes that contain nitroxyl radical ligands, researchers have also explored the magnetic properties of these radicals coupled to lanthanide ions. Owing to the large magnetic anisotropy of lanthanides, their complexes with nitronyl nitroxide radical were expected to possess stronger magnetic coupling. Additionally, the ability of lanthanides to accommodate high coordination numbers offered possibilities of extended Ln^{III}-radical networks.

In parallel with the objective of synthesizing complexes incorporating highly anisotropic lanthanide ions, Gd^{III}-containing species have been pursued to enable quantification of exchange coupling. Indeed, the Gd^{III} center, with its isotropic half-filled 4f valence shell, exhibits magnetic behavior that is free of complications associated with spin-orbit coupling. Such magnetic behavior is suitable for a spin-only analysis, similar to that employed for most transition metal complexes, wherein the orbital moment is quenched by the environment of the ligand field. As such, among all lanthanide nitronyl nitroxide radical complexes, those involving Gd^{III} are the most thoroughly studied, and great emphasis has been placed on maximizing the value of J and deducing the factors that influence the sign and magnitude of J. Table 2 summarizes the relevant coupling constants obtained for Gd^{III}-radical complexes, the majority of which involve nitronyl nitroxide radicals.

Historically, it was thought that the coupling between Gd^{III} and nitronyl nitroxide radicals was intrinsically ferromagnetic, independent of any ligand field effects, as many early examples exhibited such behavior [251,292]. Specifically, it was proposed that the exchange mechanism involves a transfer of a fraction of the unpaired electron of the radical into an empty Gd 6s or 5d orbital, which would then maintain a spin parallel in alignment to the 4f electrons, in accordance with Hund's rules [293,294]. In addition, it was assumed that any antiferromagnetic interactions involving direct exchange between the Gd^{III} center and the radical would be negligible, given the contracted nature of the 4f orbitals. However, this theory lost traction following the first observations of antiferromagnetic coupling between Gd^{III} and a radical in the complexes $[Gd(NITBzImH)_4]^{3+}$ and $[Gd(NITMeBzImH)_4]^{3+}$ [281].

Evidently, the coupling between 4f electrons and radical cannot be neglected, and the observed coupling can be considered as a sum of competing ferromagnetic and antiferromagnetic interactions, $J_{obs} = J_F + J_{AF}$. The magnitude of J_{AF} is determined by the degree of effective overlap between the 4f orbitals and the radical. As a result, ligands that are more strongly donating give rise to antiferromagnetic coupling, as in the case of $Gd(Hbpz_3)_2(dtbsq)$ [287]. A decrease in overlap of ligand π^* and 6s or 5d metal orbital also leads to observance of antiferromagnetic coupling. For instance, the more planar chelate ring in the imino nitroxide complex $Gd(hfac)_3$(IM2py) [277], compared to the related nitronyl nitroxide complex $Gd(hfac)_3$(NIT2py) [254], results in the ligand π^* orbital being more fully orthogonal to the 6s or 5d orbital. Hence, no fraction of the unpaired electron is transferred, leading to observance of antiferromagnetic metal-radical coupling in $Gd(hfac)_3$(IM2py). Indeed, all Gd^{III} complexes involving imino nitroxide ligands exhibit antiferromagnetic coupling. The low spin density on the donor atoms of nitronyl nitroxides is responsible for providing only weak to moderate coupling, as shown in Table 2. In further support of the current hypothesis regarding the nature of metal-radical coupling, the largest observed antiferromagnetic coupling for a Gd^{3+} nitronyl nitroxide complex, $Gd(hfac)_3$(6bpyNO), was very recently reported to be

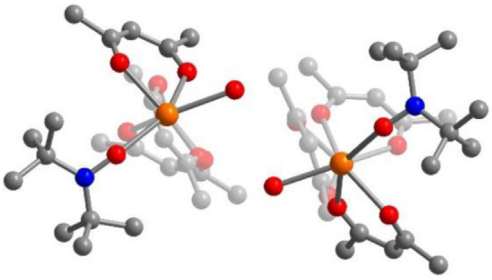

Fig. 19. Structure of $Gd(hfac)_3(DTBNO)(H_2O)$ (**22**) and nearest-neighbor molecular arrangement. Orange, blue, red and gray spheres represent Gd, N, O and C atoms, respectively; H and F atoms are omitted and selected C and O atoms are faded for clarity.

$J_{Gd-L} = -5.53\ cm^{-1}$.[286] Accordingly, the authors describe a close to planar coordination of the nitronyl nitroxide ligand to the metal, with a small Gd—O—N—C torsion angle of 16.5(5)°. Additionally, the radical ligand π* orbital is orthogonal to the Gd 5d orbital, thus disfavoring the ferromagnetic state.

Recent efforts to increase the coupling strength in nitroxide radical-containing lanthanide complexes have been directed toward the use of aliphatic nitronyl nitroxides. Hyperfine coupling provides a good measure of spin localization, and it has been shown that the hyperfine coupling constants for di-*tert*-butyl nitroxide (DTBNO) of $a_N = 1.5$ mT is larger than the values of $a_N = 0.5–0.75$ mT observed for common nitronyl nitroxides [284,295,296]. Typically, the higher the spin density at the N and O atoms is, the stronger the coupling with paramagnetic ions [297]. As a proof of concept, the antiferromagnetic coupling between the Gd^{III} center and DTBNO in the lanthanide amidoxyl radical complex $Gd(hfac)_3(DTBNO)(H_2O)$ (**22**) was shown to exhibit relatively strong ferromagnetic coupling, with $J_{Gd-L} = +4.03\ cm^{-1}$, accompanied by a ferromagnetic interaction between gadolinium centers with $J_{Gd-Gd} = +0.042\ cm^{-1}$, the second strongest value for Gd–Gd coupling (Fig. 19).

The use of nitronyl nitroxide radicals has found considerable success in the pursuit of single-molecule magnets. The terbium complex $Tb(hfac)_3(NIT2Py)\cdot C_6H_{17}$ (**23**) represents the first mononuclear lanthanide species containing a nitronyl nitroxide ligand to exhibit single-molecule magnet behavior (Fig. 20) [298]. Frequency-dependent ac magnetic susceptibility data collected for **23** reveal a relaxation barrier of $U_{eff} = 12\ cm^{-1}$ (Table 3) [298,299]. Note that ferromagnetic coupling between metal and radical was reported for the related complex $Gd(hfac)_3(NIT2Py)\cdot C_6H_{17}$, with $J_{Gd-L} = +1.52\ cm^{-1}$ [254]. The complex $Tb(hfac)_3(NITPhOEt)_2$ (**24**) represents the first example of a mononuclear lanthanide-based single-molecule magnet where both radical units coordinate the metal ion only through the N—O unit (Fig. 21) [300]. This complex exhibits single-molecule magnet behavior with $U_{eff} = 20\ cm^{-1}$ [300]. In the analogous $Gd(hfac)_3(NITPhOEt)_2$, a ferromagnetic

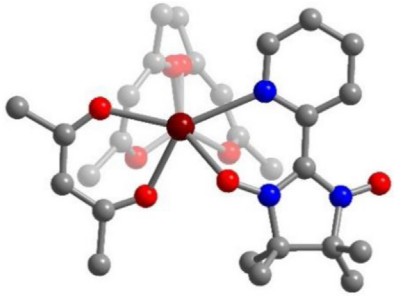

Fig. 20. Structure of $Tb(hfac)_3(NIT2Py)\cdot C_6H_{17}$ (**23**) with dark red, blue, red and gray spheres representing Tb, N, O and C atoms, respectively; H, F atoms, and C_6H_{17} are omitted and selected C and O atoms are faded for clarity.

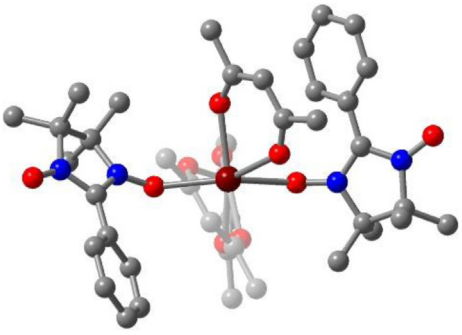

Fig. 21. Structure of $Tb(hfac)_3(NITPhOEt)_2$ (**24**) with dark red, blue, red and gray spheres representing Tb, N, O and C atoms, respectively; H and F atoms are omitted and selected C and O atoms are faded for clarity.

metal-radical interaction was observed with $J_{Gd-L} = +0.27\ cm^{-1}$, along with an antiferromagnetic radical–radical interaction of $J_{L-L} = -2.97\ cm^{-1}$ [259].

Similarly, the complex $Dy(acac)_3(NIT2Py)$ behaves as a single-molecule magnet with $U_{eff} = 15\ cm^{-1}$ [275], and a ferromagnetic metal-radical ligand exchange constant of $J_{Gd-L} = +2.23\ cm^{-1}$ was observed for the Gd^{III} analog [275]. Recently, the terbium derivative, $Tb(acac)_3NIT2Py\cdot 0.5H_2O$, was also shown to exhibit slow magnetic relaxation with spin relaxation barriers of $U_{eff} = 15\ cm^{-1}$ and $U_{eff} = 18\ cm^{-1}$ at 1000 Oe and 3500 Oe, respectively.[299] Within the series $Ln(tfa)_3(NITBzImH)$ (Ln = Gd, Tb, Dy; tfa^- = trifluoroacetyl-acetonate), both the Tb^{III} and Dy^{III} complexes exhibit slow magnetic relaxation, with barriers of $U_{eff} = 10\ cm^{-1}$ and $3.2\ cm^{-1}$, respectively [272]. Additionally, the Gd^{III} complex was shown to exhibit ferromagnetic exchange with $J_{Gd-L} = +0.99\ cm^{-1}$ [272]. As a result of π–π stacking, the biradical dysprosium complex $Dy(hfac)_3(NITmbis)$ (**25**; *m*bis = 1,3-bis-(1′-oxyl-3′-oxido-4′,4′,5′,5′-tetramethyl-4,5-hydro-1H-imidazol-2-yl)benzene) was also shown to display single-molecule magnet behavior (Fig. 22). Here, the relaxation was found to be thermally activated down to 1.2 K, with $U_{eff} = 8.1\ cm^{-1}$, and a sharp transition to a pure quantum tunneling regime at lower temperature [307].

The terdentate picolinate-functionalized nitronyl nitroxide ligand (NITpic) was employed in the synthesis of the neutral homoleptic complex $Tb(NITpic)_3$ (**26**) (Fig. 23) [304]. This complex exhibits a relaxation barrier of $U_{eff} = 16\ cm^{-1}$. Notably, it displays magnetic hysteresis below 1 K, marking the first observation of magnetic hysteresis for a mononuclear lanthanide-radical complex [304].

The stable aliphatic nitronyl nitroxide radical 2,2,6,6-tetramethylpiperidin-1-oxyl (TEMPO) has also been employed in

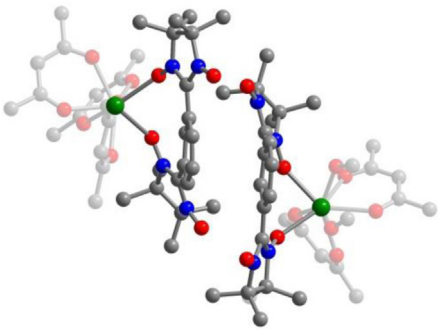

Fig. 22. Structure of $Dy(hfac)_3(NITmbis)$ (**25**), with green, blue, red and gray spheres representing Dy, N, O and C atoms, respectively; H and F atoms are omitted and selected C atoms are faded for clarity.

Table 3
Spin relaxation barriers U_{eff} (cm^{-1}) and pre-exponential factors τ_0 (s) for lanthanide-radical single-molecule magnets.

Complexes	Structure	H_{dc} (kOe)	U_{eff} (cm^{-1})	τ_0 (s)	Hysteresis (K)	Reference
$Tb(Pc)(Pc(O(C_6H_4)$-*p*-$tBu)_8)$	Mononuclear	0	652	1.1×10^{-11}	2	[225]
$Tb(Pc)(Pc(tBu)_4)$	Mononuclear	0	642	2.2×10^{-11}	2	[225]
$Tb\{Pc(O(C_6H_4)$-*p*-$tBu)_8\}_2$	Mononuclear	0	504	2.2×10^{-11}	2	[225]
$[Tb(Pc(S\text{-}DOP)_8)_2]_{cr}$	Mononuclear	0	480	6.9×10^{-12}		[232]
$[Tb(Pc(S\text{-}DOP)_8)_2]_{dis}$	Mononuclear	0	422	1.7×10^{-10}		[232]
$TbPc_2$	Mononuclear	0	410	1.5×10^{-9}		[223]
$[K(18\text{-}C\text{-}6)][((Me_3Si)_2N)_2(THF)Tb]_2(N_2)$	Dinuclear	0	227	8.2×10^{-9}	14	[301]
$[K(18\text{-}C\text{-}6)][((Me_3Si)_2N)_2(THF)Dy]_2(N_2)$	Dinuclear	0	123	8×10^{-9}	8.3	[290]
$[(Cp^*_2Dy)_2(\mu\text{-bpym})][BPh_4]$	Dinuclear	0	88	1.0×10^{-7}	6.5	[289]
$[K(18\text{-}C\text{-}6)][((Me_3Si)_2N)_2(THF)Ho]_2(N_2)$	Dinuclear	0	73	3×10^{-8}		[301]
$[Dy(hfac)_3(boaDTDA)]_2$	Dinuclear	0	71	7.3×10^{-8}		[302]
$[(Cp^*_2Tb)_2(\mu\text{-bpym})][BPh_4]$	Dinuclear	0	44	4×10^{-8}	2	[289]
$[K][((Me_3Si)_2N)_2(THF)Tb]_2(N_2)$	Dinuclear	0	41	3.9×10^{-6}	3.8	[291]
$[K(18\text{-}C\text{-}6)][((Me_3Si)_2N)_2(THF)Er]_2(N_2)$	Dinuclear	1	36	4×10^{-11}		[301]
$[(Cp^*_2Dy)_2(\mu\text{-tppz}^{\bullet})]^+$	Dinuclear	0	36	2.1×10^{-7}	Below 3.25	[288]
$Dy(Pc(\alpha\text{-}OC_5H_{11})_4)(TClPP)$	Mononuclear	2	30	7.4×10^{-8}		[233]
$Tb(hfac)_3(NITPhOEt)_2$	Mononuclear	0	20	3.0×10^{-8}		[300]
$[Tb(hfac)_3(NIT\text{-}5\text{-}Py\text{-}3Br)]_2$	Dinuclear	0	20	5.9×10^{-9}		[303]
$Tb(acac)_3NIT2Py^{\bullet}0.5H_2O$	Mononuclear	1/3.5	15/18	$1.0 \times 10^{-7}/3 \times 10^{-8}$		[299]
$[Tb(Phtfac)_3(NIT4Py)]_2$	Dinuclear	0	18	4.1×10^{-8}		[271]
$[Tb(hfac)_3(NITPhPO(OEt)_2)]_2$[a]	Dinuclear	2	17	3.4×10^{-9}		[270]
$Dy(Pc)(TClPP)$	Mononuclear	0	16	2.5×10^{-7}		[233]
$Tb(NITpic)_3$	Mononuclear	0	16	5.5×10^{-9}	Below 1	[304]
$[K][((Me_3Si)_2N)_2(THF)Dy]_2(N_2)$	Dinuclear	0	15	3.2×10^{-7}		[291]
$[Dy(acac)_3(NIT2Py)]\cdot0.5NIT^{o}Py$	Mononuclear	0	15	1.5×10^{-8}		[275]
$[Tb(hfac)_3(NITPhPO(OEt)_2)]_2$[b]	Dinuclear	2	15	1.8×10^{-9}		[270]
$[Dy(Phtfac)_3(NIT4Py)]_2$	Dinuclear	3	14	1.8×10^{-6}		[271]
$[Tb(hfac)_3(NIT3Py)]_2$	Dinuclear	3	13	8.8×10^{-8}		[305]
$[Tb(hfac)_3(NIT2Py)]\cdot0.5C_7H_{16}$	Mononuclear	0	12	9.6×10^{-7}		[298]
$Tb(tfa)_3NITBzImH$	Mononuclear	0	10	4.6×10^{-7}		[272]
$[Dy(hfac)_3(NIT4Py)]_2$	Dinuclear	2	10	6.7×10^{-7}		[306]
$[Dy(hfac)_3(NIT4Py)]_2$	Dinuclear	0	9.2	2.3×10^{-8}		[306]
$[Dy(hfac)_3(NIT\text{-}m\text{bis})]_2$	Dinuclear	0	8.1	2.3×10^{-8}		[307]
$[Dy(hfac)_2(NITPhO)]_2$	Dinuclear	0	5.3	3.0×10^{-6}		[308]
$[(Cp^*_2Tb)_2(\mu\text{-tppz}^{\bullet})]^+$	Dinuclear	0	5.1	6×10^{-6}		[288]
$Dy(tfa)_3(NITBzImH)$	Mononuclear	0	3.2	3.6×10^{-7}		[272]

[a] Isolated molecule in crystal packing.
[b] Short contacts between molecules in crystal packing.

the synthesis of mononuclear lanthanide compounds. Its hyperfine coupling constant a_N implies the spin localization at the N—O unit is 1.5 mT [309], indicating that a strong exchange-bias could be generated. Although this stable radical, along with its derivatives, is well-established for spin-probe and -labeled agents [310–312], only recently were the first lanthanide complexes containing TEMPO ligands reported: $Ln(hfac)_3(TEMPO)_2$ (Ln = Y, La, Gd) [313]. The radical ligands coordinate *trans* to the metal center, leading to spin triads S_{R1}-S_{Ln}-S_{R2} (Fig. 24). Variable-temperature dc susceptibility and low-temperature magnetization data for the Gd^{III} complex suggested a ground state of $S = 7/2$ for this molecule. This ground state indicates that the TEMPO radical spins cancel one another at low temperature. Similarly, strong superexchange interactions across diamagnetic lanthanide ions were first observed for radical–radical interactions across Y^{III} and La^{III} centers, with $J_{TEMPO1-TEMPO2} = -5.2(1)$ and $-17.3(2)\,cm^{-1}$, respectively. Taking the isomorphous yttrium complex into account, the exchange interactions between Gd and the organic radicals have been evaluated to be $J_{Gd-TEMPO} = -4.5(1)$ and $+2.8(1)\,cm^{-1}$.

3.2.3. A mononuclear gadolinium benzosemiquinonate radical complex

The occurrence of ferromagnetic coupling in Gd^{III}-radical complexes was originally explained by a mechanism involving overlap of the magnetic orbitals of the radical ligands with the empty 5d

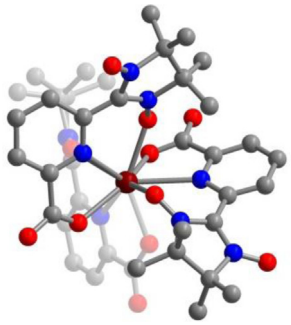

Fig. 23. Structure of $Tb(NITpic)_3$ (**26**), with dark red, blue, red and gray spheres representing Tb, N, O and C atoms, respectively; H and F atoms are omitted and selected C atoms are faded for clarity.

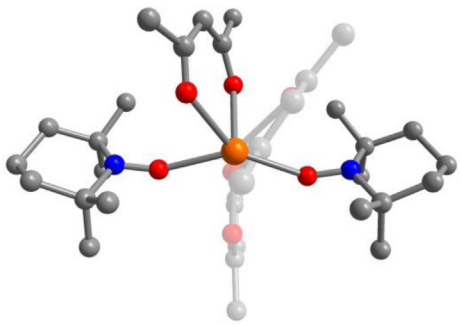

Fig. 24. Structure of $Gd(hfac)_3(TEMPO)_2$, with orange, blue, red and gray spheres representing Gd, N, O and C atoms, respectively; H and F atoms are omitted and selected C are faded for clarity.

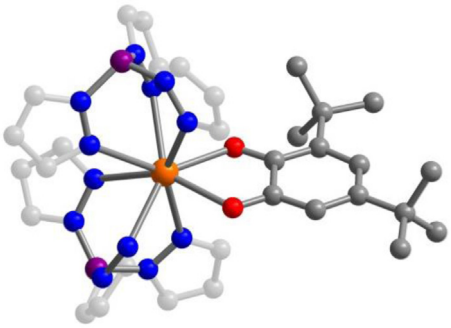

Fig. 25. Structure of Gd(Hbpz$_3$)$_2$(dtbsq) (**27**), with orange, blue, purple, red and gray spheres representing Gd, N, B, O and C atoms, respectively; H atoms are omitted and selected C are faded for clarity.

and 6s orbits of gadolinium, thereby polarizing the 4f electrons with their spins parallel to that of the radical ligand [294,314]. When the first antiferromagnetic coupling for a gadolinium radical complex was observed (see above), the coupling was proposed as the total of two contributions. The first arises from direct overlap of the radical orbitals with the 4f-orbitals, commonly leading to an antiferromagnetic interaction, and the second stems from the overlap with 5d and 6s orbitals to give a ferromagnetic interaction. Here, the former contribution was proposed to be more important for stronger donor ligands [287]. As a proof of concept, the gadolinium semiquinonate complex Gd(Hbpz$_3$)$_2$(dtbsq) (**27**) was prepared by treating the parent Gd^{III} benzoate derivative with 3,5-di-*tert*-butylcatechol and KOH (Fig. 25).

For this complex, variable-temperature dc susceptibility data reveal an antiferromagnetic interaction with $J = -5.7\ cm^{-1}$ between the Gd^{III} center and the semiquinonate radical to give an $S = 3$ ground state.

3.2.4. Mononuclear ytterbium radical metallocenes

The decamethylytterbocene bipyridyl complex Cp*$_2$Yb(bipy) (**28**) represents the most prominent radical-containing lanthanide metallocene complex and is interesting by virtue of its multiconfigurational nature (Fig. 26) [315–318]. The coordination of a bipyridyl radical anion to the [Cp*$_2$Yb]$^+$ cation fragment forms the main configuration, $|f^{13}, bipy^{\bullet -}\rangle$, while the minor configuration, $|f^{14}, bipy\rangle$, comprises a neutral bipyridyl ligand that coordinates to the neutral Cp*$_2$Yb moiety. Computations revealed that the multiconfigurational ground state stems from a mixing of low-lying excited states into the ground state [316,317]. Quantification of the coupling between two non-identical spin carriers, such as a Ln^{III}-organic radical pair, is very difficult [319] when contrasted with the modeling of variable-temperature magnetic susceptibility of two equivalent exchange-coupled Ln ions [320]. One way to determine the strength of this coupling involves the

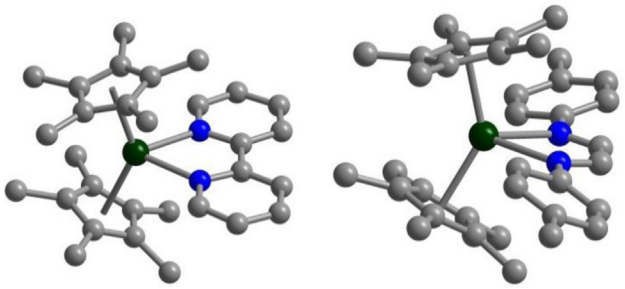

Fig. 26. Structure of Cp*$_2$Yb(bipy) (**28**) (left) and Cp*$_2$Yb(dad-p-tolyl), with dark green, blue and gray spheres representing Yb, N and C atoms, respectively; H atoms are omitted for clarity.

temperature-independent paramagnetism (TIP) of the open-shell singlet ground state through employing Griffith's methodology for metal ions with unquenched orbital angular momentum [321]. Another method to quantify the strong exchange coupling in **28** is through employing the Hubbard molecule model (HMM) [322,323], which is essentially the Hubbard model [324] adapted to a single molecule [325]. This bonding model encloses the electron correlation and represents an extension of Hückel theory by adding a parameter that considers electron pairing energy [326]. By extending the spin-only Heisenberg, Dirac, van Vleck (HDVV) Hamiltonian to metal ions with unquenched orbital angular momentum, an extraordinarily large exchange coupling of Cp*$_2$Yb(bipy) was quantified as $J = -460\ cm^{-1}$, in agreement with the predicted value from computations [325]. Remarkably, this coupling is about three orders of magnitude larger than typical coupling constants found for lanthanide ions [316,317].

In pursuit of a better understanding of the electronic structure of Cp*$_2$Yb(bipy), a number of related metallocenes incorporating heterocyclic amine ligands were explored [327]. In these intermediate-valence compounds, the valence of ytterbium in the Cp*$_2$Yb moiety is between Yb^{II} and Yb^{III} [328–331]. Among the complexes examined were Cp*$_2$Yb(bipy-X) (X = Me, *t*-Bu, OMe, Ph, CO_2Me, CO_2Et) [316,327,328,332], Cp*$_2$Yb(dad-R) (R = *t*-Bu, *i*-Pr, adamantyl, *p*-tolyl, *p*-anisyl, mesityl) [316,329], and Cp*$_2$Yb(terpy) (Fig. 26) [333,334]. A number of these complexes display intriguing magnetic properties comprising reduced magnetic moments that are consistent with strong antiferromagnetic coupling. The coupling constants were estimated typically from the temperature of the peak in the magnetic susceptibility, resulting in $|J| = \sim 100\ cm^{-1}$.

Despite this exceptionally strong coupling, studies of other lanthanide-bearing analogs that may exhibit slow magnetic relaxation have not yet been reported.

3.3. Dinuclear lanthanide radical complexes

A particularly promising route to the design of single-molecule magnets with high blocking temperatures is through engendering strong exchange coupling in multinuclear lanthanide complexes containing highly anisotropic metal centers. Indeed, strong coupling can be successfully realized by employing radical ligands to bridge lanthanide ions. The radical can serve to significantly enhance the magnitude of the coupling, as certain radical species possess diffuse spin orbitals able to penetrate the core electron density of the lanthanide ions where the 4f spin orbitals lie buried. Here, the delocalization of the electron in the radical ligand and thus its ability to provide an efficient exchange-bias is extremely important with respect to the strength of the magnetic exchange coupling and the suppression of quantum tunneling relaxation pathways.

3.3.1. Nitronyl nitroxide radical-bridged lanthanide complexes

In addition to mononuclear complexes, nitronyl nitroxide ligands have been employed in the synthesis of dinuclear lanthanide complexes. The bridging capability of the pyridine-functionalized nitronyl nitroxide ligand, NIT4Py, was exploited in linking two Dy^{III} centers to afford the single-molecule magnet [Dy(hfac)$_3$(NIT4Py)]$_2$ (**29**), which exhibits a spin relaxation barrier of $U_{eff} = 9.2(5)\ cm^{-1}$ under zero dc field and $U_{eff} = 9.5(1)\ cm^{-1}$ under a 2000 Oe dc field [306]. Notably, this dinuclear complex represents the first lanthanide-based single-molecule magnet incorporating a radical ligand. The analog [Gd(hfac)$_3$(NIT4Py)]$_2$ (**30**) exhibits weak ferromagnetic coupling between the Gd^{III} and radical centers with $J = +0.89\ cm^{-1}$, which was attributed to an operative spin polarization mechanism (Fig. 27) [254]. Bridging nitronyl nitroxide ligands between Gd^{III} centers can give rise to four-spin systems that display two different types of magnetic interaction: coupling between the metal center and the N—O group of the nitronyl nitroxide radical

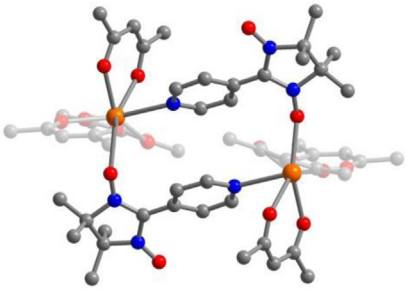

Fig. 27. Structure of $[Gd(hfac)_3(NIT4Py)]_2$ (**30**), with orange, blue, red and gray spheres representing Gd, N, O and C atoms, respectively; H and F atoms are omitted and selected C atoms are faded for clarity.

(J_{Gd-L1}), and the generally weaker interaction of the Gd^{III} center – with the ancillary R group of the radical ligand (J_{Gd-L2}).

The related radical ligand NIT-5-Py-3Br bridges two lanthanide ions in a series of lanthanide-nitronyl nitroxide compounds of the type $[Ln(hfac)_3(NIT\text{-}5\text{-}Py\text{-}3Br)]_2$ (Ln = Pr, Sm, Eu, Gd, Tb, Tm). The Tb^{III} congener (**31**) displays single-molecule magnet behavior under a zero dc field with a relaxation barrier of $U_{eff} = 20\ cm^{-1}$ (Fig. 28) [303], while the coupling constants for the Gd^{III} species was determined to be $J_{1,Gd-L} = +2.60\ cm^{-1}$ and $J_{2,Gd-L} = -0.24\ cm^{-1}$ [256]. A related complex, $[Tb(hfac)_3(NIT3Py)]_2$, in which *meta* pyridyl-substituted nitronyl nitroxide ligands link two Tb^{III} centers, also displayed slow magnetic relaxation under a 3 kOe dc field, featuring a barrier of $13.2\ cm^{-1}$ [305].

Phosphine oxide-substituted nitronyl nitroxide (NITPhPO$(OEt)_2$) radical ligands were employed in the syntheses of the complexes $[Ln(hfac)_3(NITPhPO(OEt)_2)]_2$ (Ln = Gd, Tb, Dy). In the case of Ln = Tb, single crystals exhibiting two distinct packing modes were obtained. The molecular structure of $[Tb(hfac)_3(NITPhPO(OEt)_2)]_2{\cdot}2CH_2Cl_2$ shows well-isolated molecules, as opposed to $[Tb(hfac)_3(NITPhPO(OEt)_2)]_2$, which features intermolecular interactions involving adjacent N—O radicals [270]. The former compound exhibits slow magnetic relaxation, showing out-of-phase signals under an applied dc field of 2 kOe associated with a relaxation barrier of $U_{eff} = 17\ cm^{-1}$, while the latter displays a barrier of $U_{eff} = 15\ cm^{-1}$ [270]. For this system, the Gd^{III} analog, $[Gd(hfac)_3(NITPhPO(OEt)_2)]_2$, exhibits ferromagnetic coupling with $J_{Gd-L} = 1.73\ cm^{-1}$ [270]. Although phenol-substituted nitronyl nitroxide compound $[Dy(hfac)_2(NITPhO)]_2$ shows a small relaxation barrier of $U_{eff} = 5.3\ cm^{-1}$ [308], the related Dy^{III} species with a brominated phenol-substituted nitronyl nitroxide radical does not show slow magnetic relaxation. Finally, ac magnetic susceptibility measurements performed on the phenyltrifluoroacetylacetonate (Phtfac)-containing complexes $[Tb(Phtfac)_3(NIT4Py)]_2$ and $[Dy(Phtfac)_3(NIT4Py)]_2$ revealed relaxation barriers of 18 and $14\ cm^{-1}$, respectively, under a 3-kOe dc field [271]. The analogous complex $[Gd(Phtfac)_3(NIT4Py)]_2$ exhibits ferromagnetic coupling, with constants of $J_{Gd-L1} = 1.84\ cm^{-1}$ and $J_{Gd-L2} = 0.12\ cm^{-1}$ [271].

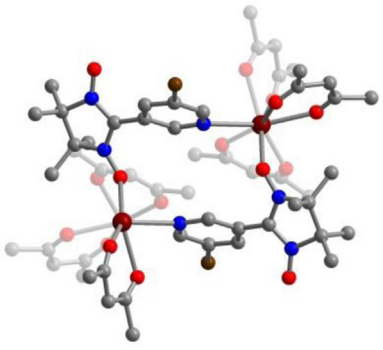

Fig. 28. Structure of $[Tb(hfac)_3(NIT\text{-}5\text{-}Py\text{-}3Br)]_2$, with dark red, blue, red and gray spheres representing Tb, N, O and C atoms, respectively; H and F atoms are omitted and selected C atoms are faded for clarity.

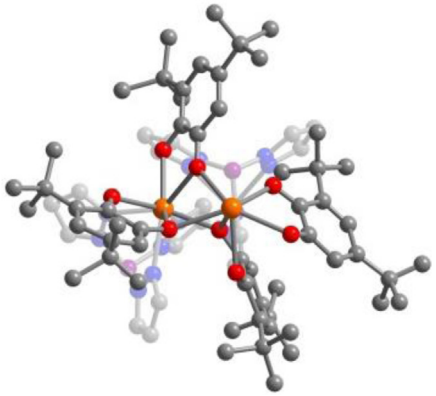

Fig. 29. Structure of $Gd_2(Hbpz_3)_2(dtbsq)_4$ (**32**), with orange, blue, purple, red and gray spheres representing Gd, N, B, O and C atoms, respectively; H atoms are omitted and selected N, B and C are faded for clarity.

3.3.2. Dinuclear gadolinium benzosemiquinonate radical complex

The relatively strong antiferromagnetic exchange of $J = -5.7\ cm^{-1}$ in the mononuclear complex $Gd(Hbpz_3)_2(dtbsq)$, arising from non-negligible overlap between the magnetic orbitals of the radical and the 4f orbitals of the lanthanide center, inspired researchers to increase the number of spin carriers. This led to isolation of the dinuclear complex $Gd_2(Hbpz_3)_2(dtbsq)_4$ (**32**), where two metal centers are bridged by three benzosemiquinonate radical ligands ($dtbsq_B$), and the fourth ligand ($dtbsq_{NB}$) is coordinated to only one Gd^{III} center (Fig. 29).[335] Variable-temperature dc susceptibility data, in conjunction with high-field EPR measurements, suggest an $S = 7$ ground state for this complex. The three exchange interactions Gd-$dtbsq_B$ (J_1), Gd-$dtbsq_{NB}$ (J_2), $dtbsq_B$-$dtbsq_{NB}$ (J_3) were estimated using two differing Hamiltonians to give $J_1 = +1.26\ cm^{-1}/0.88\ cm^{-1}$, $J_2 = -0.3\ cm^{-1}/0.18\ cm^{-1}$, and $J_3 = +9.08\ cm^{-1}/6.43\ cm^{-1}$. While these values differ depending on the Hamiltonian employed, one can qualitatively note that the coupling of the bridging benzosemiquinone radicals to the metals is weaker than the interaction between the terminal radical and one of the metal centers. Here, the weaker coupling was attributed to each of three radicals coordinated to two Gd ions and to an average larger Gd-O(benzosemiquinonate)-distance compared to the Gd–O($dtbsq_{NB}$) distance. More importantly, the overall Gd-radical coupling strength is substantially smaller than that observed for the mononuclear complex. This result signifies that geometric arrangements of the radical ligands with respect to the lanthanide ion may be of utmost importance in generating an appreciable antiferromagnetic interaction.

3.3.3. Dinuclear lanthanide-tetrathiafulvalene radical complexes

Although tetrathiafulvalene radicals have been used to construct mononuclear lanthanide complexes and extended solids, their dynamic magnetic behavior has not been investigated [336]. However, radical cation tetrathiafulvalene-based ligands have also been used to construct dinuclear lanthanide complexes wherein the radical tetrathiafulvalene ($ttf^{\bullet+}$) does not coordinate to the metals via the S atoms. In the original compound $[Gd(hfac)_3(\mu\text{-}TTF^{\bullet+}COO^{-})]_2$ (**33**), the radical ligands gave rise to very weak exchange interactions, as concluded by the small value of the Weiss constant $\Theta = -43\ K$ (Fig. 30) [337].

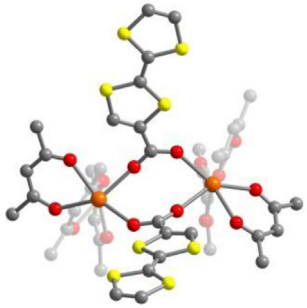

Fig. 30. Structure of $[Gd(hfac)_3(\mu\text{-}TTF^{\bullet+}COO^{-})]_2$ (**33**), with orange, red, yellow and carbon spheres representing Gd, O, S and C atoms, respectively; H and F atoms are omitted and selected C and O atoms are faded for clarity.

The radical cation $ttf^{\bullet+}$-containing dysprosium complex $[(Dy(hfac)_2(SO_3CF_3)(L^{\bullet+}))_2]^{2+}$ (L = 4,5-bis(3-pyridyl-*N*-oxidemethylthio)-4′,5′-methyldithiotetrathiafulvene) represents the first $ttf^{\bullet+}$-based single-molecule magnet [338]. The radical cationic ligand is attached to the metal via two distinct coordination modes, involving 3-py-*N*-oxide functionalities. This molecule displays out-of-phase ac susceptibility peaks under an applied dc field of 800 Oe and possesses a rather small spin relaxation barrier of $U_{eff} = 8.3\ cm^{-1}$. Since the radical is not directly bridging the metal ions, the coupling between the two Dy^{III} centers can be expected to be weak. Consequently, the observation of slow magnetic relaxation likely primarily stems from the magnetic anisotropy of the isolated Dy^{III} centers.

3.3.4. A dinuclear lanthanide thiazyl radical complex

The dimeric compound $[Dy(hfac)_3(boaDTDA)]_2$ (**34**; boaDTDA = 4-(benzoxazol-2′-yl)-1,2,3,5-dithiadiazolyl), which contains two dithiadiazolyl radicals, exhibits slow magnetic relaxation with a barrier of $U_{eff} = 71\ cm^{-1}$ [302]. Here, the authors attribute the relaxation dynamics to a single supramolecular entity since the two radical ligands pair leading to weak antiferromagnetic coupling between the metal centers. The gadolinium analog was estimated to possess a coupling strength of $J_{Gd\text{–}Gd} < -0.007\ cm^{-1}$. The weak antiferromagnetic interaction between the two Dy^{III} ions can be compensated by the application of a 700 Oe dc field leading to two distinct relaxation modes. Alternatively, the origin of single-molecule magnet behavior may be the result of single-ion effects which is not discussed in the report (Fig. 31).

3.3.5. N_2^{3-} radical-bridged lanthanide complexes

3.3.5.1. Discovery and bonding in N_2^{3-}. The biggest success in the design of single-molecule magnets possessing high blocking temperatures has been achieved by bridging two lanthanide ions

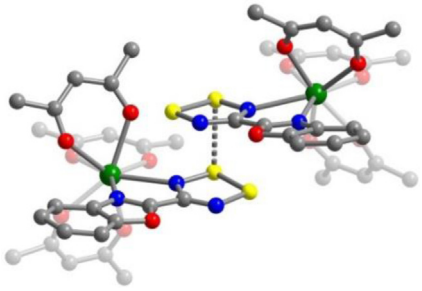

Fig. 31. Structure of $[Dy(hfac)_3(boaDTDA)]_2$ (**34**), with green, blue, red, yellow and carbon spheres representing Dy, N, O, S and C atoms, respectively; H and F atoms are omitted and selected C and O atoms are faded for clarity. The shortest intermolecular distance between S atoms is 2.901(4) Å.

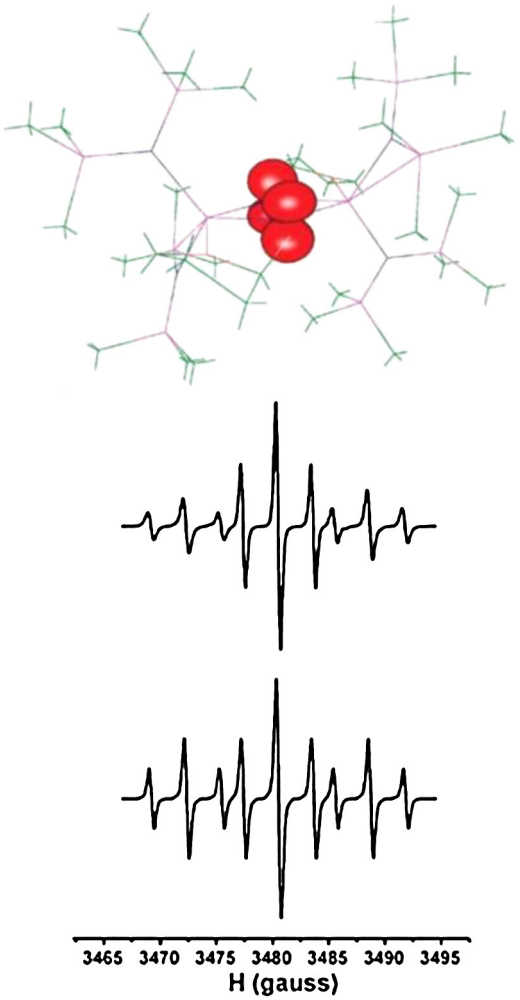

Fig. 32. Computed spin density (top) and X-EPR spectra (bottom) of $\{[(Me_3Si)_2N]_2(THF)Y\}_2(\mu\text{-}\eta^2\text{:}\eta^2\text{-}N_2)[K(THF)_6]$ **35**-$^{15}N_2$ at 293 K in millimolar THF solution.

Source: Figure was reproduced from Ref. [339], with permission of the copyright holders.

with a $N_2^{3-\bullet}$ radical anion, giving rise to an exchange bias with extraordinarily strong coupling. The dinuclear Y^{III} complexes in the salts $[K(THF)_6]\{[((Me_3Si)_2N)_2(THF)Y]_2(\mu\text{-}\eta^2\text{:}\eta^2\text{-}N_2)\}$ (**35**) and $K\{[((Me_3Si)_2N)_2(THF)Y]_2(\mu^3\text{-}\eta^2\text{:}\eta^2\text{:}\eta^2\text{-}N_2)\}$ allowed both a full experimental characterization and computation analysis due to the presence of diamagnetic metal ions [339]. The calculations performed on the N_2^{2-} congeners revealed that the N—N bonding in a diamagnetic N_2^{2-} unit arises from the formation of a 4d-π^* back-bonding interaction where the energetically high and diffuse, occupied 4d-orbital of yttrium interacts with one of the π^* orbitals of the N_2 unit. Hence, the lowest unoccupied molecular orbital of a N_2^{2-}-bridged complex results from the intrinsically unperturbed π^* orbital of N_2 that is perpendicular to the YN_2Y plane. By contrast, in a $N_2^{3-\bullet}$ bridged complex, this π^* orbital is occupied by a single electron, leading to a decrease of the bond order to 1.5 and the majority of the unpaired spin density is restricted to the N_2 unit. Moreover, EPR spectra featured a nine-line pattern, in accordance with a triplet of triplets that arises from the splitting by two ^{15}N ($I = 1/2$) and ^{89}Y ($I = 1/2$) nuclei. The hyperfine coupling constant 8.2 G for nitrogen is in good agreement with the other nitrogen-centered radicals (Fig. 32). The diffuse radical character of the $N_2^{3-\bullet}$ bridging ligand originates from electron–electron repulsions associated with the large negative formal charge and is

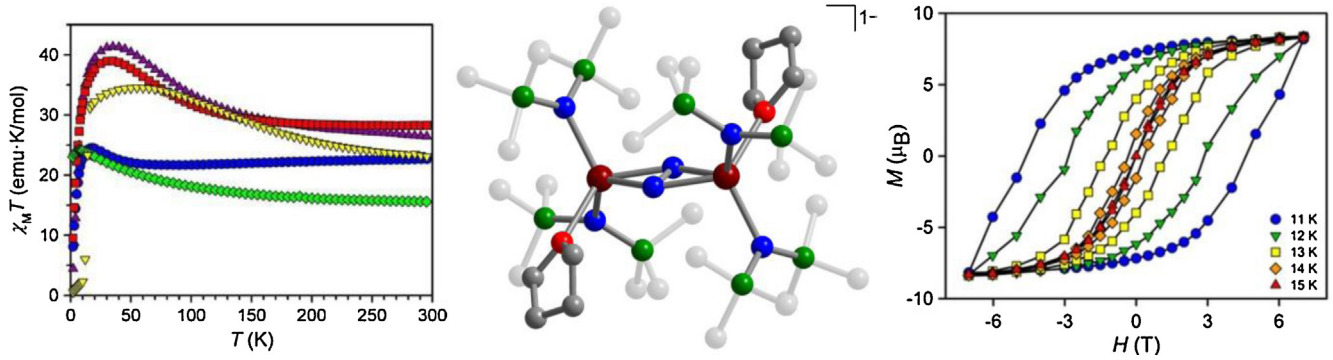

Fig. 33. Left: Dc magnetic susceptibility data for **36-Ln** with green, yellow, red, purple, and blue data for **36-Gd**, **36-Tb**, **36-Dy**, **36-Ho** and **36-Er**. Middle: structure of **36-Tb** with dark red, green, blue, red and gray spheres representing Tb, Si, N, O and C atoms, respectively. H atoms are omitted for clarity. Right: variable-field magnetization (*M*) data collected for **36-Tb** collected from 11 to 15 K at an average sweep rate of 0.9 mT/s.

Source: Figures (left and right) were reproduced from Ref. [301] with permission of the copyright holders.

anticipated to increase the exchange coupling with lanthanide ions substantially.

3.3.5.2. N_2^{3-} radical-bridged lanthanide complexes with outer-sphere K^+ ion. To probe the magnetism of $N_2^{3-\bullet}$ radical-bridged lanthanide compounds, the series of dinuclear lanthanide compounds [K(18-crown-6)]{[((Me$_3$Si)$_2$N)$_2$(THF)Ln]$_2$(μ-η^2:η^2-N$_2$)} (**36**, Ln = Gd, Tb, Dy, Ho and Er) was synthesized through the reduction of the corresponding N_2^{2-}-bridged complexes [((Me$_3$Si)$_2$N)$_2$(THF)Ln]$_2$(μ-η^2:η^2-N$_2$) with KC$_8$ in THF [290,301]. In these compounds, each complex anion features two Ln^{III} centers bridged by a $N_2^{3-\bullet}$ radical anion. Within the isostructural series, each metal ion resides in a pseudo-tetrahedral coordination environment, where one vertex is occupied by the $N_2^{3-\bullet}$ unit to give a planar Ln$_2$N$_2$ moiety.

As the temperature decreases from 300 K, a rise in $\chi_M T$ is apparent for **36-Ln**, indicative of strong antiferromagnetic lanthanide-radical exchange, followed by a gradual decrease in the data for **36-Gd**, **36-Ho** and **36-Er** and a precipitous drop for **36-Tb** and **36-Dy** (Fig. 33). Remarkably, a fit to the data for the Gd^{III} analog revealed by far the strongest exchange coupling yet observed for Gd^{III}, with $J = -27\ cm^{-1}$. Additionally, the precipitous drop in $\chi_M T$ for **36-Tb** and **36-Dy** at the low temperature indicates the onset of magnetic blocking, in which the strong magnetic anisotropy pinned the orientation of the total molecular spin, rendering it unresponsive to the magnetic field. Indeed, the sharp divergence apparent in zero-field and field-cooled data affirmed that the moments are effectively blocked.

In line with the observation of magnetic blocking, ac susceptibility data for **36-Dy** and **36-Tb** demonstrated that both are single-molecule magnets, with relaxation barriers of $U_{eff} = 123\ cm^{-1}$ and $227\ cm^{-1}$, respectively. Notably, the latter barrier is the highest yet reported for a multinuclear single-molecule magnet. By contrast, the holmium and erbium congeners **36-Ho** and **36-Er** afforded lower barriers of $U_{eff} = 73(6)\ cm^{-1}$ and $U_{eff} = 36(1)\ cm^{-1}$, respectively, and the latter required the application of a 1000 Oe dc field. The strong deviation from Arrhenius behavior was attributed to a much weaker coupling or weaker anisotropy stemming from the more spherical and contracted f electron densities of holmium and erbium.

Hysteresis loops obtained for **36-Dy** and **36-Tb** do not exhibit steps, demonstrating that strong coupling can successfully suppress tunneling pathways. The striking hysteresis loops for **36-Dy** and **36-Tb** are widely open up to 8.3 K and 14 K, respectively, with the latter representing by far the highest magnetic blocking temperature for any molecular species.

To better understand the remarkable blocking temperatures observed for **36-Dy** and **36-Tb**, DFT methods along with MO and NBO analysis were applied to probe the nature of the magnetic exchange interaction [340]. The computational results indicated that the unpaired electron in the N_2^{3-} unit resides in a π* orbital that is perpendicular to the {Gd$_2$N$_2$} plane. Furthermore, DFT analysis revealed that the coupling essentially arises from the strong overlap of the lanthanide 4f orbitals with the N_2^{3-} ligand orbitals (π^*_{py}) and gave a computed coupling constant of $J = -23.7\ cm^{-1}$, close to the experimental value of $J = -27\ cm^{-1}$. Importantly, NBO studies categorized the exchange mechanism to be direct (charge transfer).

Another DFT contribution including ab initio methods suggested that the slow magnetic relaxation in the parent molecules originates from strong Ln-N_2^{3-} coupling, which is antiferromagnetic for the Gd, Tb, Dy, and Ho species, but contradictory to the experimental result ferromagnetic for the Er congener (B3LYP) [341]. Here, however, the computed coupling constant of $J = -38.2\ cm^{-1}$ for **36-Ln** varies tremendously from the experimental value. Further, CASSCF calculations on molecular Ln-N_2^{3-} fragments attested that a synergy between strong Tb-N_2^{3-} coupling ($J = -145.8\ cm^{-1}$) and the largest energy barrier for a single Tb ion ($\Delta E_i = 133.1\ cm^{-1}$) gave rise to the highest U_{eff} for **36-Ln**. Moreover, the energy barrier for a single Er ion ($\Delta E_i = 92.3\ cm^{-1}$) was computed to be the second largest in magnitude, however, the weak Er-N_2^{3-} coupling ($J = 28.8\ cm^{-1}$) leads to the small U_{eff} for the Er species among the series **36-Tb** through **36-Er**. Enhancing both the strength of the lanthanide-radical coupling and the single-ion anisotropy was proposed to increase the spin relaxation barrier of exchange-coupled lanthanide single-molecule magnets.

The third computational approach yielded values of $2J = 21$, 83 and $102\ cm^{-1}$ for the Dy, Ho and Er species, similar to their experimentally determined relaxation barriers of $U_{eff} = 36$, 73 and $123\ cm^{-1}$ [325]. The Hubbard Molecule Model employed to elucidate the strong exchange interaction suggested two strategies to enhance the coupling. The first focuses on lessening the electron repulsion by matching redox properties of the lanthanide and the radical. The selection of lanthanides with their intrinsic large negative reduction potentials to couple with certain radical ligands hinges on the accessibility of the metal oxidation state. Pairing strongly reducing ligands (like N_2^{3-} or bipy) with lanthanides that are stable in their divalent oxidation state (Nd, Eu, Sm, Dy, Tm, Yb) or coupling strongly oxidizing ligands to lanthanides with accessible tetravalent oxidation state (Ce, Pr, Tb) is proposed to lower the electron repulsion. The second strategy suggested that increasing the overlap between the metal and the radical ligand results in the stabilization of the bonding orbital. Albeit no definite solution is

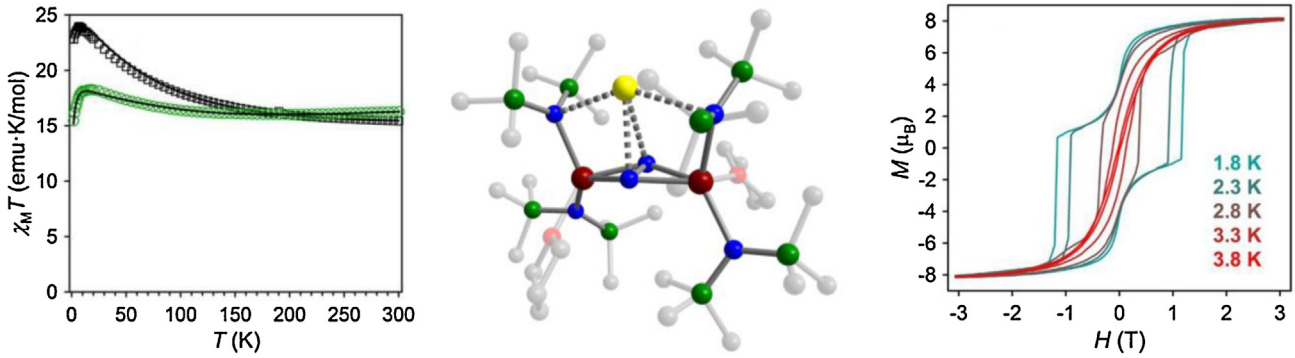

Fig. 34. Left: Dc magnetic susceptibility data for **37-Gd** (black circles) and **37-Gd** (green circles). Middle: structure of **37-Tb** with dark red, green, blue, red, gray and yellow spheres representing Tb, Si, N, O, C and K atoms, respectively. H atoms are omitted for clarity. Right: variable-field magnetization (*M*) data collected for Tb-X, collected from 1.8 to 3.8 K at an average sweep rate of 1 mT/s.

Source: Figures (left and right) were reproduced from Ref. [291] with permission of the copyright holders. Images (left and right) taken from Ref. [282].

proposed for lanthanides, note that the latter strategy is conceivably feasible with the use of actinides since the radical radial wave extensions of 5f orbitals is substantially greater than the lanthanide 4f orbitals.

3.3.5.3. N_2^{3-} radical-bridged lanthanide complexes with an inner-sphere K^+ ion. Computations suggest that the coupling in **36** arises from direct overlap of the 4f orbitals with the N_2^{3-} ligand orbitals [340]. As such, a weaker coupling may result if the dihedral angle between the lanthanide and the radical ligand deviates from planarity. This effect was probed by a second family of $N_2^{3-\bullet}$ radical-bridged dilanthanide compounds of formula $K[(R_2N)_2(THF)Ln]_2(\mu^3\text{-}\eta^2\text{:}\eta^2\text{-}N_2)$ (**37-Ln**; Ln = Gd, Tb, Dy and R = $SiMe_3$), synthesized from chemical reductions of N_2^{2-}-bridged $[(R_2N)_2(THF)Ln]_2(\mu\text{-}\eta^2\text{:}\eta^2\text{-}N_2)$ with KC_8 [291].

Notably, the inner-sphere potassium counterion exhibits a distance of 2.9 Å to the $N_2^{3-\bullet}$ radical, resulting in a folding of the planar $N_2^{3-\bullet}$ unit in **37-Ln**. This bending leads to dihedral angles between the two LnN_2 planes of 13.64°, 16.12° and 15.27° in the Gd, Tb and Dy species, respectively, and influences the magnetic behavior of **37-Ln** dramatically. The molar susceptibility of **37-Gd** ascends up to a lower maximum of 18.25 cm^3 K/mol vs 24.38 cm^3 K/mol found for **36-Gd** (Fig. 34). While the antiferromagnetic Gd-radical coupling of $J = -27.1(4)\ cm^{-1}$ is similar to the parent **36-Gd**, the bending in the $Gd^{III}(N_2^{3-\bullet})Gd^{III}$ unit presumably facilitates superexchange through the $N_2^{3-\bullet}$ ligand and therefore causes a sizable antiferromagnetic Gd–Gd coupling, with $J' = -2.28(1)\ cm^{-1}$. This effect leads to an $S = 9/2$ ground state that is only separated from the first excited state ($S = 11/2$) by 0.29 cm^{-1}. Moreover, the relaxation for the **37-Tb** and **37-Dy** primarily proceeds through a thermally activated Orbach process that affords $U_{eff} = 41.13(4)\ cm^{-1}$ and 14.95(8) cm^{-1}, respectively. Further, the hysteresis loops for **37-Tb** are open up to 3.8 K exhibiting at 1.8 K a remanent magnetization of 4.28 μ_B and a coercive field of 1.1 T (Fig. 34). The steps in the hysteresis loops stem from little separation between ground and first excited state as a result of antiferromagnetic Tb^{III}–Tb^{III} coupling or from significant dipolar interactions leading to tunneling at zero fields.

3.3.6. 2,2-Bipyrimidine radical-bridged lanthanide complexes

While engendering strong coupling in lanthanide complexes, the highly reactive $N_2^{3-\bullet}$ unit presents a synthetic challenge in building larger clusters or extended networks. In addition, synthetic modifications on $N_2^{3-\bullet}$ to enhance the magnetic exchange are not feasible. Thus, the exploration of more stable organic radical ligands that could possibly deliver similar coupling strengths is necessary. For instance, 2,2-bipyrimidyl radical anion has recently been shown to facilitate strong coupling with two lanthanide ions in the complexes $[(Cp^*_2Ln)(\mu\text{-bpym}^\bullet)]^+$ (**38-Ln**; Ln = Gd, Tb, Dy; Fig. 35) [289]. Consistent with radical character, the central C—C bond distance of the bpym unit is short at ca. 1.40 Å. Computed LUMO molecular orbital for bpym revealed that the radical spin orbital of bpym has major contributions from both in-phase $2p_z$ orbitals on the central two C atoms and opposite phase from the $2p_z$ orbitals on the four N atoms.

A fit to the variable-temperature dc susceptibility data collected for **38-Gd** revealed the presence of antiferromagnetic coupling between the Gd^{III} centers and the bridging $bpym^{-\bullet}$ ligand, with $J = -10\ cm^{-1}$. This value is the largest yet reported for an organic radical coupled to a Gd^{III} center, and second overall only to the $J = -27\ cm^{-1}$ observed in the $N_2^{3-\bullet}$ radical-bridged complex.

Despite the presence of strong coupling, tunneling pathways are apparent in the ac data of **38-Tb** below 3 K. Nevertheless, the higher-temperature data indicated a relaxation barrier of

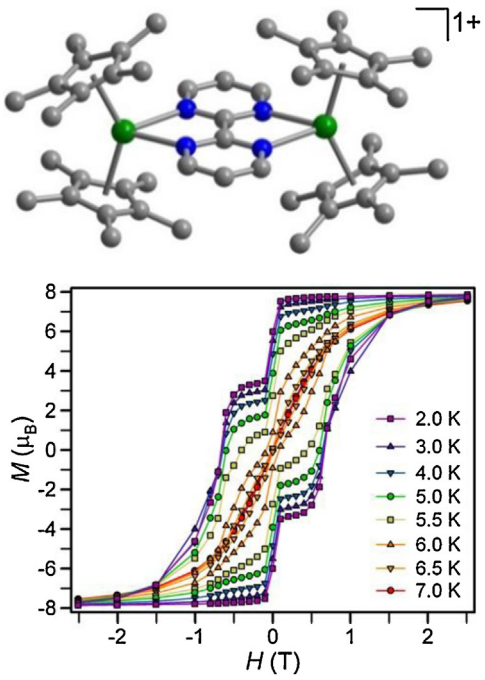

Fig. 35. Top: structure of $[(Cp^*_2Dy)_2(\mu\text{-bpym}^\bullet)]^+$ (**38-Dy**), with green, blue and gray spheres representing Dy, N, and C atoms, respectively; H atoms are omitted for clarity. Bottom: variable-field magnetization data collected for **38-Dy** at various temperatures and an average sweep rate of 0.002 T/s.

Source: Figure was reproduced from Ref. [289], with permission of the copyright holders.

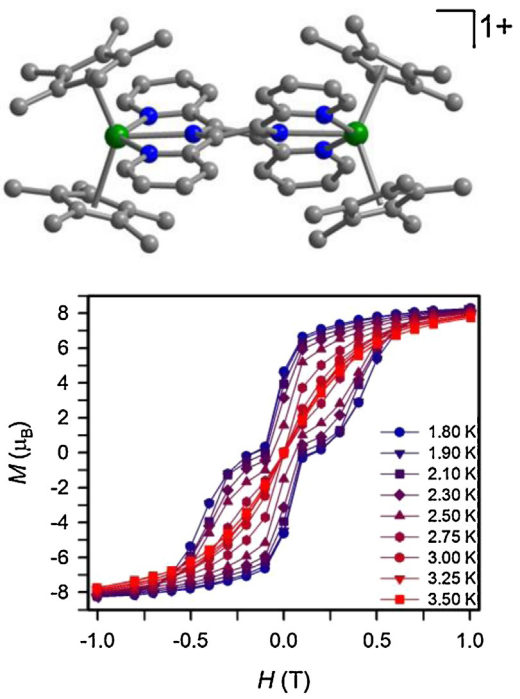

Fig. 36. Top: structure of $[(Cp^*_2Dy)_2(\mu\text{-ttpz}^{\bullet})]^+$ (**39-Dy**), with green, blue, and gray spheres representing Dy, N, and C atoms, respectively; H atoms are omitted for clarity. Bottom: variable-field magnetization data collected for **39-Dy** at various temperatures and an average sweep rate of 0.003 T/s.

Source: Reproduced by permission of The Royal Society of Chemistry [288]. http://pubs.rsc.org/en/Content/ArticleLanding/2014/SC/C4SC02154A#!divAbstract.

$U_{eff} = 44(2)\,cm^{-1}$. In contrast, the ac measurements for **38-Dy** revealed solely thermally activated dynamics in the temperature range 7.5–17.5 K, with $U_{eff} = 87.8(3)\,cm^{-1}$.

3.3.7. Tetra-2-pyridinylpyrazine radical-bridged lanthanide complexes

In order to further probe the nature of magnetic exchange between lanthanide ions and radical spin centers, dinuclear lanthanide complexes with multi-electron redox-active ligands have been explored. Specifically, owing to its bridging capability and propensity to accept multiple electrons, tetra-2-pyridinylpyrazine (tppz) was employed in the synthesis of the complexes $[(Cp^*_2Ln)_2(\mu\text{-tppz}^{\bullet})]^+$ (**39-Ln**; Ln = Gd, Tb, Dy) and $[(Cp^*_2Ln)_2(\mu\text{-tppz}^{\bullet})]^-$ (**40-Ln**; Ln = Gd, Tb, Dy), which contain bridging mono- and trianionic radicals, $tppz^{3-\bullet}$ and $tppz^{3-\bullet}$, respectively [288]. The coupling constant of $J_{Gd-L} = -6.91(4)\,cm^{-1}$ observed for **39-Gd** is smaller than those of the $bpym^{\bullet-}$ and $N_2^{3-\bullet}$ radical-bridged complexes, which is expected given the larger region over which the electron is delocalized. Complex **39-Dy** shows single-molecule magnet behavior at low temperature, with $U_{eff} = 35.9(2)\,cm^{-1}$, significantly larger than that of $U_{eff} = 5.1(1)\,cm^{-1}$ determined for **39-Tb**. Moreover, **39-Dy** displayed open hysteresis loops at zero field at temperatures below 3.25 K with a coercive field of $H_c = 0.1$ T at 1.8 K (Fig. 36). While the coupling between Ln^{III} center and $tppz^{3-\bullet}$ is strong enough to suppress a small degree of quantum tunneling, the steps apparent in the hysteresis curves indicate that tunneling pathways are nonetheless still present in the system.

For **40-Gd**, a value of $J = -6.29(3)\,cm^{-1}$ was determined, smaller but comparable to the $tppz^{-\bullet}$ analog. The calculated SOMOs of $tppz^{-\bullet}$ and $tppz^{3-\bullet}$ of an yttrium-containing model compound offered an explanation for this unanticipated result, as it revealed a perpendicular orientation of the π-interactions to the Ln–Ln axis, whereas in $tppz^{3-\bullet}$ most intra-ligand π-bonding interactions are oriented parallel to the Ln–Ln axis. Finally, neither **40-Tb** nor **40-Dy** exhibited slow magnetic relaxation, likely a result of the symmetry change of the electron/spin bearing orbitals provided by the above calculations.

4. Exchange in actinide complexes

4.1. Introduction

An exciting route to the synthesis of single-molecule magnets with higher blocking temperatures involves the incorporation of actinide elements, owing to their large spin-orbit coupling and appreciable metal–ligand covalency [342]. Additionally, in contrast to lanthanides, actinides provide a wide range of accessible oxidation states [320]. However, only a few actinide complexes have been shown to exhibit slow magnetic relaxation, with nearly all of these being uranium complexes [343–351]. Nevertheless, despite the difficulties associated with handling of the more radioactive transuranic elements, neptunium and plutonium-based single-molecule magnets have also been reported [352–354].

As a common approach in designing mononuclear actinide-based magnets, a qualitative method of matching ligand field symmetry with the electron density distribution of the maximal M_J state has been proposed [355]. This strategy led to the isolation of the first actinide-containing single-molecule magnets that possesses axial ligand fields [347,348]. Moreover, exchange coupling has been estimated in U^{IV} and U^{V} complexes [356–361] with coupling constants of up to $|J| = 48\,cm^{-1}$, however, the presence of single-molecule magnet behavior has not been reported in these compounds. Another approach to the design of single-molecule magnets involves strong superexchange in actinyl systems via well-established cation–cation interactions, such as that observed in the mixed-valence neptunyl cluster compound $(NpO_2Cl_2)[NpO_2Cl(THF)_3]_2$ [352]. The coupling constant for the Np^{IV}-Np^{V} interaction was reported as $J = 7.5\,cm^{-1}$, an order of magnitude larger than the typical superexchange in multinuclear lanthanide complexes, ultimately leading to a high relaxation barrier of $U_{eff} = 97\,cm^{-1}$. Superexchange was also observed in a large 5f-3d $U_{12}Mn_6$ wheel-shaped cluster complex, exhibiting open hysteresis loops up to 4 K and a spin relaxation barrier of $99\,cm^{-1}$, representing the highest barrier yet observed in an actinide-containing single-molecule magnet [362].

Given the observed strong coupling in actinide complexes induced by exchange or superexchange involving cation–cation interactions [352,362–364], the use of radical ligands promises to yield even higher magnetic blocking temperatures. Indeed, owing to their large single-ion anisotropies and the greater radical extension of 5f valence orbitals, the better overlap between metal and radical ligands should lead to much stronger coupling than observed for lanthanide-based systems. However, radical-containing actinide species are scarce since their synthesis is challenging due to the redox activity of the early actinides. The few known examples of radical-containing uranium compounds are presented below.

4.2. Radical-containing uranium complexes

Reduction of Tp^*_2UI (Tp^* = hydrotris(3,5-dimethylpyrazolyl) borate) with KC_8 in the presence of 2,2′-bipyridine affords the U^{III} bipyridyl radical complex, $Tp^*_2U(2,2'\text{-bpy}^{-\bullet})$, **41**, Fig. 37 [365]. This uranium complex displays slow magnetic relaxation under zero dc field with an $U_{eff} = 19.8\,cm^{-1}$ ($U_{eff} = 22.6\,cm^{-1}$, 0.05 T) [366]. The spin relaxation barrier measured at zero field is slightly higher than that of the complex containing the non-radical bipyridyl ligand [345].

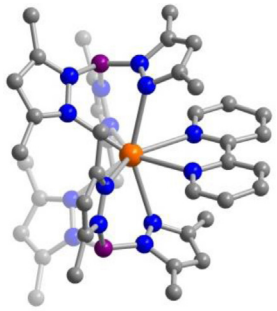

Fig. 37. Structure of $Tp^*_2U(2,2'\text{-bpy}^{-\bullet})$ (41), with orange, blue, purple and gray spheres representing U, N, B and C atoms, respectively; H atoms are omitted for clarity; selected C and B atoms are faded for clarity.

The U^{III} complex bearing the hexadentate ligand (1,4,7-tris(3-adamantyl-5-*tert*-butyl-2-hydroxybenzyl)-1,4,7-triazacyclonane) ($(^{Ad}ArO)_3tacn$) was shown to reduce CO_2 by one electron to form the U^{IV} radical complex ($(^{Ad}ArO)_3tacn)U^{IV}(CO_2^{-\bullet})$ (**42**; Fig. 38) [367]. Variable-temperature magnetic susceptibility data for **42** were compared with the analogous data of the U^{IV} azide complex, $(^{Ad}ArO)_3tacn)U^{IV}(N_3)$. The corresponding plots of μ_{eff} vs T for the two compounds are nearly identical from 300 K to 120 K. Below 120 K, the μ_{eff} data for the azide complex drops sharply until it reaches ca. 0.7 μ_B at 5 K while that of uranium CO_2 radical complex rests at 1.5 μ_B at 5 K. The increased magnetic moment of the $U{-}CO_2^{-\bullet}$ complex compared to $U{-}N_3$ at 5 K was attributed to the single unpaired electron residing on CO_2. Furthermore, the similar μ_{eff} vs T behavior above 120 K for both complexes may indicate antiferromagnetic coupling between the U^{IV} center and unpaired electron on CO_2 ligand. The same research group later reported the one-electron reduction of diphenyldiazomethane by trivalent $((^{t\text{-}Bu}ArO)_3tacn)U^{III}$ ($(^{t\text{-}Bu}ArO)_3tacn$ = 1,4,7-tris(3,5-di-*tert*-butyl-2-hydroxybenzyl)-1,4,7-triazacyclononane) to produce the uranium radical complex, $((^{t\text{-}Bu}ArO)_3tacn)U^{IV}(Ph_2CN_2^{-\bullet})$. Here, a μ_{eff} of 1.75 μ_B at 4 K was also attributed to the ligand-centered radical. In a related reaction, one-electron reduction of Ph_2CN_2 by $(^{Ad}ArO)_3tacn)U^{III}$ prompted aryl C—H activation to form the U^{IV} indazole complex ($(^{Ad}ArO)_3tacn)U(\eta^2\text{-3-phen(Ind)})$. A uranium radical intermediate, $[(^{Ad}ArO)_3tacn]U^{IV}(Ph_2CN_2^{-\bullet})$, was invoked in formation of the C—H activated product, however, it was too reactive to be isolated. A related trivalent system, $((^{t\text{-}Bu}ArO)_3tacn)U$, was found to also singly reduce di-*tert*-butylbenzophenone affording $((^{t\text{-}Bu}ArO)_3tacn)U^{IV}(^{\bullet}OC(t\text{-}BuPh)_2)$ [368]. The low-temperature range of the μ_{eff} vs T plot shows a similar trend compared to $U{-}CO_2^{\bullet}$ and $(^{Ad}ArO)_3tacn)U^{IV}(Ph_2CN_2^{\bullet})$ complexes where an elevated magnetic moment of 1.61 μ_B at 5 K was due to the unpaired spin on the benzophenone ligand. Coupling between the uranium center and radical ligand was not apparent but may be possible based on calculations that show a SOMO comprising both metal and ligand character. A trivalent uranium benzophenone radical complex, $[Tp^*_2U(OC^{\bullet}Ph_2)]$, was also recently reported [369].

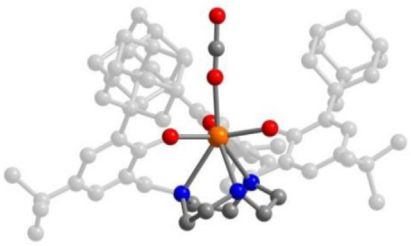

Fig. 38. Structure of $((^{Ad}ArO)_3tacn)U^{IV}(CO_2^{\bullet-})$ (**42**), with orange, blue, red and gray spheres representing U, N, O and C atoms, respectively; H atoms, adamantyl groups and *t*Bu groups on phenyl rings are omitted for clarity; selected carbon atoms are faded for clarity.

The uranium(III) terpyridyl radical complex $U(Cp^*)_2(terpy^{\bullet})$, synthesized from a one-electron reduction of $[U(Cp^*)_2(terpy)]^+$ with Na/Hg, represents the first instance where magnetic exchange interaction was observed between a U^{III} center and radical, as evidenced by a precipitous drop in $\chi_M T$ below 20 K [370]. The respective uranium(III) bipyridyl radical congener, $Cp^*_2U(bipy^{\bullet})$ was also furnished through reduction of $Cp^*_2UI(bipy)$ with Na/Hg [370]. Similarly, reduction of Cp'_2UCl_2 (Cp′ = 1,2,4-tri-*tert*-butyl cyclopentadienyl) with 2 equiv of Na/naphthalene yields U(III) bipyridiyl radical complex, $Cp'_2U(bipy^{\bullet})$ [371].

The uranium(IV) bis(amidophenolate) complexes $(^{R}ap)_2U(THF)_2$ (R = *t*-butyl, adamantyl) bind halogens via "oxidative addition" induced by the amidophenolate ligands to afford the corresponding uranium(IV) iminobenzosemiquinone radical complexes $[(^{R}isq)_2UCl]_2(\mu_2\text{-}Cl)_2$ [372]. The radical ligand was confirmed by both electronic absorption spectra that show the characteristic $\pi{-}\pi^*$ transitions between 700 and 800 nm for the open-shell, iminosemiquinone ligand, and by X-ray crystallography, which revealed the expected bond distortions for a radical species. A diisopropyl-substituted uranium(IV) bis(amidophenolate) complex was shown to undergo a similar oxidative addition in the presence of $PhICl_2$, giving rise to a transient iminosemiquinone containing uranium complex.

The redox-active pyridine(diimine) ligand, $^{Mes}PDI^{Me}$, has been employed in the formation of two series of uranium(IV) complexes that contain either ancillary Cp^* or 1-(7,7-dimethylbenzyl)cyclopentadienyl (Cp^P) ligand. The multielectron redox capacity of the $^{Mes}PDI^{Me}$ ligand in these complexes enabled the storage of electrons and their subsequent employment in carbon–carbon bond formation reactions with benzophenone and aldehyde substrates. Magnetic susceptibility measurements performed on the uranium(IV) radical complexes $Cp^PUI_2(^{Mes}PDI^{Me})$ and $Cp^PU(O_2C_2Ph_4)(^{Mes}PDI^{Me})$ revealed moments of 1.25 μ_B and 1.44 μ_B at 5 K, respectively. In both cases, the lower than expected moment for a single radical electron (1.73 μ_B) was attributed to weak antiferromagnetic interaction between the U^{IV} ion and the ligand-centered radical.

Reductive elimination was observed in the reaction between $U(CH_2Ph)_4$ and the iminoquinone ligand 4,6-di-*t*-butyl-2-[(2,6-diisopropylphenyl)-imino]quinone (^{dipp}iq). This reaction proceeds through a purported uranium(IV) iminosemiquinone radical intermediate that reductively eliminates bibenzyl to generate a uranium(IV) amidophenolate bis(benzyl) complex. The viability of the intermediate was probed by synthesizing the uranium(IV) complex $UI_3(THF)_2(^{dipp}iq^{-\bullet})$ and treating it with benzyl potassium, whereupon the uranium(IV) amidophenolate bis(benzyl) complex was regenerated along with 0.5 equiv of bibenzyl. Variable-temperature magnetization data collected on $UI_3(THF)_2(^{dipp}iq^{-\bullet})$ revealed an effective magnetic moment of 3.23 μ_B at 300 K and 1.50 μ_B at 2 K. The elevated moment at 2 K was assigned to the single unpaired electron residing on the ligand, much like previously reported complexes $((^{Ad}ArO)_3tacn)U^{IV}(CO_2^{-\bullet})$, $((^{t\text{-}Bu}ArO)_3tacn)U^{IV}(Ph_2CN_2^{-\bullet})$, and $((^{t\text{-}Bu}ArO)_3tacn)U^{IV}\text{-}(^{-\bullet}OC(t\text{-}BuPh)_2)$.

While dc magnetic susceptibility measurements on the aforementioned uranium-radical compounds have been performed, the corresponding dynamic magnetic susceptibility data have not yet been reported.

5. Concluding remarks

Strong coupling to yield high-spin ground states along with effective suppression of fast quantum tunneling pathways and

isolated spin ground states are requisites in the design of single-molecule magnets that exhibit high blocking temperatures. The foregoing discussion surveys the current state of research into ligand-radical containing single-molecule magnets and highlights other classes of ligand radical-containing metal complexes that may be exploiting in the design of future single-molecule magnets. Indeed, the work highlighted above has demonstrated the impact of radical ligands on exchange interactions and also slow magnetic relaxation. Depending on the nature of both the radical unit and the metal centers, strong coupling was shown both to isolate the spin ground state and to quench quantum tunneling of the magnetization. Moreover, more reducing radical ligands such as azophenine$^{3-\bullet}$, bipyrimidine$^{1-\bullet}$ and $N_2^{3-\bullet}$ have been shown to afford even stronger coupling than other ligand radicals. In addition, the nature of the incorporated metal ion involved in exchange coupling is of utmost importance with respect to engendering magnetic hysteresis at higher temperatures. Along this line, high-anisotropy metal ions hold the greatest promise in the design of single-molecule magnets that operate at high temperatures, in particular lanthanide and actinide ions, but possibly also transition metal ions with enhanced spin-orbit coupling through ligand field considerations.

One particular line of research that can perhaps be exploited more in the future is the synthesis of radical ligand-containing actinide complexes. Actinide ions are particularly attractive in that the spin-orbit coupling is approximately twice that of the lanthanides, giving rise to much larger single-ion anisotropies compared to both transition metals and lanthanides. Furthermore, the greater radial extension of the 5f valence orbitals can better facilitate magnetic exchange through enhanced overlap with radical-ligands, potentially leading to much stronger coupling than observed for lanthanide-based systems. An increase of magnetic exchange coupling could potentially give rise to longer relaxation times and thus, higher blocking temperatures. In addition, the wide range of accessible oxidation states for the early actinides makes the usage of oxidizing and reducing ligands conceivable in the design of single-molecule magnets that operate at higher temperatures [325]. Specifically, metal centers featuring the electron configuration $5f^3$ (e.g. U^{III}, Np^{IV} and Pu^{V}) or $5f^1$ (e.g. U^{V}, Np^{VI}) are of particular interest. Unfortunately, the synthetic strategies employed for lanthanide systems often cannot be directly applied to actinides owing to the much greater reactivity of trivalent actinides, such as U^{III} compared to Ln^{III}. As such, the development of radical ligand-containing actinide complexes as single-molecule magnets offers a formidable yet exciting challenge to synthetic chemists.

Conflict of interest

The authors declare no competing financial interest.

Acknowledgment

This research was funded by the National Science Foundation through grants CHE-1111900 (JRL) and DMR-1351959 (TDH).

References

[1] L. Bogani, W. Wernsdorfer, Nat. Mater. 7 (2008) 179–186.
[2] W. Liang, M.P. Shores, M. Bockrath, J.R. Long, H. Park, Nature 417 (2002) 725–729.
[3] M.-H. Jo, J.E. Grose, K. Baheti, M.M. Deshmukh, J.J. Sokol, E.M. Rumberger, D.N. Hendrickson, J.R. Long, H. Park, D.C. Ralph, Nano Lett. 6 (2006) 2014–2020.
[4] H.B. Heersche, Z. de Groot, J.A. Folk, H.S.J. van der Zant, C. Romeike, M.R. Wegewijs, L. Zobbi, D. Barreca, E. Tondello, A. Cornia, Phys. Rev. Lett. 96 (2006) 206801.
[5] M. Urdampilleta, N.-V. Nguyen, J.-P. Cleuziou, S. Klyatskaya, M. Ruben, W. Wernsdorfer, Int. J. Mol. Sci. 12 (2011) 6656–6667.
[6] S. Thiele, R. Vincent, M. Holzmann, S. Klyatskaya, M. Ruben, F. Balestro, W. Wernsdorfer, Phys. Rev. Lett. 111 (2013) 037203.
[7] M. Mannini, F. Pineider, P. Sainctavit, C. Danieli, E. Otero, C. Sciancalepore, A.M. Talarico, M.-A. Arrio, A. Cornia, D. Gatteschi, R. Sessoli, Nat. Mater. 8 (2009) 194–197.
[8] A. Ardavan, S.J. Blundell, J. Mater. Chem. 19 (2009) 1754–1760.
[9] C.T. Lyons, T.D.P. Stack, Coord. Chem. Rev. 257 (2013) 528–540.
[10] R.G. Hicks, Stable Radicals – Fundamentals and Applied Aspects of Odd-Electron Compounds, John Wiley and Sons, Ltd., United Kingdom, 2010.
[11] W. Kaim, B. Schwederski, Coord. Chem. Rev. 254 (2010) 1580–1588.
[12] S. Sproules, K. Wieghardt, Coord. Chem. Rev. 255 (2011) 837–860.
[13] W. Kaim, Inorg. Chem. 50 (2011) 9752–9765.
[14] M. Abe, Chem. Rev. 113 (2013) 7011–7088.
[15] O.R. Luca, R.H. Crabtree, Chem. Soc. Rev. 42 (2013) 1440–1459.
[16] M.L. Kirk, D.A. Shultz, Coord. Chem. Rev. 257 (2013) 218–233.
[17] W.I. Dzik, X.P. Zhang, B. de Bruin, Inorg. Chem. 50 (2011) 9896–9903.
[18] S. Kaizaki, Bull. Chem. Soc. Jpn. 76 (2003) 673–688.
[19] S. Kaizaki, Coord. Chem. Rev. 250 (2006) 1804–1818.
[20] K.E. Torraca, L. McElwee-White, Coord. Chem. Rev. 206–207 (2000) 469–491.
[21] A.I.O. Suarez, V. Lyaskovskyy, J.N.H. Reek, J.I. van der Vlugt, B. de Bruin, Angew. Chem. Int. Ed. 52 (2013) 12510–12529.
[22] H.L.C. Feltham, S. Brooker, Coord. Chem. Rev. 276 (2014) 1–33.
[23] P. Zhang, Y.-N. Guo, J. Tang, Coord. Chem. Rev. 257 (2013) 1728–1763.
[24] Y.-N. Guo, G.-F. Xu, Y. Guo, J. Tang, Dalton Trans. 40 (2011) 9953–9963.
[25] P. Zhang, L. Zhang, J. Tang, Curr. Inorg. Chem. 3 (2013) 101–111.
[26] L. Ungur, S.-Y. Lin, J. Tang, L.F. Chibotaru, Chem. Soc. Rev. 43 (2014) 6894–6905.
[27] S.-Y. Lin, J. Tang, Polyhedron 83 (2014) 185–196.
[28] R.A. Layfield, Organometallics 33 (2014) 1084–1099.
[29] D.N. Woodruff, R.E.P. Winpenny, R.A. Layfield, Chem. Rev. 113 (2013) 5110–5148.
[30] F. Habib, M. Murugesu, Chem. Soc. Rev. 42 (2013) 3278–3288.
[31] R. Sessoli, H.L. Tsai, A.R. Schake, S. Wang, J.B. Vincent, K. Folting, D. Gatteschi, G. Christou, D.N. Hendrickson, J. Am. Chem. Soc. 115 (1993) 1804–1816.
[32] T. Lis, Acta Crystallogr. Sect. B 36 (1980) 2042–2046.
[33] A. Caneschi, D. Gatteschi, R. Sessoli, A.L. Barra, L.C. Brunel, M. Guillot, J. Am. Chem. Soc. 113 (1991) 5873–5874.
[34] R. Sessoli, D. Gatteschi, A. Caneschi, M.A. Novak, Nature 365 (1993) 141–143.
[35] S.L. Castro, Z. Sun, C.M. Grant, J.C. Bollinger, D.N. Hendrickson, G. Christou, J. Am. Chem. Soc. 120 (1998) 2365–2375.
[36] S.M.J. Aubin, N.R. Dilley, L. Pardi, J. Krzystek, M.W. Wemple, L.-C. Brunel, M.B. Maple, G. Christou, D.N. Hendrickson, J. Am. Chem. Soc. 120 (1998) 4991–5004.
[37] A.L. Barra, A. Caneschi, A. Cornia, F. Fabrizi de Biani, D. Gatteschi, C. Sangregorio, R. Sessoli, L. Sorace, J. Am. Chem. Soc. 121 (1999) 5302–5310.
[38] E.K. Brechin, M. Soler, J. Davidson, D.N. Hendrickson, S. Parsons, G. Christou, Chem. Commun. (2002) 2252–2253.
[39] C. Dendrinou-Samara, M. Alexiou, C.M. Zaleski, J.W. Kampf, M.L. Kirk, D.P. Kessissoglou, V.L. Pecoraro, Angew. Chem. Int. Ed. 42 (2003) 3763–3766.
[40] J.R. Long, in: P. Yang (Ed.), Chemistry of Nanostructured Materials, World Scientific, Hong Kong, 2003, pp. 291–315.
[41] E.M. Rumberger, S.J. Shah, C.C. Beedle, L.N. Zakharov, A.L. Rheingold, D.N. Hendrickson, Inorg. Chem. 44 (2005) 2742–2752.
[42] H. Oshio, N. Hoshino, T. Ito, M. Nakano, J. Am. Chem. Soc. 126 (2004) 8805–8812.
[43] S. Maheswaran, G. Chastanet, S.J. Teat, T. Mallah, R. Sessoli, W. Wernsdorfer, R.E.P. Winpenny, Angew. Chem. Int. Ed. 44 (2005) 5044–5048.
[44] N.E. Chakov, S.-C. Lee, A.G. Harter, P.L. Kuhns, A.P. Reyes, S.O. Hill, N.S. Dalal, W. Wernsdorfer, K.A. Abboud, G. Christou, J. Am. Chem. Soc. 128 (2006) 6975–6989.
[45] C.J. Milios, A. Vinslava, W. Wernsdorfer, S. Moggach, S. Parsons, S.P. Perlepes, G. Christou, E.K. Brechin, J. Am. Chem. Soc. 129 (2007) 2754–2755.
[46] T.C. Stamatatos, V. Nastopoulos, A.J. Tasiopoulos, E.E. Moushi, W. Wernsdorfer, G. Christou, S.P. Perlepes, Inorg. Chem. 47 (2008) 10081–10089.
[47] C. Lampropoulos, G. Redler, S. Data, K.A. Abboud, S. Hill, G. Christou, Inorg. Chem. 49 (2010) 1325–1336.
[48] D.I. Alexandropoulos, C. Papatriantafyllopoulou, G. Aromí, O. Roubeau, S.J. Teat, S.P. Perlepes, G. Christou, T.C. Stamatatos, Inorg. Chem. 49 (2010) 3962–3964.
[49] M. Hołyńska, N. Frank, C. Pichon, I.-R. Jeon, R. Clérac, S. Dehnen, Inorg. Chem. 52 (2013) 7317–7319.
[50] A. Caneschi, D. Gatteschi, R. Sessoli, P. Rey, Acc. Chem. Res. 22 (1989) 392–398.
[51] C.G. Pierpont, Coord. Chem. Rev. 219–221 (2001) 415–433.
[52] C.G. Pierpont, Coord. Chem. Rev. 216–217 (2001) 99–125.
[53] C.G. Pierpont, R.M. Buchanan, Coord. Chem. Rev. 38 (1981) 45–87.
[54] A. Caneschi, D. Gatteschi, P. Rey, in: S.J. Lippard (Ed.), Progress in Inorganic Chemistry, John Wiley & Sons, Inc., 1991, pp. 331–429.
[55] B.D. Koivisto, R.G. Hicks, Coord. Chem. Rev. 249 (2005) 2612–2630.
[56] K.E. Preuss, Dalton Trans. (2007) 2357–2369.
[57] N. Koga, S. Karasawa, Bull. Chem. Soc. Jpn. 78 (2005) 1384–1400.
[58] W. Kaim, M. Moscherosch, Coord. Chem. Rev. 129 (1994) 157–193.
[59] L. Ballester, A. Gutiérrez, M.F. Perpiñán, M.T. Azcondo, Coord. Chem. Rev. 190–192 (1999) 447–470.
[60] J.M. Manriquez, G.T. Yee, R.S. McLean, A.J. Epstein, J.S. Miller, Science 252 (1991) 1415–1417.
[61] W.E. Broderick, J.A. Thompson, E.P. Day, B.M. Hoffman, Science 249 (1990) 401–403.

[62] J.S. Miller, J.C. Calabrese, R.S. McLean, A.J. Epstein, Adv. Mater. 4 (1992) 498–501.
[63] P.J. Kunkeler, P.J. van Koningsbruggen, J.P. Cornelissen, A.N. van der Horst, A.M. van der Kraan, A.L. Spek, J.G. Haasnoot, J. Reedijk, J. Am. Chem. Soc. 118 (1996) 2190–2197.
[64] J.S. Miller, A.J. Epstein, Chem. Commun. (1998) 1319–1325.
[65] H. Zhao, R.A. Heintz, X. Ouyang, K.R. Dunbar, C.F. Campana, R.D. Rogers, Chem. Mater. 11 (1999) 736–746.
[66] D.A. Pejaković, C. Kitamura, J.S. Miller, A.J. Epstein, Phys. Rev. Lett. 88 (2002) 057202.
[67] R. Clérac, S. O'Kane, J. Cowen, X. Ouyang, R. Heintz, H. Zhao, M.J. Bazile, K.R. Dunbar, Chem. Mater. 15 (2003) 1840–1850.
[68] H. Miyasaka, T. Izawa, N. Takahashi, M. Yamashita, K.R. Dunbar, J. Am. Chem. Soc. 128 (2006) 11358–11359.
[69] H. Miyasaka, T. Madanbashi, K. Sugimoto, Y. Nakazawa, W. Wernsdorfer, K.-I. Sugiura, M. Yamashita, C. Coulon, R. Clérac, Chem. Eur. J. 12 (2006) 7028–7040.
[70] R. Ishikawa, K. Katoh, B.K. Breedlove, M. Yamashita, Inorg. Chem. 51 (2012) 9123–9131.
[71] D. Maspoch, D. Ruiz-Molina, K. Wurst, C. Rovira, J. Veciana, Polyhedron 22 (2003) 1929–1934.
[72] D. Maspoch, D. Ruiz-Molina, K. Wurst, J. Vidal-Gancedo, C. Rovira, J. Veciana, Dalton Trans. (2004) 1073–1082.
[73] D. Maspoch, N. Domingo, D. Ruiz-Molina, K. Wurst, J.M. Hernández, F. Lloret, J. Tejada, C. Rovira, J. Veciana, Inorg. Chem. 46 (2007) 1627–1633.
[74] D. Maspoch, N. Domingo, D. Ruiz-Molina, K. Wurst, G. Vaughan, J. Tejada, C. Rovira, J. Veciana, Angew. Chem. Int. Ed. 43 (2004) 1828–1832.
[75] N. Roques, N. Domingo, D. Maspoch, K. Wurst, C. Rovira, J. Tejada, D. Ruiz-Molina, J. Veciana, Inorg. Chem. 49 (2010) 3482–3488.
[76] A. Caneschi, D. Gatteschi, N. Lalioti, C. Sangregorio, R. Sessoli, G. Venturi, A. Vindigni, A. Rettori, M.G. Pini, M.A. Novak, Angew. Chem. Int. Ed. 40 (2001) 1760–1763.
[77] S. Karasawa, G. Zhou, H. Morikawa, N. Koga, J. Am. Chem. Soc. 125 (2003) 13676–13677.
[78] H. Tobinaga, M. Suehiro, T. Ito, G. Zhou, S. Karasawa, N. Koga, Polyhedron 26 (2007) 1905–1911.
[79] S. Karasawa, K. Nakano, J.-I. Tanokashira, N. Yamamoto, T. Yoshizaki, N. Koga, Dalton Trans. 41 (2012) 13656–13667.
[80] S. Kanegawa, S. Karasawa, M. Nakano, N. Koga, Bull. Chem. Soc. Jpn. 79 (2006) 1372–1382.
[81] S. Karasawa, Y. Sano, T. Akita, N. Koga, T. Itoh, H. Iwamura, P. Rabu, M. Drillon, J. Am. Chem. Soc. 120 (1998) 10080–10087.
[82] S. Karasawa, K. Nakano, D. Yoshihara, N. Yamamoto, J.-I. Tanokashira, T. Yoshizaki, Y. Inagaki, N. Koga, Inorg. Chem. 53 (2014) 5447–5457.
[83] K.S. Cole, R.H. Cole, J. Chem. Phys. 9 (1941) 341–351.
[84] D. Yoshihara, S. Karasawa, N. Koga, J. Am. Chem. Soc. 130 (2008) 10460–10461.
[85] D. Yoshihara, S. Karasawa, N. Koga, Polyhedron 30 (2011) 3211–3217.
[86] I.-R. Jeon, J.G. Park, D.J. Xiao, T.D. Harris, J. Am. Chem. Soc. 135 (2013) 16845–16848.
[87] S. Fortier, O.G.-d. Moral, C.-H. Chen, M. Pink, J.J. Le Roy, M. Murugesu, D.J. Mindiola, K.G. Caulton, Chem. Commun. 48 (2012) 11082–11084.
[88] M.H. Dickman, R.J. Doedens, Inorg. Chem. 20 (1981) 2677–2681.
[89] M.H. Dickman, L.C. Porter, R.J. Doedens, Inorg. Chem. 25 (1986) 2595–2599.
[90] L.C. Porter, M.H. Dickman, R.J. Doedens, Inorg. Chem. 27 (1988) 1548–1552.
[91] D. Gatteschi, J. Laugier, P. Rey, C. Zanchini, Inorg. Chem. 26 (1987) 938–943.
[92] A. Caneschi, D. Gatteschi, J.P. Renard, P. Rey, R. Sessoli, Inorg. Chem. 28 (1989) 2940–2944.
[93] J. Laugier, P. Rey, C. Benelli, D. Gatteschi, C. Zanchini, J. Am. Chem. Soc. 108 (1986) 6931–6937.
[94] L.C. Porter, M.H. Dickman, R.J. Doedens, Inorg. Chem. 25 (1986) 678–684.
[95] A. Cogne, J. Laugier, D. Luneau, P. Rey, Inorg. Chem. 39 (2000) 5510–5514.
[96] Y.Y. Lim, R.S. Drago, Inorg. Chem. 11 (1972) 1334–1338.
[97] J values were estimated based on the general Hamiltonian $H = -2J_1S_MS_{L1} - 2J_2S_MS_{L2} - 2J_{L\text{-}L}S_{L1}S_{L2}$ and are shown in units of cm^{-1}.
[98] A. Caneschi, D. Gatteschi, A. Grand, J. Laugier, L. Pardi, P. Rey, Inorg. Chem. 27 (1988) 1031–1035.
[99] D. Luneau, G. Risoan, P. Rey, A. Grand, A. Caneschi, D. Gatteschi, J. Laugier, Inorg. Chem. 32 (1993) 5616–5622.
[100] D. Luneau, J. Laugier, P. Rey, G. Ulrich, R. Ziessel, P. Legoll, M. Drillon, J. Chem. Soc., Chem. Commun. (1994) 741–742.
[101] D. Luneau, F.M. Romero, R. Ziessel, Inorg. Chem. 37 (1998) 5078–5087.
[102] K. Fegy, N. Sanz, D. Luneau, E. Belorizky, P. Rey, Inorg. Chem. 37 (1998) 4518–4523.
[103] G. Francese, F.M. Romero, A. Neels, H. Stoeckli-Evans, S. Decurtins, Inorg. Chem. 39 (2000) 2087–2095.
[104] K. Osanai, A. Okazawa, T. Nogami, T. Ishida, J. Am. Chem. Soc. 128 (2006) 14008–14009.
[105] A. Okazawa, T. Nogami, T. Ishida, Chem. Mater. 19 (2007) 2733–2735.
[106] A. Okazawa, Y. Nagaichi, T. Nogami, T. Ishida, Inorg. Chem. 47 (2008) 8859–8868.
[107] A. Ito, Y. Nakano, M. Urabe, K. Tanaka, M. Shiro, Eur. J. Inorg. Chem. 2006 (2006) 3359–3368.
[108] I.A. Gass, C.J. Gartshore, D.W. Lupton, B. Moubaraki, A. Nafady, A.M. Bond, J.F. Boas, J.D. Cashion, C. Milsmann, K. Wieghardt, K.S. Murray, Inorg. Chem. 50 (2011) 3052–3064.
[109] I.A. Gass, S. Tewary, A. Nafady, N.F. Chilton, C.J. Gartshore, M. Asadi, D.W. Lupton, B. Moubaraki, A.M. Bond, J.F. Boas, S.-X. Guo, G. Rajaraman, K.S. Murray, Inorg. Chem. 52 (2013) 7557–7572.
[110] S. Kanegawa, S. Karasawa, M. Nakano, N. Koga, Chem. Commun. (2004) 1750–1751.
[111] S. Kanegawa, S. Karasawa, M. Maeyama, M. Nakano, N. Koga, J. Am. Chem. Soc. 130 (2008) 3079–3094.
[112] A. Caneschi, D. Gatteschi, J. Laugier, P. Rey, R. Sessoli, C. Zanchini, J. Am. Chem. Soc. 110 (1988) 2795–2799.
[113] N. Ishii, Y. Okamura, S. Chiba, T. Nogami, T. Ishida, J. Am. Chem. Soc. 130 (2008) 24–25.
[114] A.L. Balch, R.H. Holm, J. Am. Chem. Soc. 88 (1966) 5201–5209.
[115] F. Rohrscheid, A.L. Balch, R.H. Holm, Inorg. Chem. 5 (1966) 1542–1551.
[116] R.M. Buchanan, S.L. Kessel, H.H. Downs, C.G. Pierpont, D.N. Hendrickson, J. Am. Chem. Soc. 100 (1978) 7894–7900.
[117] S.R. Boone, G.H. Purser, H.R. Chang, M.D. Lowery, D.N. Hendrickson, C.G. Pierpont, J. Am. Chem. Soc. 111 (1989) 2292–2299.
[118] M.W. Lynch, R.M. Buchanan, C.G. Pierpont, D.N. Hendrickson, Inorg. Chem. 20 (1981) 1038–1046.
[119] B.J. Attia, B.J. Conklin, C.W. Lange, C.G. Pierpont, Inorg. Chem. 35 (1996) 1033–1038.
[120] A. Bencini, C. Carbonera, A. Dei, M.G.F. Vaz, Dalton Trans. (2003) 1701–1706.
[121] O. Kahn, R. Prins, J. Reedijk, J.S. Thompson, Inorg. Chem. 26 (1987) 3557–3561.
[122] A.I. Poddel'sky, V.K. Cherkasov, G.A. Abakumov, Coord. Chem. Rev. 253 (2009) 291–324.
[123] H. Chun, P. Chaudhuri, T. Weyhermüller, K. Wieghardt, Inorg. Chem. 41 (2002) 790–795.
[124] H. Chun, E. Bill, T. Weyhermüller, K. Wieghardt, Inorg. Chem. 42 (2003) 5612–5620.
[125] G.A. Abakumov, A.I. Poddel'sky, M.P. Bubnov, G.K. Fukin, L.G. Abakumova, V.N. Ikorskii, V.K. Cherkasov, Inorg. Chim. Acta 358 (2005) 3829–3840.
[126] E. Bill, E. Bothe, P. Chaudhuri, K. Chlopek, D. Herebian, S. Kokatam, K. Ray, T. Weyhermüller, F. Neese, K. Wieghardt, Chem. Eur. J. 11 (2005) 204–224.
[127] S. Ye, B. Sarkar, F. Lissner, T. Schleid, J. van Slageren, J. Fiedler, W. Kaim, Angew. Chem. Int. Ed. 44 (2005) 2103–2106.
[128] K. Chłopek, E. Bill, T. Weyhermüller, K. Wieghardt, Inorg. Chem. 44 (2005) 7087–7098.
[129] K. Chłopek, E. Bothe, F. Neese, T. Weyhermüller, K. Wieghardt, Inorg. Chem. 45 (2006) 6298–6307.
[130] M.M. Khusniyarov, E. Bill, T. Weyhermüller, E. Bothe, K. Harms, J. Sundermeyer, K. Wieghardt, Chem. Eur. J. 14 (2008) 7608–7622.
[131] N. Muresan, C.C. Lu, M. Ghosh, J.C. Peters, M. Abe, L.M. Henling, T. Weyhermöller, E. Bill, K. Wieghardt, Inorg. Chem. 47 (2008) 4579–4590.
[132] D. Herebian, E. Bothe, F. Neese, T. Weyhermüller, K. Wieghardt, J. Am. Chem. Soc. 125 (2003) 9116–9128.
[133] D. Herebian, K.E. Wieghardt, F. Neese, J. Am. Chem. Soc. 125 (2003) 10997–11005.
[134] D.N. Hendrickson, C.G. Pierpont, in: P. Guetlich, H.A. Goodwin (Eds.), Spin Crossover in Transition Metal Compounds II. Topics in Current Chemistry, Springer, Berlin, Heidelberg, 2004, pp. 63–95.
[135] H. Ohtsu, K. Tanaka, Angew. Chem. Int. Ed. 43 (2004) 6301–6303.
[136] D. Ruiz, J. Yoo, D.N. Hendrickson, I.A. Guzei, A.L. Rheingold, Chem. Commun. (1998) 2089–2090.
[137] D.M. Adams, A. Dei, A.L. Rheingold, D.N. Hendrickson, Angew. Chem. Int. Ed. 32 (1993) 880–882.
[138] R.M. Buchanan, C.G. Pierpont, J. Am. Chem. Soc. 102 (1980) 4951–4957.
[139] L. Norel, F. Pointillart, C. Train, L.-M. Chamoreau, K. Boubekeur, Y. Journaux, A. Brieger, D.J.R. Brook, Inorg. Chem. 47 (2008) 2396–2403.
[140] J.-B. Rota, L. Norel, C. Train, N.B. Amor, D. Maynau, V. Robert, J. Am. Chem. Soc. 130 (2008) 10380–10385.
[141] T.M. Barclay, R.G. Hicks, M.T. Lemaire, L.K. Thompson, Inorg. Chem. 40 (2001) 5581–5584.
[142] N.G.R. Hearns, K.E. Preuss, J.F. Richardson, S. Bin-Salamon, J. Am. Chem. Soc. 126 (2004) 9942–9943.
[143] J. Britten, N.G.R. Hearns, K.E. Preuss, J.F. Richardson, S. Bin-Salamon, Inorg. Chem. 46 (2007) 3934–3945.
[144] N.G.R. Hearns, E.M. Fatila, R. Clérac, M. Jennings, K.E. Preuss, Inorg. Chem. 47 (2008) 10330–10341.
[145] J. Wu, D.J. MacDonald, R. Clérac, I.-R. Jeon, M. Jennings, A.J. Lough, J. Britten, C. Robertson, P.A. Dube, K.E. Preuss, Inorg. Chem. 51 (2012) 3827–3839.
[146] T.M. Barclay, R.G. Hicks, M.T. Lemaire, L.K. Thompson, Chem. Commun. (2000) 2141–2142.
[147] T.M. Barclay, R.G. Hicks, M.T. Lemaire, L.K. Thompson, Inorg. Chem. 42 (2003) 2261–2267.
[148] D.J.R. Brook, C.J. Richardson, B.C. Haller, M. Hundley, G.T. Yee, Chem. Commun. 46 (2010) 6590–6592.
[149] K. Matsuda, N. Nakamura, K. Takahashi, K. Inoue, N. Koga, H. Iwamura, J. Am. Chem. Soc. 117 (1995) 5550–5560.
[150] I. Fujita, Y. Teki, T. Takui, T. Kinoshita, K. Itoh, F. Miko, Y. Sawaki, H. Iwamura, A. Izuoka, T. Sugawara, J. Am. Chem. Soc. 112 (1990) 4074–4075.
[151] Y. Teki, T. Takui, K. Itoh, H. Iwamura, K. Kobayashi, J. Am. Chem. Soc. 108 (1986) 2147–2156.
[152] A. Izuoka, S. Murata, T. Sugawara, H. Iwamura, J. Am. Chem. Soc. 109 (1987) 2631–2639.
[153] N. Nakamura, K. Inoue, H. Iwamura, T. Fujioka, Y. Sawaki, J. Am. Chem. Soc. 114 (1992) 1484–1485.

[154] N. Koga, Y. Ishimaru, H. Iwamura, Angew. Chem. Int. Ed. Engl. 35 (1996) 755–757.
[155] S. Karasawa, N. Koga, Inorg. Chem. 50 (2011) 5186–5195.
[156] S. Karasawa, D. Yoshihara, N. Watanabe, M. Nakano, N. Koga, Dalton Trans. (2008) 1418–1420.
[157] Y. Sano, M. Tanaka, N. Koga, K. Matsuda, H. Iwamura, P. Rabu, M. Drillon, J. Am. Chem. Soc. 119 (1997) 8246–8252.
[158] S. Mukherjee, T. Weyhermüller, E. Bill, K. Wieghardt, P. Chaudhuri, Inorg. Chem. 44 (2005) 7099–7108.
[159] C. Benelli, A. Dei, D. Gatteschi, L. Pardi, Inorg. Chem. 27 (1988) 2831–2836.
[160] G.A. Abakumov, V.K. Cherkasov, M.P. Bubnov, O.G. Éllert, Y.V. Rakitin, L.N. Zakharov, Y.T. Struchkov, Y.N. Saf'yanov, Bull. Russ. Acad. Sci., Div. Chem. Sci. 41 (1992) 1813–1818.
[161] C.W. Lange, C.G. Pierpont, Inorg. Chim. Acta 263 (1997) 219–224.
[162] C.G. Attia, Pierpont, Inorg. Chem. 37 (1998) 3051–3056.
[163] H.-C. Chang, T. Ishii, M. Kondo, S. Kitagawa, J. Chem. Soc., Dalton Trans. (1999) 2467–2476.
[164] H. Chun, T. Weyhermüller, E. Bill, K. Wieghardt, Angew. Chem. Int. Ed. 40 (2001) 2489–2492.
[165] S. Mukherjee, T. Weyhermuller, E. Bothe, K. Wieghardt, P. Chaudhuri, Dalton Trans. (2004) 3842–3853.
[166] D.E. Wheeler, J.K. McCusker, Inorg. Chem. 37 (1998) 2296–2307.
[167] P. Chaudhuri, C.N. Verani, E. Bill, E. Bothe, T. Weyhermüller, K. Wieghardt, J. Am. Chem. Soc. 123 (2001) 2213–2223.
[168] A. Caneschi, A. Dei, D. Gatteschi, V. Tangoulis, Inorg. Chem. 41 (2002) 3508–3512.
[169] K. Sik Min, T. Weyhermuller, K. Wieghardt, Dalton Trans. (2003) 1126–1132.
[170] R.G. Hicks, M.T. Lemaire, L.K. Thompson, T.M. Barclay, J. Am. Chem. Soc. 122 (2000) 8077–8078.
[171] T.M. Barclay, R.G. Hicks, M.T. Lemaire, L.K. Thompson, Z. Xu, Chem. Commun. (2002) 1688–1689.
[172] S. Kitagawa, S. Kawata, Coord. Chem. Rev. 224 (2002) 11–34.
[173] A. Dei, D. Gatteschi, L. Pardi, Inorg. Chim. Acta 189 (1991) 125–128.
[174] A. Dei, D. Gatteschi, L. Pardi, U. Russo, Inorg. Chem. 30 (1991) 2589–2594.
[175] M.D. Ward, Inorg. Chem. 35 (1996) 1712–1714.
[176] K. Heinze, G. Huttner, L. Zsolnai, A. Jacobi, P. Schober, Chem. Eur. J. 3 (1997) 732–743.
[177] K. Heinze, G. Huttner, O. Walter, Eur. J. Inorg. Chem. 1999 (1999) 593–600.
[178] C. Carbonera, A. Dei, J.-F. Létard, C. Sangregorio, L. Sorace, Angew. Chem. Int. Ed. 43 (2004) 3136–3138.
[179] P. Gupta, A. Das, F. Basuli, A. Castineiras, W.S. Sheldrick, H. Mayer-Figge, S. Bhattacharya, Inorg. Chem. 44 (2005) 2081–2088.
[180] K.S. Min, A.L. Rheingold, A. DiPasquale, J.S. Miller, Inorg. Chem. 45 (2006) 6135–6137.
[181] J. Tao, H. Maruyama, O. Sato, J. Am. Chem. Soc. 128 (2006) 1790–1791.
[182] K.S. Min, A.G. DiPasquale, J.A. Golen, A.L. Rheingold, J.S. Miller, J. Am. Chem. Soc. 129 (2007) 2360–2368.
[183] D. Guo, J.K. McCusker, Inorg. Chem. 46 (2007) 3257–3274.
[184] S. Ghumaan, B. Sarkar, S. Maji, V.G. Puranik, J. Fiedler, F.A. Urbanos, R. Jimenez-Aparicio, W. Kaim, G.K. Lahiri, Chem. Eur. J. 14 (2008) 10816–10828.
[185] B. Li, J. Tao, H.-L. Sun, O. Sato, R.-B. Huang, L.-S. Zheng, Chem. Commun. (2008) 2269–2271.
[186] K.S. Min, K. Swierczek, A.G. DiPasquale, A.L. Rheingold, W.M. Reiff, A.M. Arif, J.S. Miller, Chem. Commun. (2008) 317–319.
[187] K.S. Min, A.G. DiPasquale, A.L. Rheingold, H.S. White, J.S. Miller, J. Am. Chem. Soc. 131 (2009) 6229–6236.
[188] P.B. Chatterjee, K. Bhattacharya, N. Kundu, K.-Y. Choi, R. Clérac, M. Chaudhury, Inorg. Chem. 48 (2009) 804–806.
[189] A.E. Baum, S.V. Lindeman, A.T. Fiedler, Chem. Commun. 49 (2013) 6531–6533.
[190] R. Dinnebier, H.-W. Lerner, L. Ding, K. Shankland, W.I.F. David, P.W. Stephens, M. Wagner, Z. Anorg. Allg. Chem. 628 (2002) 310–314.
[191] T.E. Keyes, R.J. Forster, P.M. Jayaweera, C.G. Coates, J.J. McGarvey, J.G. Vos, Inorg. Chem. 37 (1998) 5925–5932.
[192] G. Margraf, T. Kretz, F.F. de Biani, F. Laschi, S. Losi, P. Zanello, J.W. Bats, B. Wolf, K. Remović-Langer, M. Lang, A. Prokofiev, W. Assmus, H.-W. Lerner, M. Wagner, Inorg. Chem. 45 (2006) 1277–1288.
[193] H.-W. Lerner, G. Margraf, T. Kretz, J.W. Bats, G. Dürner, O. Schiemann, F.F. de Biani, P. Zanello, M. Bolte, M. Wagner, Zeitschrift fur Naturforschung B: J. Phys. Sci. B61 (2006) 252.
[194] S.L. Caldwell, J.B. Gilroy, R. Jain, E. Crawford, B.O. Patrick, R.G. Hicks, Can. J. Chem. 86 (2008) 976–981.
[195] L.R. Pignotti, N. Kongprakaiwoot, W.W. Brennessel, J. Baltrusaitis, R.L. Luck, E. Urnezius, J. Organomet. Chem. 693 (2008) 3263–3272.
[196] S. Kar, B. Sarkar, S. Ghumaan, D. Janardanan, J. van Slageren, J. Fiedler, V.G. Puranik, R.B. Sunoj, W. Kaim, G.K. Lahiri, Chem. Eur. J. 11 (2005) 4901–4911.
[197] H.S. Das, A.K. Das, R. Pattacini, R. Hubner, B. Sarkar, P. Braunstein, Chem. Commun. (2009) 4387–4389.
[198] H.S. Das, F. Weisser, D. Schweinfurth, C.-Y. Su, L. Bogani, J. Fiedler, B. Sarkar, Chem. Eur. J. 16 (2010) 2977–2981.
[199] F. Weisser, R. Huebner, D. Schweinfurth, B. Sarkar, Chem. Eur. J. 17 (2011) 5727–5736.
[200] D. Schweinfurth, H.S. Das, F. Weisser, D. Bubrin, B. Sarkar, Inorg. Chem. 50 (2011) 1150–1159.
[201] M.G. Sommer, D. Schweinfurth, F. Weisser, S. Hohloch, B. Sarkar, Organometallics 32 (2013) 2069–2078.
[202] D. Schweinfurth, Y. Rechkemmer, S. Hohloch, N. Deibel, I. Peremykin, J. Fiedler, R. Marx, P. Neugebauer, J. van Slageren, B. Sarkar, Chem. Eur. J. 20 (2014) 3475–3486.
[203] O. Siri, J.-P. Taquet, J.-P. Collin, M.-M. Rohmer, M. Bénard, P. Braunstein, Chem. Eur. J. 11 (2005) 7247–7253.
[204] J.-P. Taquet, O. Siri, P. Braunstein, R. Welter, Inorg. Chem. 45 (2006) 4668–4676.
[205] Y.-B. Huang, G.-R. Tang, G.-Y. Jin, G.-X. Jin, Organometallics 27 (2007) 259–269.
[206] D. Schweinfurth, M.M. Khusniyarov, D. Bubrin, S. Hohloch, C.-Y. Su, B. Sarkar, Inorg. Chem. 52 (2013) 10332–10339.
[207] S.R. Oakley, G. Nawn, K.M. Waldie, T.D. MacInnis, B.O. Patrick, R.G. Hicks, Chem. Commun. 46 (2010) 6753–6755.
[208] G. Nawn, K.M. Waldie, S.R. Oakley, B.D. Peters, D. Mandel, B.O. Patrick, R. McDonald, R.G. Hicks, Inorg. Chem. 50 (2011) 9826–9837.
[209] S. Fortier, J.J. Le Roy, C.-H. Chen, V. Vieru, M. Murugesu, L.F. Chibotaru, D.J. Mindiola, K.G. Caulton, J. Am. Chem. Soc. 135 (2013) 14670–14678.
[210] N. Ishikawa, M. Sugita, T. Ishikawa, S.-Y. Koshihara, Y. Kaizu, J. Am. Chem. Soc. 125 (2003) 8694–8695.
[211] N. Ishikawa, M. Sugita, T. Ishikawa, S.-Y. Koshihara, Y. Kaizu, J. Phys. Chem. B 108 (2004) 11265–11271.
[212] N. Ishikawa, Y. Mizuno, S. Takamatsu, T. Ishikawa, S.-Y. Koshihara, Inorg. Chem. 47 (2008) 10217–10219.
[213] M.A. AlDamen, J.M. Clemente-Juan, E. Coronado, C. Martí-Gastaldo, A. Gaita-Ariño, J. Am. Chem. Soc. 130 (2008) 8874–8875.
[214] M.A. AlDamen, S. Cardona-Serra, J.M. Clemente-Juan, E. Coronado, A. Gaita-Ariño, C. Martí-Gastaldo, F. Luis, O. Montero, Inorg. Chem. 48 (2009) 3467–3479.
[215] S.-D. Jiang, B.-W. Wang, H.-L. Sun, Z.-M. Wang, S. Gao, J. Am. Chem. Soc. 133 (2011) 4730–4733.
[216] J.J. Le Roy, I. Korobkov, M. Murugesu, Chem. Commun. 50 (2014) 1602–1604.
[217] L. Ungur, J.J. Le Roy, I. Korobkov, M. Murugesu, L.F. Chibotaru, Angew. Chem. Int. Ed. 53 (2014) 4413–4417.
[218] K.R. Meihaus, J.R. Long, J. Am. Chem. Soc. 135 (2013) 17952–17957.
[219] D. Gatteschi, R. Sessoli, J. Villain, Molecular Nanomagnets, Oxford University Press, Oxford, 2006.
[220] J.J. Le Roy, L. Ungur, I. Korobkov, L.F. Chibotaru, M. Murugesu, J. Am. Chem. Soc. 136 (2014) 8003–8010.
[221] K.L. Trojan, J.L. Kendall, K.D. Kepler, W.E. Hatfield, Inorg. Chim. Acta 198–200 (1992) 795–803.
[222] A.G. Gürek, T. Basova, D. Luneau, C. Lebrun, E. Kol'tsov, A.K. Hassan, V. Ahsen, Inorg. Chem. 45 (2006) 1667–1676.
[223] N. Ishikawa, M. Sugita, N. Tanaka, T. Ishikawa, S.-Y. Koshihara, Y. Kaizu, Inorg. Chem. 43 (2004) 5498–5500.
[224] S. Takamatsu, N. Ishikawa, Polyhedron 26 (2007) 1859–1862.
[225] C.R. Ganivet, B. Ballesteros, G. de la Torre, J.M. Clemente-Juan, E. Coronado, T. Torres, Chem. Eur. J. 19 (2013) 1457–1465.
[226] S. Takamatsu, T. Ishikawa, S.-Y. Koshihara, N. Ishikawa, Inorg. Chem. 46 (2007) 7250–7252.
[227] A.V. Ivanov, P.A. Svinareva, I.V. Zhukov, L.G. Tomilova, N.S. Zefirov, Russ. Chem. Bull. 55 (2006) 281–286.
[228] M. Gonidec, E.S. Davies, J. McMaster, D.B. Amabilino, J. Veciana, J. Am. Chem. Soc. 132 (2010) 1756–1757.
[229] M. Gonidec, I. Krivokapic, J. Vidal-Gancedo, E.S. Davies, J. McMaster, S.M. Gorun, J. Veciana, Inorg. Chem. 52 (2013) 4464–4471.
[230] A.T. Chang, J.-C. Marchon, Inorg. Chim. Acta 53 (1981) L241–L243.
[231] G.A. Corker, B. Grant, N.J. Clecak, J. Electrochem. Soc. 126 (1979) 1339–1343.
[232] M. Gonidec, F. Luis, À. Vílchez, J. Esquena, D.B. Amabilino, J. Veciana, Angew. Chem. Int. Ed. 49 (2010) 1623–1626.
[233] H. Wang, K. Wang, J. Tao, J. Jiang, Chem. Commun. 48 (2012) 2973–2975.
[234] R. Biagi, J. Fernandez-Rodriguez, M. Gonidec, A. Mirone, V. Corradini, F. Moro, V. De Renzi, U. del Pennino, J.C. Cezar, D.B. Amabilino, J. Veciana, Phys. Rev. B 82 (2010) 224406.
[235] J. Gomez-Segura, I. Diez-Perez, N. Ishikawa, M. Nakano, J. Veciana, D. Ruiz-Molina, Chem. Commun. (2006) 2866–2868.
[236] M. Gonidec, R. Biagi, V. Corradini, F. Moro, V. De Renzi, U. del Pennino, D. Summa, L. Muccioli, C. Zannoni, D.B. Amabilino, J. Veciana, J. Am. Chem. Soc. 133 (2011) 6603–6612.
[237] A. Candini, S. Klyatskaya, M. Ruben, W. Wernsdorfer, M. Affronte, Nano Lett. 11 (2011) 2634–2639.
[238] M. Lopes, A. Candini, M. Urdampilleta, A. Reserbat-Plantey, V. Bellini, S. Klyatskaya, L. Marty, M. Ruben, M. Affronte, W. Wernsdorfer, N. Bendiab, ACS Nano 4 (2010) 7531–7537.
[239] S. Kyatskaya, J.R.G. Mascarós, L. Bogani, F. Hennrich, M. Kappes, W. Wernsdorfer, M. Ruben, J. Am. Chem. Soc. 131 (2009) 15143–15151.
[240] S. Stepanow, J. Honolka, P. Gambardella, L. Vitali, N. Abdurakhmanova, T.-C. Tseng, S. Rauschenbach, S.L. Tait, V. Sessi, S. Klyatskaya, M. Ruben, K. Kern, J. Am. Chem. Soc. 132 (2010) 11900–11901.
[241] L. Vitali, S. Fabris, A.M. Conte, S. Brink, M. Ruben, S. Baroni, K. Kern, Nano Lett. 8 (2008) 3364–3368.
[242] A. Lodi Rizzini, C. Krull, T. Balashov, J.J. Kavich, A. Mugarza, P.S. Miedema, P.K. Thakur, V. Sessi, S. Klyatskaya, M. Ruben, S. Stepanow, P. Gambardella, Phys. Rev. Lett. 107 (2011) 177205.
[243] L. Margheriti, D. Chiappe, M. Mannini, P.E. Car, P. Sainctavit, M.-A. Arrio, F.B. de Mongeot, J.C. Cezar, F.M. Piras, A. Magnani, E. Otero, A. Caneschi, R. Sessoli, Adv. Mater. 22 (2010) 5488–5493.

[244] K. Katoh, Y. Yoshida, M. Yamashita, H. Miyasaka, B.K. Breedlove, T. Kajiwara, S. Takaishi, N. Ishikawa, H. Isshiki, Y.F. Zhang, T. Komeda, M. Yamagishi, J. Takeya, J. Am. Chem. Soc. 131 (2009) 9967–9976.
[245] K. Katoh, T. Komeda, M. Yamashita, Dalton Trans. 39 (2010) 4708–4723.
[246] M. Urdampilleta, S. Klyatskaya, J.P. Cleuziou, M. Ruben, W. Wernsdorfer, Nat. Mater. 10 (2011) 502–506.
[247] K. Katoh, H. Isshiki, T. Komeda, M. Yamashita, Coord. Chem. Rev. 255 (2011) 2124–2148.
[248] A. Cornia, M. Mannini, P. Sainctavit, R. Sessoli, Chem. Soc. Rev. 40 (2011) 3076–3091.
[249] T. Ishida, R. Murakami, T. Kanetomo, H. Nojiri, Polyhedron 66 (2013) 183–187.
[250] N. Ikegaya, T. Kanetomo, R. Murakami, T. Ishida, Chem. Lett. 41 (2012) 82–83.
[251] C. Benelli, A. Caneschi, D. Gatteschi, L. Pardi, P. Rey, D.P. Shum, R.L. Carlin, Inorg. Chem. 28 (1989) 272–275.
[252] C. Benelli, A. Caneschi, D. Gatteschi, L. Pardi, P. Rey, Inorg. Chem. 29 (1990) 4223–4228.
[253] C. Benelli, A. Caneschi, A.C. Fabretti, D. Gatteschi, L. Pardi, Inorg. Chem. 29 (1990) 4153–4155.
[254] C. Benelli, A. Caneschi, D. Gatteschi, L. Pardi, Inorg. Chem. 31 (1992) 741–746.
[255] C. Lescop, D. Luneau, P. Rey, G. Bussière, C. Reber, Inorg. Chem. 41 (2002) 5566–5574.
[256] J.-X. Xu, Y. Ma, G.-F. Xu, C. Wang, D.-Z. Liao, Z.-H. Jiang, S.-P. Yan, L.-C. Li, Inorg. Chem. Commun. 11 (2008) 1356–1358.
[257] Q.-H. Zhao, Y.-P. Ma, L. Du, R.-B. Fang, Transit. Met. Chem. 31 (2006) 593–597.
[258] X.-L. Wang, J. Coord. Chem. 64 (2011) 4334–4343.
[259] N. Zhou, Y. Ma, C. Wang, G.-F. Xu, J. Tang, S.-P. Yan, D.-Z. Liao, J. Solid State Chem. 183 (2010) 927–932.
[260] X.-L. Wang, Inorg. Chim. Acta 387 (2012) 20–24.
[261] X. Wang, P. Xu, X. Bao, F. Wang, Y. Chen, Y. Wei, Z. Anorg. Allg. Chem. 639 (2013) 176–180.
[262] Y.-L. Wang, Y.-Y. Gao, Y. Ma, Q.-L. Wang, L.-C. Li, D.-Z. Liao, CrystEngComm 14 (2012) 4706–4712.
[263] C.-X. Zhang, N.-N. Sun, X.-Y. Zhao, Y.-Y. Zhang, Y.-L. Guo, Inorg. Chem. Commun. 14 (2011) 166–168.
[264] C.-X. Zhang, H.-W. Chen, W.-M. Wang, Y.-Y. Zhang, Inorg. Chem. Commun. 24 (2012) 177–180.
[265] R.N. Liu, S.P. Zhao, C.X. Xiong, Russ. J. Coord. Chem. 39 (2013) 808–812.
[266] Y.-L. Wang, Y.-Y. Gao, Y. Ma, Q.-L. Wang, L.-C. Li, D.-Z. Liao, J. Solid State Chem. 202 (2013) 276–281.
[267] Y.-y. Gao, Y.-l. Wang, P. Hu, M.-f. Yang, Y. Ma, Q.-l. Wang, L.-c. Li, D.-z. Liao, Inorg. Chem. Commun. 27 (2013) 31–35.
[268] C.-X. Zhang, W.-M. Wang, X.-Y. Zhao, L.-F. Ji, Y.-Y. Zhang, Polyhedron 30 (2011) 3177–3181.
[269] C. Wang, Y.-l. Wang, Z.-x. Qin, Y. Ma, Q.-l. Wang, L.-c. Li, D.-z. Liao, Inorg. Chem. Commun. 20 (2012) 112–116.
[270] F. Pointillart, K. Bernot, G. Poneti, R. Sessoli, Inorg. Chem. 51 (2012) 12218–12229.
[271] X.-L. Mei, R.-N. Liu, C. Wang, P.-P. Yang, L.-C. Li, D.-Z. Liao, Dalton Trans. 41 (2012) 2904–2909.
[272] P. Hu, M. Zhu, X. Mei, H. Tian, Y. Ma, L. Li, D. Liao, Dalton Trans. 41 (2012) 14651–14656.
[273] J.-P. Sutter, M.L. Kahn, S. Golhen, L. Ouahab, O. Kahn, Chemistry – Eur. J. 4 (1998) 571–576.
[274] X. Mei, X. Wang, J. Wang, Y. Ma, L. Li, D. Liao, New J. Chem. 37 (2013) 3620–3626.
[275] X.-L. Mei, Y. Ma, L.-C. Li, D.-Z. Liao, Dalton Trans. 41 (2012) 505–511.
[276] Z.-H. Jiang, W. Zhang, D.-Z. Liao, Z.-W. Huan, B.-W. Sun, G.-L. Wang, Chin. J. Chem. 13 (1995) 423–428.
[277] T. Tsukuda, T. Suzuki, S. Kaizaki, J. Chem. Soc., Dalton Trans. (2002) 1721–1726.
[278] J.W. Raebiger, J.S. Miller, Inorg. Chem. 41 (2002) 3308–3312.
[279] L. Norel, L.-M. Chamoreau, Y. Journaux, O. Oms, G. Chastanet, C. Train, Chem. Commun. (2009) 2381–2383.
[280] A.A. Trifonov, I.D. Gudilenkov, J. Larionova, C. Luna, G.K. Fukin, A.V. Cherkasov, A.I. Poddel'sky, N.O. Druzhkov, Organometallics 28 (2009) 6707–6713.
[281] C. Lescop, D. Luneau, E. Belorizky, P. Fries, M. Guillot, P. Rey, Inorg. Chem. 38 (1999) 5472–5473.
[282] T. Tsukuda, T. Suzuki, S. Kaizaki, Inorg. Chim. Acta 358 (2005) 1253–1257.
[283] T. Tsukuda, T. Suzuki, S. Kaizaki, Mol. Cryst. Liquid Cryst. 379 (2002) 159–164.
[284] T. Kanetomo, T. Ishida, Chem. Commun. 50 (2014) 2529–2531.
[285] C. Lescop, E. Belorizky, D. Luneau, P. Rey, Inorg. Chem. 41 (2002) 3375–3384.
[286] T. Kanetomo, T. Ishida, Inorg. Chem. 53 (2014) 10794–10796.
[287] A. Caneschi, A. Dei, D. Gatteschi, L. Sorace, K. Vostrikova, Angew. Chem. Int. Ed. 39 (2000) 246–248.
[288] S. Demir, M. Nippe, M.I. Gonzalez, J.R. Long, Chem. Sci. 5 (2014) 4701–4711.
[289] S. Demir, J.M. Zadrozny, M. Nippe, J.R. Long, J. Am. Chem. Soc. 134 (2012) 18546–18549.
[290] J.D. Rinehart, M. Fang, W.J. Evans, J.R. Long, Nat. Chem. 3 (2011) 538–542.
[291] K.R. Meihaus, J.F. Corbey, M. Fang, J.W. Ziller, J.R. Long, W.J. Evans, Inorg. Chem. 53 (2014) 3099–3107.
[292] C. Benelli, A. Caneschi, D. Galleschi, J. Laugier, P. Rey, Angew. Chem. Int. Ed. 26 (1987) 913–915.
[293] C. Benelli, A. Caneschi, D. Gatteschi, R. Sessoli, J. Appl. Phys. 73 (1993) 5333–5337.
[294] M. Andruh, I. Ramade, E. Codjovi, O. Guillou, O. Kahn, J.C. Trombe, J. Am. Chem. Soc. 115 (1993) 1822–1829.
[295] J. Goldman, T.E. Petersen, K. Torssell, J. Becher, Tetrahedron 29 (1973) 3833–3843.
[296] E.F. Ullman, J.H. Osiecki, D.G.B. Boocock, R. Darcy, J. Am. Chem. Soc. 94 (1972) 7049–7059.
[297] H.M. McConnell, J. Chem. Phys. 39 (1963) 1910.
[298] X.-L. Wang, L.-C. Li, D.-Z. Liao, Inorg. Chem. 49 (2010) 4735–4737.
[299] A. Lannes, M. Intissar, Y. Suffren, C. Reber, D. Luneau, Inorg. Chem. 53 (2014) 9548–9560.
[300] N. Zhou, Y. Ma, C. Wang, G. Feng Xu, J.-K. Tang, J.-X. Xu, S.-P. Yan, P. Cheng, L.-C. Li, D.-Z. Liao, Dalton Trans. (2009) 8489–8492.
[301] J.D. Rinehart, M. Fang, W.J. Evans, J.R. Long, J. Am. Chem. Soc. 133 (2011) 14236–14239.
[302] E.M. Fatila, M. Rouzières, M.C. Jennings, A.J. Lough, R. Clérac, K.E. Preuss, J. Am. Chem. Soc. 135 (2013) 9596–9599.
[303] J.-X. Xu, Y. Ma, D.-z. Liao, G.-F. Xu, J. Tang, C. Wang, N. Zhou, S.-P. Yan, P. Cheng, L.-C. Li, Inorg. Chem. 48 (2009) 8890–8896.
[304] E. Coronado, C. Giménez-Saiz, A. Recuenco, A. Tarazón, F.M. Romero, A.N. Camón, F. Luis, Inorg. Chem. 50 (2011) 7370–7372.
[305] H. Tian, R. Liu, X. Wang, P. Yang, Z. Li, L. Li, D. Liao, Eur. J. Inorg. Chem. 2009 (2009) 4498–4502.
[306] G. Poneti, K. Bernot, L. Bogani, A. Caneschi, R. Sessoli, W. Wernsdorfer, D. Gatteschi, Chem. Commun. (2007) 1807–1809.
[307] K. Bernot, F. Pointillart, P. Rosa, M. Etienne, R. Sessoli, D. Gatteschi, Chem. Commun. 46 (2010) 6458–6460.
[308] R. Liu, C. Zhang, L. Li, D. Liao, J.-P. Sutter, Dalton Trans. 41 (2012) 12139–12144.
[309] O.H. Griffith, D.W. Cornell, H.M. McConnell, J. Chem. Phys. 43 (1965) 2909–2910.
[310] G.I. Likhtenshtein, J. Yamauchi, S.I. Nakatsuji, A.I. Smirnov, R. Tamura, Nitroxides, Wiley-VCH Verlag GmbH & Co. KGaA, Weinheim, 2008, pp. 405–419.
[311] L.J. Berliner, Spin-Labeling: Theory and Applications, Academic Press, New York, 1976.
[312] J.F.W. Keana, Chem. Rev. 78 (1978) 37–64.
[313] R. Murakami, T. Nakamura, T. Ishida, Dalton Trans. 43 (2014) 5893–5898.
[314] C. Benelli, A. Caneschi, D. Gatteschi, O. Guillou, L. Pardi, Inorg. Chem. 29 (1990) 1750–1755.
[315] C.H. Booth, M.D. Walter, M. Daniel, W.W. Lukens, R.A. Andersen, Phys. Rev. Lett. 95 (2005) 267202.
[316] C.H. Booth, M.D. Walter, D. Kazhdan, Y.-J. Hu, W.W. Lukens, E.D. Bauer, L. Maron, O. Eisenstein, R.A. Andersen, J. Am. Chem. Soc. 131 (2009) 6480–6491.
[317] N.A.G. Bandeira, C. Daniel, A. Trifonov, M.J. Calhorda, Organometallics 31 (2012) 4693–4700.
[318] M. Schultz, J.M. Boncella, D.J. Berg, T.D. Tilley, R.A. Andersen, Organometallics 21 (2001) 460–472.
[319] A. Palii, B. Tsukerblat, S. Klokishner, K.R. Dunbar, J.M. Clemente-Juan, E. Coronado, Chem. Soc. Rev. 40 (2011) 3130–3156.
[320] W.W. Lukens, M.D. Walter, Inorg. Chem. 49 (2010) 4458–4465.
[321] J.S. Griffith, Structure and Bonding, Springer Verlag, New York, 1972.
[322] M.C.B. Sousa, C.A. Maced, Sci. Plena 4 (2008) 094401.
[323] G. Chiappe, E. Louis, E. SanFabián, J.A. Verges, Phys. Rev. B 75 (2007) 195104.
[324] J. Hubbard, Proc. R. Soc. Lond. Ser. A: Math. Phys. Sci. 276 (1963) 238–257.
[325] W.W. Lukens, N. Magnani, C.H. Booth, Inorg. Chem. 51 (2012) 10105–10110.
[326] M.A. Fox, F.A. Matsen, J. Chem. Educ. 62 (1985) 367.
[327] C.H. Booth, D. Kazhdan, E.L. Werkema, M.D. Walter, W.W. Lukens, E.D. Bauer, Y.-J. Hu, L. Maron, O. Eisenstein, M. Head-Gordon, R.A. Andersen, J. Am. Chem. Soc. 132 (2010) 17537–17549.
[328] M.D. Walter, D.J. Berg, R.A. Andersen, Organometallics 25 (2006) 3228–3237.
[329] M.D. Walter, D.J. Berg, R.A. Andersen, Organometallics 26 (2007) 2296–2307.
[330] M.D. Walter, M. Schultz, R.A. Andersen, New J. Chem. 30 (2006) 238–246.
[331] R.E. Da Re, C.J. Kuehl, M.G. Brown, R.C. Rocha, E.D. Bauer, K.D. John, D.E. Morris, A.P. Shreve, J.L. Sarrao, Inorg. Chem. 42 (2003) 5551–5559.
[332] G. Nocton, C.H. Booth, L. Maron, R.A. Andersen, Organometallics 32 (2013) 5305–5312.
[333] J.M. Veauthier, E.J. Schelter, C.N. Carlson, B.L. Scott, R.E.D. Re, J.D. Thompson, J.L. Kiplinger, D.E. Morris, K.D. John, Inorg. Chem. 47 (2008) 5841–5849.
[334] J.M. Veauthier, E.J. Schelter, C.J. Kuehl, A.E. Clark, B.L. Scott, D.E. Morris, R.L. Martin, J.D. Thompson, J.L. Kiplinger, K.D. John, Inorg. Chem. 44 (2005) 5911–5920.
[335] A. Dei, D. Gatteschi, C.A. Massa, L.A. Pardi, S. Poussereau, L. Sorace, Chem. Eur. J. 6 (2000) 4580–4586.
[336] F. Pointillart, O. Maury, Y. Le Gal, S. Golhen, O. Cador, L. Ouahab, Inorg. Chem. 48 (2009) 7421–7429.
[337] F. Pointillart, Y. Le Gal, S. Golhen, O. Cador, L. Ouahab, Chem. Commun. (2009) 3777–3779.
[338] F. Pointillart, B. Le Guennic, S. Golhen, O. Cador, L. Ouahab, Chem. Commun. 49 (2013) 11632–11634.
[339] W.J. Evans, M. Fang, G. Zucchi, F. Furche, J.W. Ziller, R.M. Hoekstra, J.I. Zink, J. Am. Chem. Soc. 131 (2009) 11195–11202.
[340] T. Rajeshkumar, G. Rajaraman, Chem. Commun. 48 (2012) 7856–7858.
[341] Y.-Q. Zhang, C.-L. Luo, B.-W. Wang, S. Gao, J. Phys. Chem. A 117 (2013) 10873–10880.
[342] J.J. Baldovi, S. Cardona-Serra, J.M. Clemente-Juan, E. Coronado, A. Gaita-Arino, Chem. Sci. 4 (2013) 938–946.
[343] J.T. Coutinho, M.A. Antunes, L.C.J. Pereira, H. Bolvin, J. Marcalo, M. Mazzanti, M. Almeida, Dalton Trans. 41 (2012) 13568–13571.

[344] J.D. Rinehart, J.R. Long, Dalton Trans. 41 (2012) 13572–13574.
[345] M.A. Antunes, L.C.J. Pereira, I.C. Santos, M. Mazzanti, J. Marçalo, M. Almeida, Inorg. Chem. 50 (2011) 9915–9917.
[346] D.P. Mills, F. Moro, J. McMaster, J. van Slageren, W. Lewis, A.J. Blake, S.T. Liddle, Nat. Chem. 3 (2011) 454–460.
[347] J.D. Rinehart, K.R. Meihaus, J.R. Long, J. Am. Chem. Soc. 132 (2010) 7572–7573.
[348] J.D. Rinehart, J.R. Long, J. Am. Chem. Soc. 131 (2009) 12558–12559.
[349] F. Moro, D.P. Mills, S.T. Liddle, J. van Slageren, Angew. Chem. Int. Ed. 52 (2013) 3430–3433.
[350] K.R. Meihaus, S.G. Minasian, W.W. Lukens, S.A. Kozimor, D.K. Shuh, T. Tyliszczak, J.R. Long, J. Am. Chem. Soc. 136 (2014) 6056–6068.
[351] D.M. King, F. Tuna, J. McMaster, W. Lewis, A.J. Blake, E.J.L. McInnes, S.T. Liddle, Angew. Chem. Int. Ed. 52 (2013) 4921–4924.
[352] N. Magnani, E. Colineau, R. Eloirdi, J.C. Griveau, R. Caciuffo, S.M. Cornet, I. May, C.A. Sharrad, D. Collison, R.E.P. Winpenny, Phys. Rev. Lett. 104 (2010) 197202.
[353] N. Magnani, C. Apostolidis, A. Morgenstern, E. Colineau, J.-C. Griveau, H. Bolvin, O. Walter, R. Caciuffo, Angew. Chem. Int. Ed. 50 (2011) 1696–1698.
[354] N. Magnani, E. Colineau, J.C. Griveau, C. Apostolidis, O. Walter, R. Caciuffo, Chem. Commun. 50 (2014) 8171–8173.
[355] J.D. Rinehart, J.R. Long, Chem. Sci. 2 (2011) 2078–2085.
[356] B.S. Newell, A.K. Rappé, M.P. Shores, Inorg. Chem. 49 (2010) 1595–1606.
[357] J.D. Rinehart, B.M. Bartlett, S.A. Kozimor, J.R. Long, Inorg. Chim. Acta 361 (2008) 3534–3538.
[358] S.A. Kozimor, B.M. Bartlett, J.D. Rinehart, J.R. Long, J. Am. Chem. Soc. 129 (2007) 10672–10674.
[359] R.K. Rosen, R.A. Andersen, N.M. Edelstein, J. Am. Chem. Soc. 112 (1990) 4588–4590.
[360] J.D. Rinehart, T.D. Harris, S.A. Kozimor, B.M. Bartlett, J.R. Long, Inorg. Chem. 48 (2009) 3382–3395.
[361] D. Patel, F. Moro, J. McMaster, W. Lewis, A.J. Blake, S.T. Liddle, Angew. Chem. Int. Ed. 50 (2011) 10388–10392.
[362] V. Mougel, L. Chatelain, J. Pécaut, R. Caciuffo, E. Colineau, J.-C. Griveau, M. Mazzanti, Nat. Chem. 4 (2012) 1011–1017.
[363] N.N. Krot, M.S. Grigoriev, Russ. Chem. Rev. 73 (2004) 89–100.
[364] L. Chatelain, V. Mougel, J. Pecaut, M. Mazzanti, Chem. Sci. 3 (2012) 1075–1079.
[365] S.J. Kraft, P.E. Fanwick, S.C. Bart, Inorg. Chem. 49 (2010) 1103–1110.
[366] J.T. Coutinho, M.A. Antunes, L.C.J. Pereira, J. Marcalo, M. Almeida, Chem. Commun. 50 (2014) 10262–10264.
[367] I. Castro-Rodriguez, H. Nakai, L.N. Zakharov, A.L. Rheingold, K. Meyer, Science 305 (2004) 1757–1759.
[368] O.P. Lam, C. Anthon, F.W. Heinemann, J.M. O'Connor, K. Meyer, J. Am. Chem. Soc. 130 (2008) 6567–6576.
[369] E.M. Matson, J.J. Kiernicki, N.H. Anderson, P.E. Fanwick, S.C. Bart, Dalton Trans. (2014).
[370] T. Mehdoui, J.-C. Berthet, P. Thuéry, L. Salmon, E. Rivière, M. Ephritikhine, Chem. Eur. J. 11 (2005) 6994–7006.
[371] G. Zi, L. Jia, E.L. Werkema, M.D. Walter, J.P. Gottfriedsen, R.A. Andersen, Organometallics 24 (2005) 4251–4264.
[372] E.M. Matson, S.R. Opperwall, P.E. Fanwick, S.C. Bart, Inorg. Chem. 52 (2013) 7295–7304.